Measurements of the giant dipole resonance with monoenergetic photons*

B. L. Berman and S. C. Fultz†

Lawrence Livermore Laboratory, University of California, Livermore, California 94550

Photoneutron cross-section data obtained with monoenergetic photon beams are presented, many of them in graphical form in a uniform format. Tables of values for quantities derived directly from the data, such as integrated cross sections, and for quantities derived indirectly from the data, such as parameters of Lorentz curves fitted to the data, are presented as well. Average properties of the giant dipole resonance obtained from the data are compared with theory, as are more general nuclear quantities, such as symmetry energies, deformations, and level-density parameters. Structure in the cross sections and various other special topics are discussed, and a survey and a critique of the experimental techniques used to obtain the data are included.

CONTENTS

I. Introduction 713
II. Experimental Methods 715
A. Positron annihilation in flight 715
1. Production and measurement of the photon beam 715
2. Neutron detection and multiplicity counting 718
B. Other experimental methods 719
III. Experimental Results 720
A. Photoneutron cross-section data 726
B. Specialized experiments 735
1. Caldwell's experiment 736
2. Kelly's experiment 738
3. Photon scattering 739
IV. Properties of the Giant Resonance 741
A. Quantities derived directly from the data 741
1. The integrated cross section and the TRK sum rule 741
2. The first moment of the integrated cross section 742
3. The second moment of the integrated cross section and the Migdal sum rule 743
4. The ratio of integrated cross sections and the shell model 745
B. Lorentz curves fitted to the data and their parameters 745
C. Quantities derived from the Lorentz parameters 746
1. The nuclear symmetry energy 746
2. The energy of the giant resonance 747
3. The width of the giant resonance 748
4. The extrapolated integrated cross section 749
5. The area ratio and quadrupole moment for statically deformed nuclei 750
D. Application of the data to other collective theories of the giant resonance 751
E. Statistical parameters 753
F. Structure above the giant resonance 755
1. Isospin splitting and mixing 755
2. Electric quadrupole absorption 757
V. Summary 757
VI. Perspective 758
Acknowledgments 758
References to the Data 758
References to the Text 759

I. INTRODUCTION

Over the past twenty-five years many studies of photonuclear reactions have been made, for many nuclei throughout the periodic table, in the attempt to delineate the systematics of photon absorption by nuclei in general and of the giant electric dipole resonance, which dominates the absorption process at energies between 10 and 30 MeV, in particular. The large effort that has been put into these studies is justified by the fact that the theory of the interaction of electromagnetic radiation with nuclei is perhaps the best understood in nuclear physics: if the interaction in the entrance channel is understood, then the effects of the purely nuclear forces can be studied directly by measuring either the photon absorption cross sections or the products of nuclear photodisintegration.

The giant dipole resonance always has been of central interest in photonuclear-reaction studies, both experimental and theoretical. It corresponds to the fundamental frequency for absorption of electric dipole radiation by the nucleus acting as a whole, and is most simply understood as the oscillations of the neutrons against the protons in the nucleus. This is the semiclassical hydrodynamic model of Goldhaber and Teller (1948; Steinwedel and Jensen, 1950). Alternatively, one can construct the giant resonance from a superposition of particle–hole states based on the shell model. Indeed, building upon the independent-particle-model description of the giant resonance of Wilkinson (1956), the particle–hole theory was developed, largely by Brown and co-workers, to explain the details of the giant resonance (Elliott and Flowers, 1957; Brown and Bolsterli, 1959). This latter approach is particularly suited to calculating the decay modes (branching ratios, angular distributions, polarizations, and the like) of the giant-resonance states, especially for light nuclei, where the number of states involved is small enough to be manageable. The experimental emphasis seems to be changing gradually from the exploration of the absorption process to the attempt to understand the giant-resonance states in detail by studying their decay products. Yet both these aspects have been scrutinized in ever finer detail in recent years, the former by means of systematic studies in medium and heavy nuclei and the latter through key experiments on specific light nuclei. Although measurements performed with monoenergetic photon beams have played an important role in both these aspects, they have come much closer to dominating the field in medium and heavy nuclei, and therefore the main emphasis of this review will lie there; the importance

* Work performed under the auspices of the U. S. Atomic Energy Commission.
† Deceased.

of a few key experiments on light nuclei should not, however, be underrated.

Most of the giant-resonance measurements which have been done in the past have used as the source of radiation the continuous bremsstrahlung spectrum produced when the electron beam from an accelerator, usually a betratron or synchrotron, strikes a high-Z target. This use of a continuous radiation source requires an "unfolding" of the data, in which assumed bremsstrahlung spectra for different incident electron energies are subtracted from each other. In general, one has to obtain a yield curve by stepping the incident electron energy in small increments, and then differentiate the yield curve in order to determine the cross section. This requires great stability in the accelerator parameters, enormous counting statistics, knowledge of the bremsstrahlung flux and spectrum, especially near the end point where both are exceedingly hard either to calculate or to measure, and tedious data-reduction procedures. That some systematic measurements of the giant resonance indeed were achieved (Fuller and Hayward, 1962a; Hayward, 1965) is a testimony to the diligence and patience of the early workers in the field. However, a number of systematic errors are intrinsic in the unfolding technique, and these become magnified when energies above the peak of the giant resonance are reached, because the yields increase much more slowly. This important energy region contains (a) high-multiplicity processes, such as $(\gamma,2n)$ and $(\gamma,3n)$ reactions, (b) photoexcitation of higher isospin states, (c) quadrupole giant resonances, and (d) direct-reaction contributions, among others, and has become a very important region for investigation, where accurate information on cross sections is required. Further, since the measurement even of the basic shape of the giant dipole resonance itself depends critically upon a knowledge of the multiple-neutron cross sections on the higher-energy side of the giant resonance, it became clear that continuously variable monoenergetic photon beams with good resolution and sufficient intensity were needed to delineate giant-resonance systematics in detail.

Until the advent of high-intensity linear electron accelerators, this central experimental problem in photonuclear physics could not be solved. During the past decade, however, some new methods have been introduced in which the photoprocesses have been measured with monoenergetic photons. The most fruitful of these has been the use of the annihilation in flight of fast positrons from a linear accelerator to produce monoenergetic photons, although other methods have been employed as well (Schuhl, 1973; Berman, 1974a), and several are discussed below. Historically, work in the photonuclear field which has employed annihilation-photon beams has been concentrated at the Livermore and Saclay laboratories, but it should be noted that this was not an historical accident: rather, it resulted from the recognition at an early date of the facts stated in the previous paragraph by the workers at these laboratories. Photoneutron studies were not performed at these laboratories because annihilation-photon beams and highly efficient neutron detectors were available there already; the apparatus and techniques were developed, at great cost, time, and effort, specifically in order to attack, by the most efficient method, the central problem of the detailed delineation of the systematic properties of the giant resonance.

Today, the results are clear. The use of monoenergetic photon beams has given rise to cross-section measurements with high resolution, and especially to an improved knowledge of the cross sections above the peak of the giant resonance. Higher-multiplicity cross sections have been measured directly and their systematics studied, and more accurate information on structure throughout the giant-resonance region has been obtained. In short, the quality of the data produced has justified well the effort necessary to develop and utilize monoenergetic photon beams.

The purposes of this review, then, are to survey the considerable body of photoneutron data acquired with monoenergetic photon beams, to delineate the systematics of the giant dipole resonance so determined, and to compare the results with the predictions of various nuclear models. Also, since the great majority of these data have been obtained by the annihilation-photon method, an exposition and a critique of this experimental technique are given as well. This has not been done recently, although some years ago Spicer (1964) compared the bremsstrahlung and annihilation-photon techniques for measuring photoneutron cross sections.

The present report is concerned primarily with the results obtained with monoenergetic photons. Although much fine work has been done using bremsstrahlung sources, the large discrepancies in the data reported from various laboratories and the intrinsic systematic uncertainties referred to above make it difficult to weight properly these measurements when comparing them with monoenergetic-photon data, and no such attempt is made here. Fortunately, enough data are now available from monoenergetic-photon measurements alone to justify fully a survey at this time.

Finally, the reader should be cautioned that although the principal results of this review are based almost entirely upon photoneutron measurements made with monoenergetic photons, for the reasons given above, there exists as well a considerable body of pertinent literature in the areas of electron and photon scattering, (γ,p) and capture reactions, and photon absorption, which are beyond the scope of the present report. The reader therefore is referred to the several reviews of the general subject of photonuclear reactions which are available. Levinger (1960) gives a summary of early work in the field, together with a theoretical introduction to the subject based on the analogy with the atomic photoeffect; Danos and Fuller (1965) give a theoretical exposition of the shell- and collective-model treatments of the giant resonance; Hayward (1965, 1970) gives a general survey, together with an extensive treatment of photon scattering and of angular distributions of photonucleons; Spicer (1969) gives an historical review of the theories of the giant resonance and the early experiments, together with a strong treatment of the dynamic collective model, particularly as applied to vibrational nuclei; and Firk (1970) gives a treatment of giant-resonance properties in heavy nuclei, the angular distribution and polarization of photonucleons from light nuclei, and isospin effects in photonuclear reactions. The reader also is referred to the recent experimental survey by Berman (1974a), to the textbooks by Eisenberg and Greiner (1970a, 1970b, 1972), to the bibliographic compilations of Toms (1967) and Fuller *et al.*

(1973), and to the proceedings of two recent conferences in the field (Shoda and Ui, 1972; Berman, 1973d).

II. EXPERIMENTAL METHODS

The experimental methods for producing beams of monoenergetic photons which have been used for photonuclear-reaction studies include the annihilation in flight of fast positrons, tagged bremsstrahlung, and nuclear γ rays from the capture of protons or neutrons. Most of the work surveyed here has been done with annihilation photons; therefore, this method will be treated in the most detail. [For even more details regarding the annihilation-photon technique, see Berman and Fultz (1974c).]

A. Positron annihilation in flight

The annihilation-photon method for obtaining a monoenergetic photon beam was first suggested by Tzara (1957), and has been developed or studied at several laboratories since, principally at Saclay (Miller *et al.*, 1960a; Miller *et al.*, 1960b; Schuhl and Tzara, 1961) and at Livermore (Hatcher *et al.*, 1961; Jupiter *et al.*, 1961; Seward *et al.*, 1961; Fultz *et al.*, 1962b). The method consists in producing a beam of fast positrons, transporting this beam (having the desired energy E_{e^+}) to the experimental area, and allowing it to strike a thin, low-Z target, thus producing, in the forward direction, a monoenergetic beam of annihilation photons (where the photon energy is $E_\gamma = E_{e^+} + 0.76$ MeV, the latter term being $\frac{3}{4}$ of the rest mass of the annihilating pair).

1. Production and measurement of the photon beam

Studies have been made of annihilation-photon yields (Seward *et al.*, 1961; Owens and Cardman, 1969; Audit *et al.*, 1970), positron converters (Yount and Pine, 1962; Sund *et al.*, 1964; Nunan, 1965; Toms and Godlove, 1965; Haissinski, 1967; Lobb, 1967), and annihilation-photon resolution (Hatcher *et al.*, 1961; Elliott *et al.*, 1964; Audit *et al.*, 1970). Measurements on photon energy resolution have shown that the resolution width down to the 1% level can be attributed to three sources: (a) the momentum width of the incident positron beam, (b) the dE/dX loss suffered by the positrons in the target before annihilation, and (c) multiple scattering of the positron beam in the target before annihilation. Figure 1 shows the photon energy resolution obtained for beryllium annihilation targets 0.25 and 0.76 mm thick, for a spread in the incident positron momentum of 1%. If the resolution is pushed down to the 0.1% level by reducing the momentum width of the positron beam and the thickness of the annihilation target (of course this requires a much more intense positron beam, since the photon yield decreases approximately as the square of the resolution), then other effects begin to play a role, such as the energy variation of the annihilation photons with angle (for large annihilation-target or nuclear-sample diameters) and the presence of Compton-scattered photons which have lower energy (for large sample thicknesses). Fortunately, these effects are worst for high energies ($\gtrsim$40 MeV), where high resolution is not likely to be so important because one is measuring cross sections well up in the nuclear continuum.

The annihilation cross section has been shown to increase almost linearly with positron energy (Seward *et al.*, 1961),

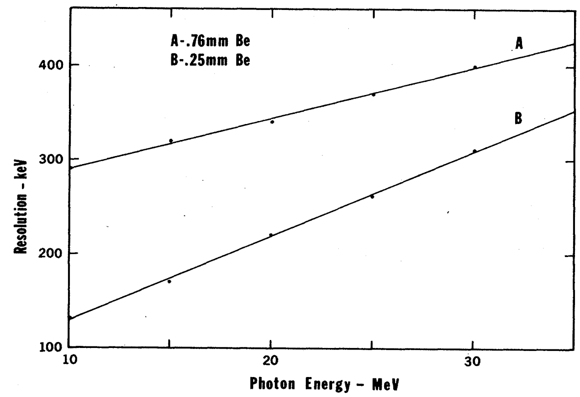

FIG. 1. Calculated energy resolution (FWHM) of the forward annihilation-photon beam produced by a positron beam having a momentum spread of 1% incident on beryllium targets 0.76 mm thick (curve A) and 0.25 mm thick (curve B) (values taken from Bramblett *et al.*, 1966b).

as does the photon yield (Audit *et al.*, 1970). Even so, the yield of unwanted photons above any given photonuclear threshold from positron bremsstrahlung increases faster still with increasing positron energy. This makes it increasingly more difficult to subtract off the results of this effect (by repeating the experimental measurements with incident electrons instead of positrons—see below), so that cross-section measurements for a given photonuclear reaction channel far above its threshold tend to become statistically poor (since they depend upon the measurement of the difference between two large numbers).

Positrons are produced by pair production from the bremsstrahlung created when the intense beam of high-energy electrons from a high-current Linac strikes a thick, high-Z converter. The materials used for these converters have included gold, tungsten, platinum, and tantalum, as well as copper, molybdenum, and other elements or alloys, and usually are about one to two radiation lengths thick. These targets must sustain great heating and mechanical stresses owing to the high power and power density of the electron beam. As a result, they often are given some motion (linear or circular) to distribute the heat load, and must be well cooled. The most successful material used at Livermore has been a carefully treated tungsten–rhenium alloy. It clearly is advantageous to use a high incident electron energy, not only because the bremsstrahlung and pair-production cross sections increase with energy, but even more so because the (relativistic) positrons are emitted into an increasingly narrower cone, thus allowing them to be captured more efficiently by the downstream components of the beam optical system.

Positrons have been produced both along the accelerator and at the end of the accelerator. In the former case (the Livermore system), the converter target is placed between two sections of the Linac. The incident electrons are focused onto the converter by a quadrupole doublet, the converter itself is immersed in a stepped solenoidal magnetic field, and the emergent positrons are focused into the next accelerator section, also by a solenoid. To select and accelerate a positron beam, all accelerator sections following the converter are operated with the radio frequency nearly 180°

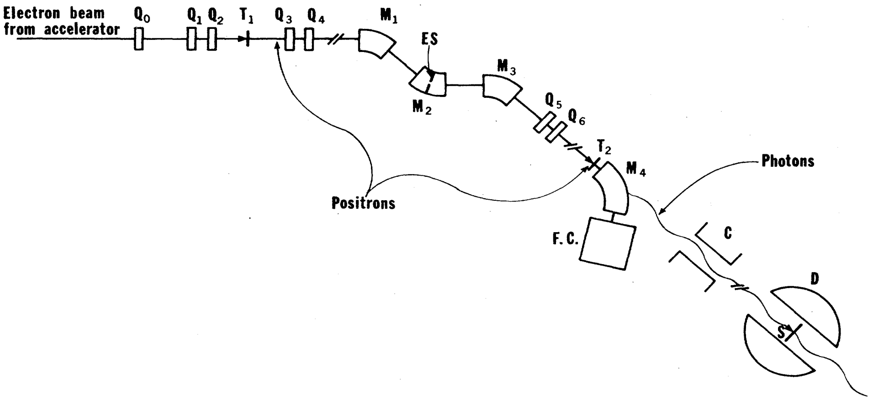

FIG. 2. Schematic diagram of the annihilation-photon beam facility at Saclay: M_i—bending magnets; Q_i—quadrupole magnets; ES—energy-analyzing slit; T_1—positron converter target; T_2—annihilation target; FC—Faraday cup; C—collimator; S—nuclear sample; D—neutron detector. (from Bayart, 1969)

out of phase with that normally used for electrons. To select the negative electrons from pair production (for performing the bremsstrahlung-subtraction measurements), all accelerator sections are operated with the normal phase. The energy of the positrons can be selected over a wide range by adjusting the power of the sections following the converter. Since the Linac sections which accelerate electrons operate at full beam loading while those which accelerate positrons operate essentially in a zero-current mode, the optimum location of the converter is determined by the energy and intensity of the positron beam required to do the experiment. Thus, by having the ability to insert the converter at any of several locations along the accelerator, one can trade energy for intensity in the way best suited to the needs of the experiment. The positron beam, having been accelerated to the desired energy, is energy analyzed with a bending magnet and slit and then transported to the experimental area.

For the case where the positrons are produced external to the accelerator (the Saclay system), the positrons pass through a series of bending and focusing magnets and energy-selection slits. By adjusting the magnetic fields the system is made to pass positron beams of various energies. This method produces the maximum positron flux of which the machine is capable, but is ideal only for the range of energies near the maximum of the intensity distribution of the positrons emerging directly from the converter. In both systems the momentum width of the positron beam is set by the width of the energy-selection slits. Figure 2 is a diagram of the setup used at the Saclay 60-MeV Linac (Schuhl and Tzara, 1961; Bayart, 1969). The neutrons from photoneutron reactions are counted by means of a 500-l spherical liquid scintillator 1 m in diameter and loaded with 0.5% gadolinium (Beil *et al.*, 1969). The energy calibration and resolution (but not the photon flux) are measured by detecting the 15.11-MeV photons scattered from a carbon sample placed in the photon beam line. The resolution also was measured at 19.15 MeV by observing the broadening of the sharp structure in the $^{28}Si(\gamma,p_0)$ reaction for various beam and target conditions by means of a Si(Li) solid-state proton detector placed in the photon beam. The absolute photon flux is determined by calibrating the Faraday cup (Fig. 2), which measures the integrated charged-particle beam flux, against a 20×20 cm NaI(Tl) crystal placed in the forward photon beam and subtracting the measured bremsstrahlung spectrum for electrons incident upon the annihilation target from the spectrum of bremsstrahlung plus annihilation photons produced by incident positrons.

Much of the experimental data included in this survey was taken with the annihilation-photon facility at the old 30-MeV Linac at Livermore. Two experimental arrangements for the beam-transport and optical system were used; these have been illustrated and described in the literature (Fultz *et al.*, 1962b; Alvarez *et al.*, 1971) and are not shown here. Figure 3 is a diagram of the beam-transport system and experimental setup currently in use at Livermore. The neutron detector consists of a 60-cm cube of paraffin in which are embedded 48 long (50 cm) high-pressure ($\sim$2 atm) $^{10}BF_3$ detectors, arranged in four concentric rings of 12 tubes each around the axial sample hole (Berman *et al.*, 1967). Up to eight samples can be loaded into the detector sequentially with a remotely controlled blower-pump-driven sample changer, so that beam-tuning conditions remain the same for different samples at a given energy. The measurement of the photon flux is achieved with a thin-walled, spherical, xenon-filled transmission ion chamber. The ion chamber was calibrated up to 45 MeV by means of a 20×20 cm NaI(Tl) scintillation crystal. Response functions for this crystal were obtained experimentally, with the use of a coincidence–anticoincidence scheme between the forward ($\sim$0°) and backward ($\sim$180° in the center-of-mass system) photons of the two-photon annihilation process (Bramblett *et al.*, 1973). Sample response functions achieved by this technique of tagging one annihilation photon with the other are shown in Fig. 4. Examples of NaI photon spectra produced by beams of 16.5-MeV positrons and electrons striking an 0.13-mm-thick beryllium target are shown in Fig. 5. The systematic uncertainty in the absolute photonuclear cross sections resulting from uncertainties in the photon flux calibration ranges from $\pm5\%$ at 15 MeV to $\pm10\%$ at 30 MeV. The energy calibration is set with reference to the peak in the $^{16}O(\gamma,n)^{15}O$ cross section at 17.28 MeV and the threshold for transitions to the third excited state of ^{15}O ($E_\gamma = 21.85$ MeV), the latter being measured by the ring-ratio technique (Caldwell *et al.*, 1965). The energy resolution has been measured using the 17.28-MeV peak in ^{16}O and also using several narrow peaks in the $^{26}Mg(\gamma,n)$ cross section.

Sund and collaborators at General Atomic (Sund *et al.*, 1968; Sund *et al.*, 1970) have used the annihilation-photon method, combined with counting of the radioactivity from

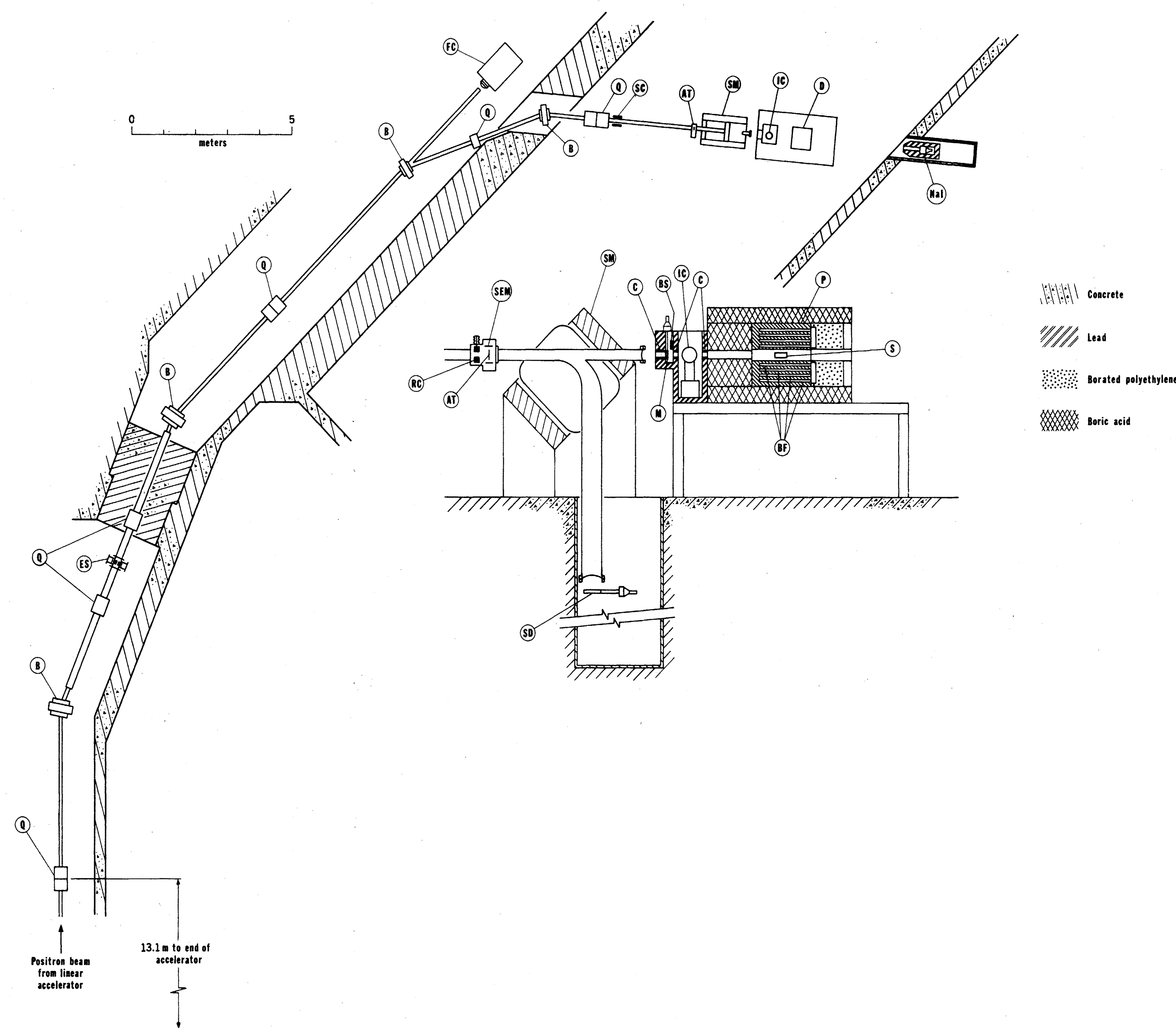

FIG. 3. Experimental layout for one of the annihilation-photon beam facilities at Livermore: B—bending magnets; Q—quadrupole magnets; ES—energy-analyzing slit; FC—Faraday cup; SC—steering coils; AT—annihilation target; SM—sweeping magnet; IC—photon ion chamber; D—detector; NaI—photon spectrometer. Inset: Detail of the 4π photoneutron experiment: RC—removable collimator; SEM—secondary-emission monitor; SD—swept-beam detector; C—collimators; M—beam-tuning monitor: BS—beam shutter; S—nuclear sample; P—paraffin moderator; BF—$^{10}BF_3$ neutron detectors (from Fultz *et al.*, 1973a).

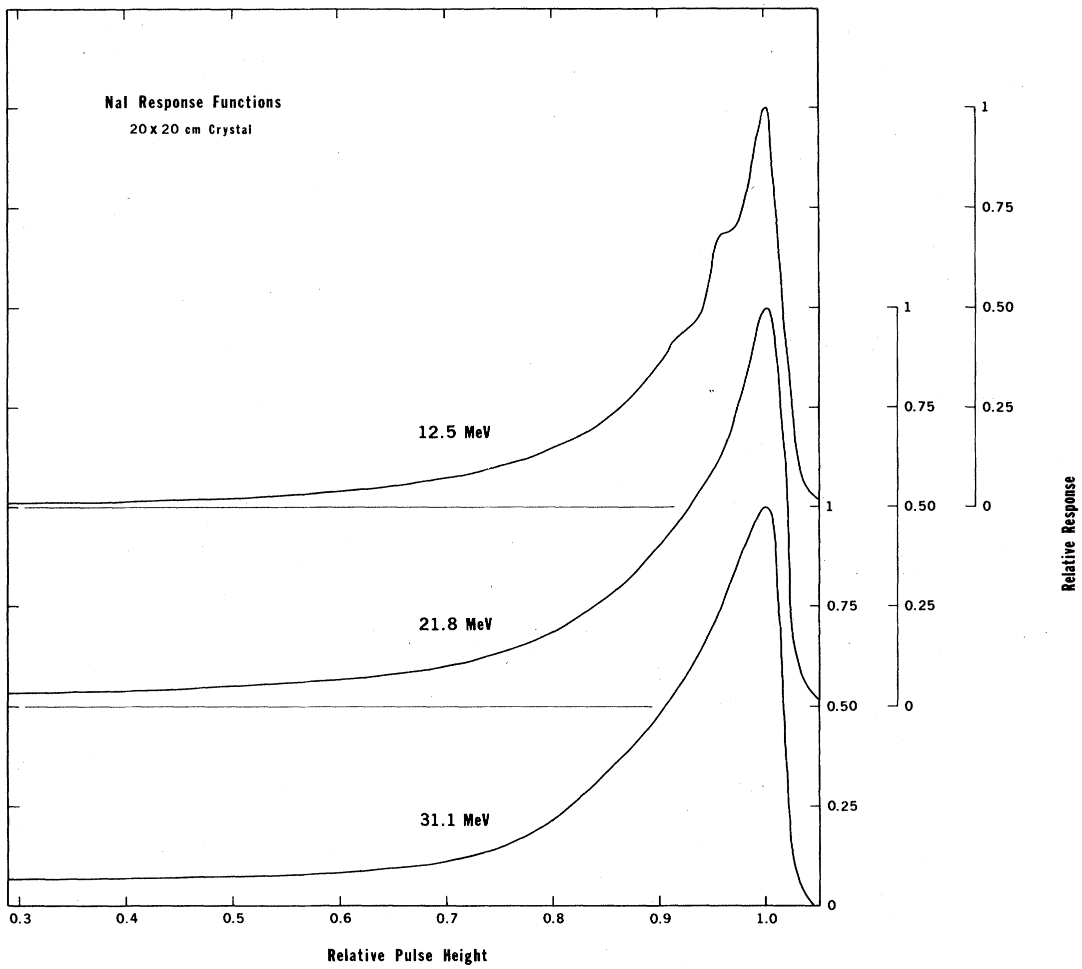

FIG. 4. Measured response functions for a 20 × 20-cm cylindrical NaI(Tl) photon spectrometer obtained with annihilation photons incident along the cylindrical axis (see text) (from Bramblett *et al.*, 1973c).

photoactivation instead of direct photoneutron counting. They have measured the (γ,n) cross sections for ^{63}Cu and ^{141}Pr with good resolution, as well as a few points for the ^{63}Cu$(\gamma,2n)$ reaction.

2. Neutron detection and multiplicity counting

The development of neutron detection techniques, which has paralleled that for monoenergetic photon beams, also has proven to be essential for giant-resonance studies. In particular, the height of the Coulomb barrier in medium and heavy nuclei results in nearly all the photon absorption strength going into the neutron-producing partial cross sections (γ,n), $(\gamma,2n)$, etc. This gives rise to the need for highly efficient 4π neutron detectors (since the efficiency for detecting two neutrons is the square of that for one) and for neutron multiplicity counting techniques [in order, for instance, to distinguish a $(\gamma,2n)$ event from two (γ,n) events]. Both these needs are satisfied by employing a "slowing-down" type of detector, in which the neutrons produced during the short beam burst of a pulsed accelerator are moderated before being detected between beam bursts. Both large arrays of ^{10}BF$_3$ tubes embedded in a paraffin or polyethylene matrix (Fultz *et al.*, 1962b; Berman *et al.*, 1967; Kelly, 1968; Kelly *et al.*, 1969) and large liquid scintillators (Beil *et al.*, 1969) have been used. In order to be able to differentiate between a $(\gamma,2n)$ event and two (γ,n) events, say, as well as to be able to measure absolute cross sections well, one must know the neutron detector efficiency (which might be 40–60% typically) rather precisely. The Livermore group has developed the ring-ratio technique for measuring the average neutron energy, and thus, with the aid of calibrated neutron sources, the efficiency for every data run, based on the fact that the ratio of the counting rate in the outer ring of ^{10}BF$_3$ detectors to that in the inner ring is a strong, monotonically increasing function of the energy of the photoneutrons. Calibration curves for the Livermore detector are shown in Fig. 6. The more recent Livermore data (published after 1964) include ring-ratio determinations of the average photoneutron energy $\bar{E}_n$. In particular, for the most recent of these, ring-ratio data for both $(\gamma,1n)$ events and $(\gamma,2n)$ events were determined separately. This enabled these partial cross sections to be obtained using detector efficiencies appropriate to each photoneutron multiplicity, thus improving the accuracy of the branching ratios, and at the same time providing more detailed information on the decay of the giant resonance for these nuclei. An example, for ^{153}Eu, is discussed below (Sec. IV.E).

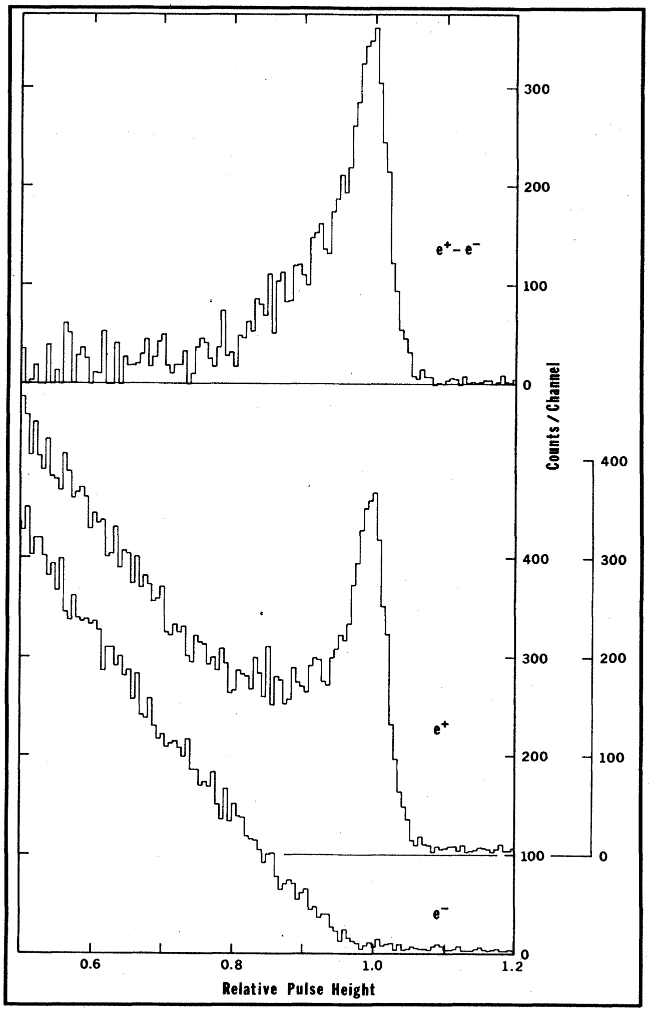

FIG. 5. Photon spectra produced by beams of 16.5-MeV positrons and electrons striking an 0.13-mm beryllium target. The annihilation-photon peak is broadened greatly by the resolution of the 20 × 20 cm NaI spectrometer. The difference spectrum is another measure of the response function of the NaI crystal (see text) (from Fultz *et al.*, 1973a).

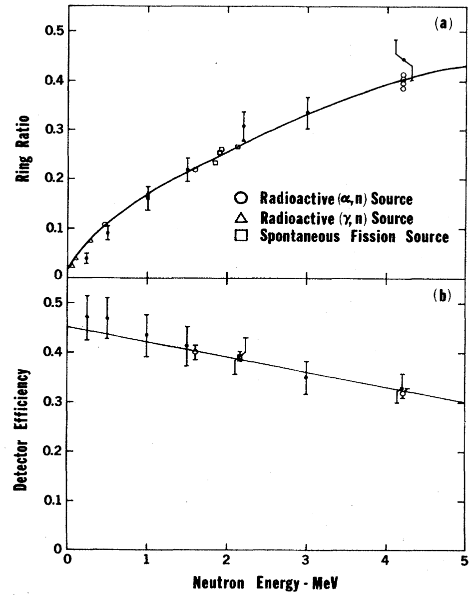

FIG. 6. Comparison of experimental measurements of (a) the ring ratio (the ratio of neutron counting rates of the outer to the inner ring of detectors) and (b) gated detector efficiency as functions of neutron energy for the Livermore 4π BF_3-plus-paraffin neutron detector (open symbols from Berman *et al.*, 1967) with theoretical Monte-Carlo calculations (solid circles, from Meyer, 1973). The values of the abscissa for the (α,n) and spontaneous fission sources are averages of broad neutron energy spectra.

The large Gd-loaded liquid scintillator used at Saclay, shown schematically in Fig. 7, was calibrated only by means of a ^{252}Cf source. A calculated efficiency curve, shown in Fig. 8, is used to justify the use of a constant value for the efficiency in the photoneutron data reduction procedure on the basis that serious discrepancies arise only above $E_n \simeq 5$ MeV (see Fig. 8), whereas the energy of most photoneutrons does not exceed ~3 MeV.

A word about the possible errors involved in the neutron detection and multiplicity counting is in order here. First, the over-all detector efficiencies over the range of neutron energies important for giant-resonance measurements are rather well known (to $\lesssim 3\%$), so that the chief uncertainty in the absolute cross-section scale results from the uncertainty in the photon flux determination. However, the branching between the various partial photoneutron cross sections depends critically upon the efficiencies used. The lower efficiency of the Livermore detector makes the complex multiplicity sorting (see Bramblett, 1962; Fultz *et al.*, 1962) inherently somewhat less reliable than for the Saclay case, although the information gleaned from the ring-ratio measurements probably compensates to a large degree. The Saclay detector, on the other hand, suffers from a much higher background rate, made up largely of single-neutron events, which introduces larger uncertainties in the background subtractions and pile-up corrections.

B. Other experimental methods

Two other methods for generating monoenergetic photon beams have been applied to giant-resonance cross-section measurements. One of these makes use of the (p,γ) reaction,

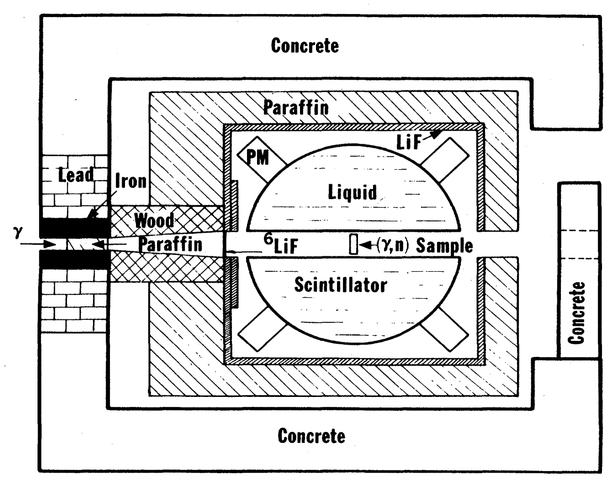

FIG. 7. Cross-section view of the Saclay 4π gadolinium-loaded liquid-scintillator neutron detector and its associated shielding (from Beil *et al.*, 1969).

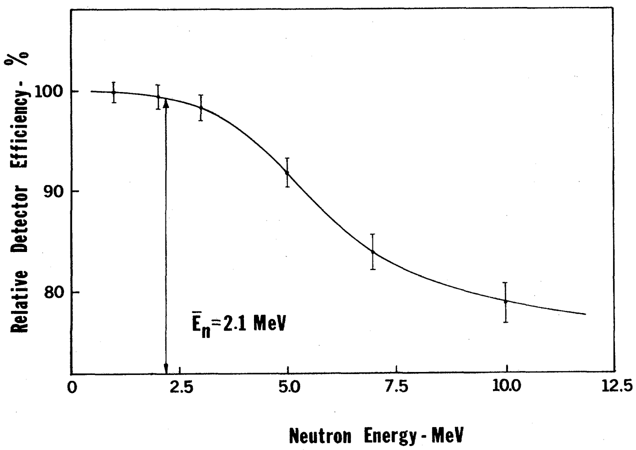

FIG. 8. Calculated relative detector efficiency as a function of neutron energy for the Saclay neutron detector (from Beil *et al.*, 1969).

usually on ^{7}Li, but sometimes on ^{3}H, to produce a beam of monoenergetic photons. Lochstet and Stephens at Pennsylvania (Lochstet and Stephens, 1966) measured the ^{12}C$(\gamma,n)^{11}$C cross section by use of ^{3}H(p,γ) reaction γ rays at a Van de Graaff accelerator. Here, use is made of the high Q value (19.8 MeV) of this reaction to reach relatively high photon energies with a moderate-energy proton beam. The main drawback to this method is the large neutron background from the ^{3}H(p,n) reaction once its threshold (corresponding to a photon energy of 20.6 MeV) is exceeded. They avoided this problem by measuring the ^{11}C activity produced, using coincidence counting of the two 0.511-MeV annihilation photons from the ^{11}C positron decay. It is notable that they achieved an energy resolution of 100 keV at 22 MeV, ranging up to 200 keV at 26 MeV. Also, Del Bianco *et al.* (1973) recently measured the (γ,n) cross sections for ^{50}Cr and ^{64}Zn in this way, but only over the limited energy range from 20.4 to 22.2 MeV.

Axel and collaborators at Illinois (O'Connell *et al.*, 1962) have developed a photon-tagging technique (the "bremsstrahlung monochromator"), which consists in bending a high-resolution electron beam from a betatron (or synchrotron) in a beta-ray spectrometer after it has passed through a thin, high-Z bremsstrahlung target and demanding a fast coincidence between a reaction product of the photonuclear event induced by a bremsstrahlung photon and the scattered electron that produced the photon. The intensity and resolution of the quasimonoenergetic photon beam thus produced are comparable to those of the annihilation-photon technique. This technique can be employed only with accelerators having a long duty cycle; it has proven most useful for photon scattering and fast photoneutron measurements below 16 MeV, but recently the Illinois group also has extended their measurements to photoneutron cross-section measurements at giant-resonance energies (Kuchnir *et al.*, 1967; Calarco, 1969; Young, 1972). Four nuclei, namely ^{89}Y, ^{141}Pr, ^{208}Pb, and ^{209}Bi, have been studied thus far, with good resolution (of the order of 100 keV). The chief disadvantage for cross-section measurements is that because of the fast-coincidence requirement a low-efficiency, small-solid-angle neutron detector (such as an organic scintillator) must be used; and since counting rates are limited by pile-up, massive samples must be used, and counting statistics are poor. This technique, however, rapidly becomes more competitive as the duty cycle of the accelerator increases; and as machines with duty cycles approaching 100%, such as pulse stretchers and superconducing Linacs, come on line it might very well become the method of choice for performing a wide variety of photonuclear measurements.

A novel approach for the special case of the (γ,p) and (γ,α) reactions on ^{28}Si is the use of a Si(Li) detector itself as the nuclear sample. This has been carried out by Matsumoto *et al.* (1964, 1965) and by Nagel (1970); the former used ^{7}Li(p,γ_0) and ^{3}H(p,γ) photons and the latter used tagged bremsstrahlung.

In addition to giant-resonance measurements proper, this survey also includes the photoneutron cross-section measurements of Donahue and collaborators at Pennsylvania State (Welsh and Donahue, 1961; Green and Donahue, 1964; Hurst and Donahue, 1967). They obtained monoenergetic γ rays from the capture of thermal neutrons from a reactor. The discrete γ-ray energies were varied by changing the neutron-capture sample; for instance, nickel gives a strong γ ray at 9.00 MeV; chromium gives one at 9.72 MeV, and nitrogen one at 10.83 MeV. Both activation counting and direct neutron detection were employed to study a large number of nuclei. Moreh and Bar-Noy (1972) recently have shown that the 11.4-MeV γ ray from ^{59}Ni(n,γ) ($\tau_{1/2} = 8 \times 10^4$ yr) can be used as a source of monoenergetic photons, thus pushing the upper-energy limit for this technique well up into the giant-resonance region for heavy nuclei.

III. EXPERIMENTAL RESULTS

The results of measurements made with the use of monoenergetic photons, mostly for the photoneutron cross sections, are discussed below. Some selection of these has been made in order to keep the data current and consistent. Nearly all of the data where the higher-multiplicity cross sections $\sigma(\gamma,2n)$, $\sigma(\gamma,3n)$, etc., were measured were selected for review, as were data taken with separated-isotopic samples. For the region of low atomic numbers, where the structure in the cross sections is prominent and of salient importance, the criterion for choice was the energy resolution; on this basis, only the data of more recent years were chosen.

A considerable number of measurements have been performed by Bergère and collaborators at Saclay very recently, but as yet have been published only in conference reports (Bergère *et al.*, 1973; Carlos *et al.*, 1973). These are not included in the figures and tables, but are referred to in the text below where appropriate, and are designated by the phrase "recent Saclay." The same is true for very recent measurements at Livermore (Berman *et al.*, 1973c). A complete set of data plots can be found in a recent compilation (Berman, 1974b).

Although much credit is due to Tzara and his collaborators for initiating the annihilation-photon work at Saclay, the early results of the original Saclay group (Miller *et al.*, 1962a; Miller *et al.*, 1962b; Miller *et al.*, 1966; Axel *et al.*, 1966) largely have been superseded by more recent mea-

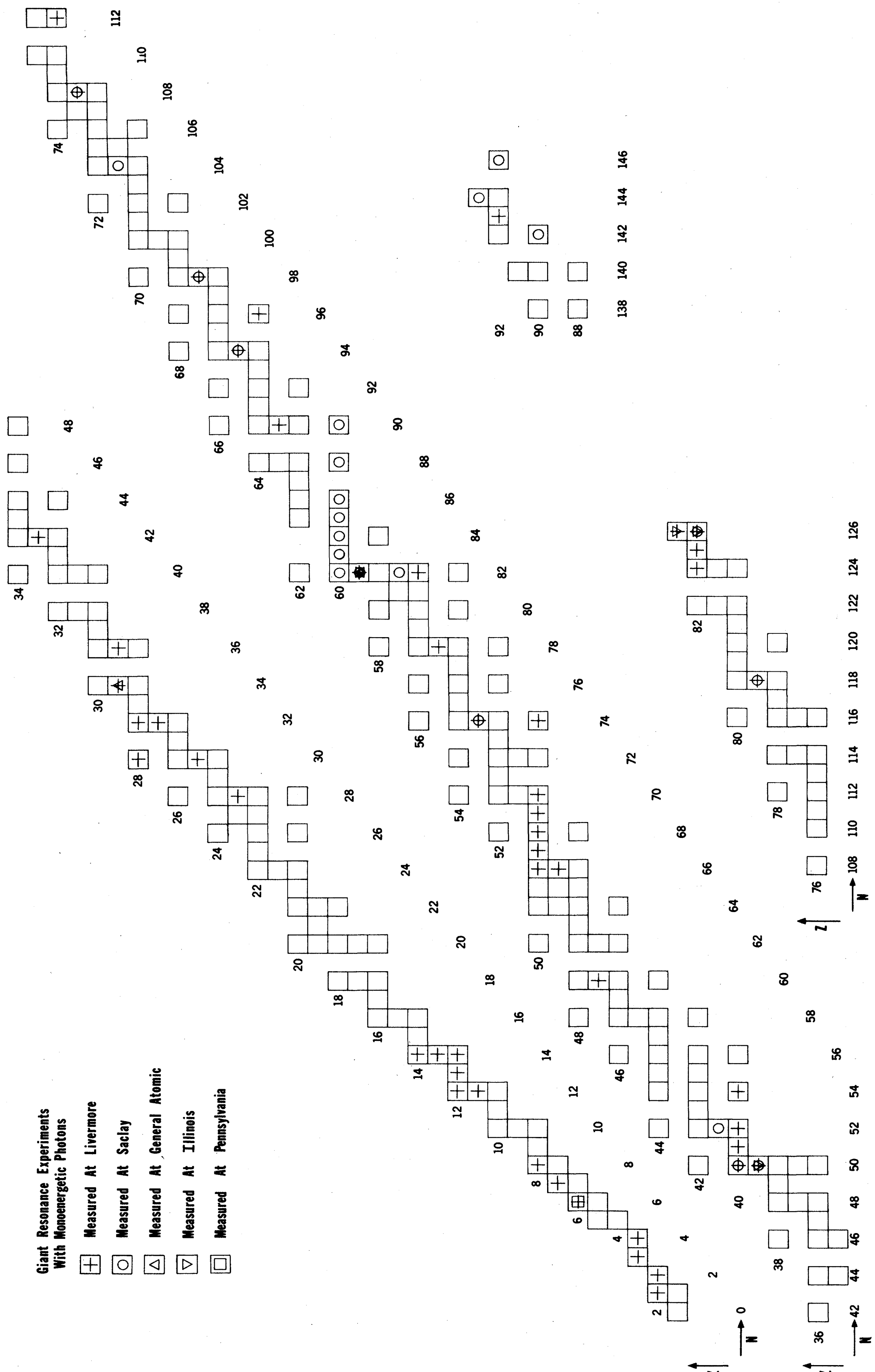

FIG. 9. Periodic table of the stable nuclei, showing those for which giant-resonance cross-section measurements have been performed with monoenergetic photons (adapted from Bramblett *et al.*, 1973a).

TABLE I. Experimental data—general.

Nucleus	Isotopic abundance (%)	Detector	Resolution (keV)	$E_{\gamma max}$ (MeV)	$\sigma_{int}(\gamma,tot)$ (MeV-mb)	$\sigma_{int}(\gamma,1n)$ (MeV-mb)	$\sigma_{int}(\gamma,2n)$ (MeV-mb)	$\sigma_{int}(\gamma,3n)$ (MeV-mb)	σ_{-1} (mb)	σ_{-2} (mb-MeV^{-1})	Figure number	Reference
^{3}He	98.6	BF_3	250–400	30.2	13.0	13.0			0.77	0.050	10	Berman *et al.*, 1970a
^{4}He	100	BF_3	350–400	31.4	7.94	7.94	0		0.30	0.012	10	Berman *et al.*, 1970a; Berman *et al.*, 1971
^{6}Li	95	BF_3	250–400	32.0	27.7	27.3	0.4		1.87	0.15	11	Berman *et al.*, 1965
^{7}Li	99	BF_3	250–400	30.5	20.1	10.1	10.0		1.15	0.071	12	Bramblett *et al.*, 1966; Bramblett *et al.*, 1973b
^{12}C	N.A.	Activ.	100–200	26.7	36	36					13	Lochstet & Stephens, 1966
	98.9	BF_3	400	25.5	29.4	29.4						Miller *et al.*, 1966
	98.9	BF_3	200–300	37.4	46.8	46.8	0		1.83	0.073	14	Fultz *et al.*, 1966
^{14}N	99.6	BF_3	300–400	29.5	97.6	97.6			4.36	0.20	14	Berman *et al.*, 1970c
^{16}O	99.8	BF_3	400	26.5	41.5	41.5						Miller *et al.*, 1966
	99.8	BF_3	200–300	28.0	41.5	41.5			1.76	0.075	14	Bramblett *et al.*, 1964; Caldwell *et al.*, 1965
^{23}Na	100	BF_3	150–300	27.1	119	118	0.6		5.74	0.29		Alvarez *et al.*, 1971
^{Nat}Mg	79.0(^{24}Mg)	BF_3	400	26.0	58[a]							Miller *et al.*, 1966
	79.0(^{24}Mg)	BF_3	150–300	28.0	75.6							Fultz *et al.*, 1971a
^{24}Mg	99.9	BF_3	150–300	28.3	51.9	51.9			2.37	0.11	15	Fultz *et al.*, 1971a
^{25}Mg	97.9	BF_3	150–300	28.9	247	245	1.5		11.5	0.56		Alvarez *et al.*, 1971
^{26}Mg	99.7	BF_3	150–300	28.6	236	164	72		11.5	0.59	16	Fultz *et al.*, 1971a
^{27}Al	100	BF_3	150–300	36.7	167	159	7.6		7.17	0.32		Fultz *et al.*, 1966
^{Nat}Si	92.2(^{28}Si)	BF_3	200–300	31.0	68.5	68.5	0		3.05	0.14	15	Caldwell *et al.*, 1963
^{40}Ca	96.9	BF_3	400	26.0	73	73						Miller *et al.*, 1966
^{51}V	99.8	BF_3	300–400	27.8	552	450	102		28.9	1.56		Fultz *et al.*, 1962a
^{55}Mn	100	BF_3	150–300	36.5	798	629	166	3.4	38.8	2.02	17	Alvarez *et al.*, 1973
^{58}Ni	99.9	BF_3	150–300	33.5	286	278	7.7		13.8	0.70	18	Fultz *et al.*, 1973a; Fultz *et al.*, 1973c
^{59}Co	100	BF_3	150–300	36.5	884	741	139	4.2	43.5	2.28		Alvarez *et al.*, 1973b
^{60}Ni	99.8	BF_3	150–300	33.2	704	632	72	0	35.6	1.90	19	Fultz *et al.*, 1973b; Fultz *et al.*, 1973c
^{63}Cu	99.4	BF_3	300–400	27.8	604	528	76		33.4	1.92	20	Fultz *et al.*, 1964
	N.A.	Activ.	150–500	25.1		498[b]	43[b]				20	Sund *et al.*, 1968
^{65}Cu	99.7	BF_3	300–400	27.8	619	421	198		36.0	2.18		Fultz *et al.*, 1964
^{Nat}Cu	...	BF_3	300–400	27.8	635	525	110					Fultz *et al.*, 1964
	...	BF_3	500	19.6	450[a]							Miller *et al.*, 1962a
^{75}As	100	BF_3	300–400	29.5	909	688	221	0	51.4	3.05	21	Berman *et al.*, 1969a
^{Nat}Rb	72.2(^{85}Rb)	Scint.	(400)	24.3	1147	1052	95		67.1	4.04		Leprêtre *et al.*, 1971
^{Nat}Sr	82.6(^{88}Sr)	Scint.	(400)	27.0	1432	1311	121		80.3	4.68	22	Leprêtre *et al.*, 1971
^{89}Y	100	BF_3	300–400	28.0	1059	960	99		59.8	3.48		Berman *et al.*, 1967
	100	Scint.	(400)	27.0	1353	1279	74		76.5	4.46		Leprêtre *et al.*, 1971
	100	NTOF	100–150	18.1	641				40.0	2.52		Young, 1972

TABLE I. (*Continued*)

Nucleus	Isotopic abundance (%)	Detector	Resolution (keV)	$E_{\gamma max}$ (MeV)	$\sigma_{int}(\gamma,tot)$ (MeV-mb)	$\sigma_{int}(\gamma,1n)$ (MeV-mb)	$\sigma_{int}(\gamma,2n)$ (MeV-mb)	$\sigma_{int}(\gamma,3n)$ (MeV-mb)	σ_{-1} (mb)	σ_{-2} (mb-MeV^{-1})	Figure number	Reference
^{90}Zr	97.8	BF_3	200–400	27.6	1060	962	98		59.1	3.38	23, 24	Berman *et al.*, 1967
	96.6	Scint.	(400)	25.9	1260	1211	49		70.8	4.08	23	Leprêtre *et al.*, 1971
^{91}Zr	90.9	BF_3	300–400	30.0	1103	903	200	0	65.4	4.07	24	Berman *et al.*, 1967
^{92}Zr	95.7	BF_3	300–400	27.8	1091	639	452	0	64.2	3.92	24	Berman *et al.*, 1967
^{93}Nb	100	Scint.	(400)	24.3	1331	1052	279		78.5	4.80		Leprêtre *et al.*, 1971
^{94}Zr	96.5	BF_3	300–400	31.1	1121	508	580	33	68.5	4.40	24	Berman *et al.*, 1967
^{107}Ag	98.5	BF_3	300–400	29.5	1356	1093	263	0	78.7	4.82		Berman *et al.*, 1969a
^{115}In	95.7	BF_3	300–400	31.1	1875	1355	508	13	113	7.13		Fultz *et al.*, 1969
^{116}Sn	95.7	BF_3	200–400	29.6	1669	1255	414	0	99	6.13	25	Fultz *et al.*, 1969
^{117}Sn	89.2	BF_3	300–400	31.1	1894	1380	476	38	114	7.30	25	Fultz *et al.*, 1969
^{118}Sn	97.2	BF_3	300–400	30.8	1853	1302	531	20	110	6.83	25	Fultz *et al.*, 1969
^{119}Sn	89.8	BF_3	300–400	31.1	1993	1326	597	69	118	7.55	25	Fultz *et al.*, 1969
^{120}Sn	98.4	BF_3	300–400	29.9	2074	1389	673	12	124	7.79	25	Fultz *et al.*, 1969
^{124}Sn	92.8	BF_3	300–400	31.1	2010	1285	670	55	123	8.02	25	Fultz *et al.*, 1969
^{127}I	100	BF_3	300–400	29.5	1729	1286	443	<20	105	6.70		Bramblett *et al.*, 1966b
	100	Scint.	400	24.9	1991	1601	390[c]	d	128	8.55		Bergère *et al.*, 1969
^{133}Cs	100	BF_3	300–400	29.5	1986	1475	503	8	124	8.09		Berman *et al.*, 1969a
^{138}Ba	99.8	BF_3	300–400	27.1	2040	1550	490	3[e]	130	8.71		Berman *et al.*, 1970c
^{Nat}Ba	71.9(^{138}Ba)	Scint.	150–250	24.3	2248	1877	371		146	9.94		Beil *et al.*, 1971
^{139}La	99.9	BF_3	500	21.2	1910[a]							Miller *et al.*, 1962a
	99.9	Scint.	150–400	24.3	1978	1687	291[f]	g	128	8.54		Bergère *et al.*, 1968 Beil *et al.*, 1971
^{Nat}Ce	88.5(^{140}Ce)	BF_3	500	21.2	1880[a]							Miller *et al.*, 1962a
	88.5(^{140}Ce)	Scint.	150–400	25.2	2165	1764	400[h]	1[i]	143	9.83		Bergère *et al.*, 1969 Beil *et al.*, 1971
^{141}Pr	100	BF_3	150–400	29.8	2062	1717	340	5[j]	128	8.37	26	Bramblett *et al.*, 1966b
	N.A.	Activ.	150–300	23.7		1714[b]					26	Sund *et al.*, 1970
	100	Scint.	150–250	16.9	1422	1422			101	7.31	26	Beil *et al.*, 1971
	100	NTOF	100–150	18.1	1395[a]				94[a]	6.41[a]	26	Young, 1972
^{Nat}Nd	...	Scint.	150–250	18.0	1559	1236	323		112	8.46		Beil *et al.*, 1971
^{142}Nd	95	Scint.	300	20.2	1873	1828	45		126	8.66	27	Carlos *et al.*, 1971
^{143}Nd	83.2	Scint.	300	19.8	1901	1722	179		132	9.51	27	Carlos *et al.*, 1971
^{144}Nd	91.5	Scint.	300	20.2	1882	1319	563		128	9.01	27	Carlos *et al.*, 1971
^{145}Nd	71	Scint.	300	20.2	2037	1380	657		147	11.34	27	Carlos *et al.*, 1971
^{146}Nd	94.7	Scint.	300	20.2	1920	1253	667		133	9.60	27	Carlos *et al.*, 1971
^{148}Nd	89.4	Scint.	300	18.8	1702	867	835		122	9.02	27	Carlos *et al.*, 1971
^{150}Nd	88.5	Scint.	300	20.2	2011	1174	837		142	10.39	27	Carlos *et al.*, 1971
^{Nat}Sm	...	Scint.	400	25.2	2413	1661	731	21[k]	163	11.5		Bergère *et al.*, 1969
^{153}Eu	98.8	BF_3	300–400	28.9	2273	1566	670	37	148	10.2		Berman *et al.*, 1969b

TABLE I. (*Continued*)

Nucleus	Isotopic abundance (%)	Detector	Resolution (keV)	$E_{\gamma max}$ (MeV)	$\sigma_{int}(\gamma,tot)$ (MeV-mb)	$\sigma_{int}(\gamma,1n)$ (MeV-mb)	$\sigma_{int}(\gamma,2n)$ (MeV-mb)	$\sigma_{int}(\gamma,3n)$ (MeV-mb)	σ_{-1} (mb)	σ_{-2} (mb-MeV^{-1})	Figure number	Reference
^{159}Tb	100	BF_3	300–400	28.0	2300	1413	887[l]		151	10.5		Bramblett *et al.*, 1964
	100	Scint.	400	27.4	2557	1936	605	16[m]	170	12.0		Bergère *et al.*, 1968
^{160}Gd	97.9	BF_3	300–400	29.5	2533	1398	1055	80	169	12.1	28	Berman *et al.*, 1969b
^{165}Ho	100	BF_3	400	19.6	2540[n]							Axel *et al.*, 1966
	100	BF_3	300–400	28.9	2523	1735	744	44	166	11.6		Berman *et al.*, 1969b
	100	Scint.	400	26.8	2871	2090	766	15[p]	194	13.9		Bergère *et al.*, 1968
^{Nat}Er	...	Scint.	400	21.1	2387	1801	586[q]	r	172	12.9		Bergère *et al.*, 1969
^{175}Lu	97.4	Scint.	400	23.0	2507	1872	635[s]	t	173	12.5	29	Bergère *et al.*, 1969
^{181}Ta	100	BF_3	500	22.0	2970[a]							Miller *et al.*, 1962a
	100	BF_3	300–400	24.6	2181	1300	881[l]		149	10.7		Bramblett *et al.*, 1963
	100	Scint.	400	25.2	2983	2180	790	13[u]	205	14.8	30	Bergère *et al.*, 1968
^{186}W	97.2	BF_3	300–400	28.6	3004	1655	1200	149	203	14.5	31	Berman *et al.*, 1969b
^{197}Au	100	BF_3	500	22.0	3000[a]							Miller *et al.*, 1962a
	100	BF_3	300–400	24.7	2967	2190	777[l]		205	14.7		Fultz *et al.*, 1962b
	100	Scint.	400	21.7	3067	2588	479[v]	w	217	15.9		Veyssière *et al.*, 1970
^{206}Pb	99.8	BF_3	300–400	26.4	2909	2377	532[l]		203	15.0		Harvey *et al.*, 1964
^{207}Pb	92.8	BF_3	300–400	26.4	2718	2169	549[l]		191	14.2		Harvey *et al.*, 1964
^{208}Pb	99.8	BF_3	300–400	26.4	2646	1786	860[l]		189	14.3		Harvey *et al.*, 1964
	91	Scint.	150–400	18.9	3059	2731	328[x]	y	229	17.6	32	Veyssière *et al.*, 1970
	72.6	NTOF	80–120	14.9	2090[a]				165[a]	13.3[a]	33	Young, 1972
^{Nat}Pb	...	BF_3	500	22.0	4100[a]							Miller *et al.*, 1962a
^{209}Bi	100	BF_3	500	22.0	3730[a]							Miller *et al.*, 1962a
	100	BF_3	300–400	26.4	3058	2344	714[l]		214	15.8		Harvey *et al.*, 1964
	100	NTOF	80–120	14.8	2129[a]				170[a]	13.8[a]		Young, 1972
^{232}Th	100	Scint.	(400)	16.3	2694	1728	787	179[z]	224	19.5		Veyssière *et al.*, 1973
^{235}U	93	BF_3 + Fission	300–400	18.5	3714	1066	1588	1060[z]	293	24.1	34	Bowman *et al.*, 1964
^{237}Np	(100)	Scint.	(400)	16.6	2756	1085	121	1550[z]	224	19.0		Veyssière *et al.*, 1973
^{238}U	99.3	Scint.	(400)	18.35	3026	1169	899	958[z]	241	20.2	35	Veyssière *et al.*, 1973

[a] Not corrected for $(\gamma,2n)$ events; the figures given are for the photoneutron yield cross section $\sigma[(\gamma,n)+(\gamma,pn)+2(\gamma,2n)]$.
[b] No data for (γ,pn) events; $(\gamma,2n)$ data consist of three values, at 22.2, 23.7, and 25.7 MeV.
[c] 508 MeV-mb up to 31.2 MeV.
[d] 31 MeV-mb up to 31.2 MeV.
[e] 13 MeV-mb up to 28.6 MeV.
[f] Some $(\gamma,2n)$ data up to 29 MeV.
[g] Some $(\gamma,3n)$ data up to 30 MeV.
[h] 473 MeV-mb up to 29.6 MeV.
[i] 19 MeV-mb up to 29.6 MeV.
[j] 36 MeV-mb up to 33.0 MeV.
[k] 59 MeV-mb up to 27.4 MeV.
[l] Includes $\frac{3}{2}\sigma_{int}(\gamma,3n)$.
[m] 46 MeV-mb up to 29.3 MeV.
[n] Extrapolated to 23 MeV.
[p] 45 MeV-mb up to 28.5 MeV.
[q] 768 MeV-mb up to 27.4 MeV.
[r] 52 MeV-mb up to 27.7 MeV.
[s] 742 MeV-mb up to 28.5 MeV.
[t] 65 MeV-mb up to 28.5 MeV.
[u] 137 MeV-mb up to 36.4 MeV; some $(\gamma,4n)$ data up to 36.4 MeV.
[v] 671 MeV-mb up to 27.1 MeV.
[w] 24 MeV-mb up to 27.1 MeV.
[x] 614 MeV-mb up to 26.3 MeV.
[y] 197 MeV-mb up to 37.8 MeV; some $(\gamma,4n)$ data up to 37.8 MeV.
[z] $\sigma_{int}(\gamma,\text{fission})$.

TABLE II. Photoneutron cross sections (in mb) obtained for single photon energies.

Nucleus \ Energy (MeV)	5.43	6.41	6.61	6.75	7.16	7.38	7.49	7.64	7.72	7.88	7.91	8.56	9.00	9.30	9.72	10.16	10.83	Reference
^{6}Li	0.42±0.07	0.6±0.1		1.3±0.2	0.9±0.1	1.2±0.2		1.3±0.2	1.13±0.12	1.0±0.2	1.1±0.2	1.6±0.3						Green & Donahue, 1964
^{7}Li						0.068±0.035		0.079±0.014	0.06±0.01		0.07±0.01	0.17±0.12	0.16±0.06		0.55±0.25		1.07±0.25	Green & Donahue, 1964
^{10}B													0.11±0.01	0.09±0.03	0.23±0.05		0.9±0.2	Green & Donahue, 1964
^{13}C			0.32±0.04		0.4±0.1	0.3±0.3		0.23±0.05	1.7±0.2	1.2±0.2	0.97±0.13		0.6±0.1				4±2	Green & Donahue, 1964
^{59}Co																	9.0±0.8	Hurst & Donahue, 1967
^{75}As																	20.4±1.7	Hurst & Donahue, 1967
^{93}Nb													0.008±0.005	1.0±0.4	2.4±0.7			Welsh & Donahue, 1961
^{93}Nb													0.53±0.10		14.6±2.2		25.8±2.1	Hurst & Donahue, 1967
^{103}Rh															10.6±1.7		38.8±3.1	Hurst & Donahue, 1967
^{107}Ag													0±0.1		4.4±1.5	22±16	23±7.5	Welsh & Donahue, 1961
^{Nat}Ag															10.0±1.5		37.6±2.9	Hurst & Donahue, 1967
^{115}In															17.1±2.6		33.3±2.7	Hurst & Donahue, 1967
^{Nat}Sb															20.7±3.1		42.5±3.6	Hurst & Donahue, 1967
^{127}I															38.7±5.8		38.8±3.1	Hurst & Donahue, 1967
^{133}Cs															31.7±4.8		52.5±3.8	Hurst & Donahue, 1967
^{139}La													8.61±0.86		40.8±6.5		63.0±5.0	Hurst & Donahue, 1967
^{141}Pr															21.5±3.2		58.3±4.1	Hurst & Donahue, 1967
^{Nat}Eu													28.9±3.2		61.3±14.7		102±18	Hurst & Donahue, 1967
^{165}Ho											0±0.1	29±15	30±18	46±21	86±31		260±93	Welsh & Donahue, 1961
^{165}Ho													35.6±4.3		92.2±27.6		150±20	Hurst & Donahue, 1967
^{181}Ta[a]							0±0.05	0.5±1	4.8±1.6		14±5	32±16	44±15		83±33		120±48	Welsh & Donahue, 1961
^{181}Ta								0.0±0.9	4.1±0.4		10.8±1.0	29±6	44±6		84±25		121±12	Green & Donahue, 1964
^{181}Ta									4.14 0.36				45.4±3.7		65.0±5.5		146±12	Hurst & Donahue, 1967
^{197}Au											0±2	34±17	44±11	64±30	80±30			Welsh & Donahue, 1961
^{197}Au													44.5±3.6		68.4±13.5		160±15	Hurst & Donahue, 1967
^{206}Pb													<34.3				238±29	Hurst & Donahue, 1967
^{208}Pb													22.6±11.3				280±31	Hurst & Donahue, 1967
^{209}Bi													36.1±12.0				226±27	Hurst & Donahue, 1967

[a] ^{181}Ta$(\gamma,n)^{180m}$Ta.

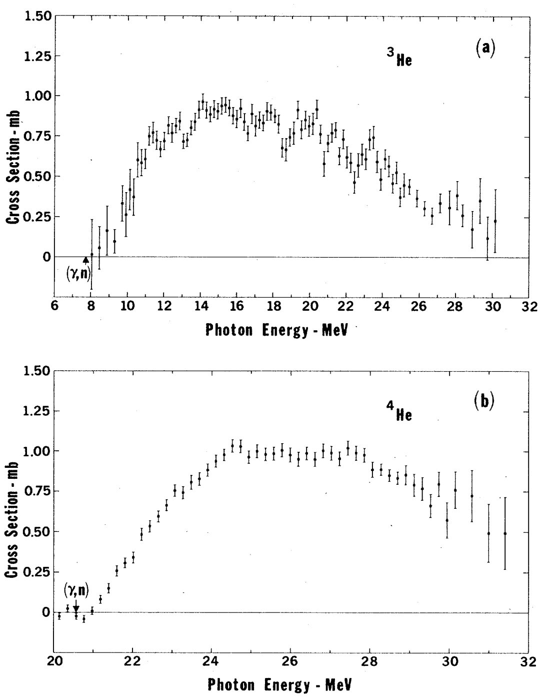

FIG. 10. (a) Photoneutron cross section for ^{3}He (Livermore). (b) Photoneutron cross section for ^{4}He (Livermore). The threshold energies, indicated by the arrows in all the cross-section figures, are taken from Wapstra and Gove (1971)

surements performed either at Saclay or at Livermore, and hence are not illustrated here. The results of these measurements are included in the tables, however, and in the discussion below.

Unfortunately, almost no (γ,p) cross-section data have been obtained with monoenergetic photons, which limits the information on sum rules (and in some cases, on details of the structure) for light nuclei. Even if such data existed, however, the fact that the cross sections for most light nuclei are still appreciable at 30 MeV (the upper limit of measurement in most cases) would preclude deriving sum-rule systematics for these nuclei. Total photon absorption cross-section measurements of the kind performed by Ziegler and his collaborators at Mainz (Ahrens *et al.*, 1973) are needed for this information.

A. Photoneutron cross-section data

The periodic table shown in Fig. 9 is marked to show the nuclei for which giant-resonance cross-section data are presented in this survey, and at which laboratories the data were taken. Sample cross-section data are shown, in a uniform format, in Figs. 10–35, in order of increasing mass number. The top (and sometimes only) data plot for each nucleus is the total photoneutron cross section

$$\sigma(\gamma,\text{total}) = \sigma[(\gamma,n) + (\gamma,pn) + (\gamma,2n) + (\gamma,p2n) + (\gamma,3n) + \cdots];$$

below it, where appropriate, are the single photoneutron cross section

$$\sigma(\gamma,1n) = \sigma[(\gamma,n) + (\gamma,pn)],$$

the double photoneutron cross section $\sigma[(\gamma,2n) + (\gamma,p2n)]$, and the triple photoneutron cross section $\sigma(\gamma,3n)$. Most of the total photoneutron data plots for medium and heavy nuclei ($A > 50$) have Lorentz-curve fits superposed. Some of the data plots for light nuclei have curves drawn to guide the eye. For the case of ^{12}C, the plot of the Pennsylvania data was taken from the original article (Lochstet and Stephens, 1966).

Table I contains the experimental parameters and the integrated cross sections: the second column gives the isotopic purity of the sample used in the measurement; the third column gives the type of neutron detector used; the fourth column gives the photon energy resolution (where a range of resolution is given, the smaller value refers to the resolution at the lowest energy at which data were taken and the larger value at the highest); the sixth through ninth columns give the unweighted integrated cross sections

$$\int_{E_{\text{thr}}(\gamma,n)}^{E_{\gamma\max}} \sigma(E)dE$$

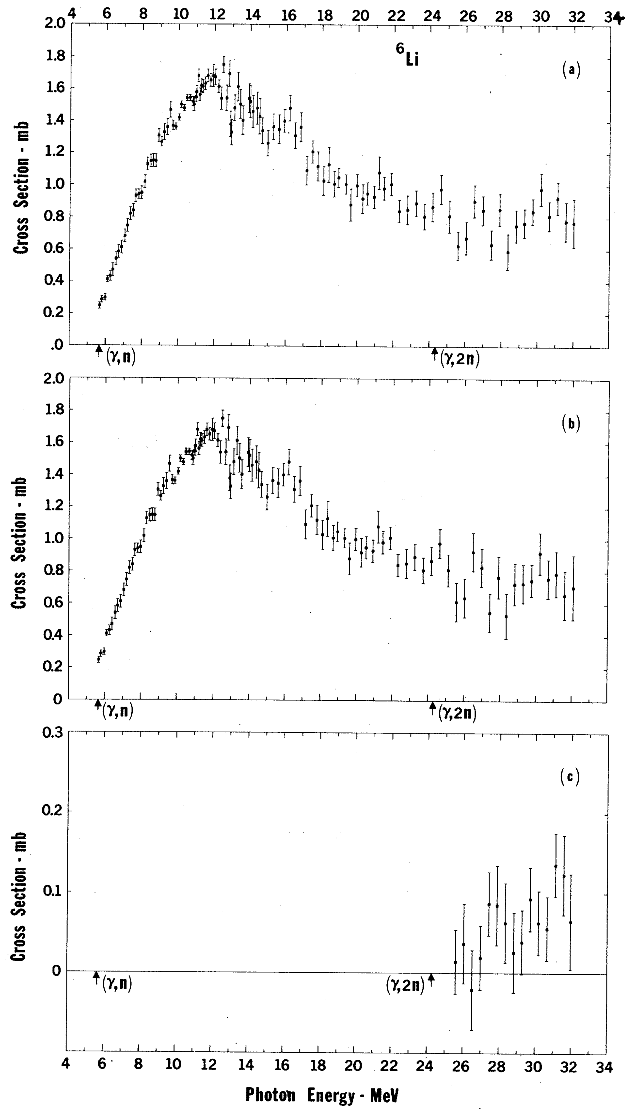

FIG. 11. Photoneutron cross sections for ^{6}Li. (a) Total; (b) single; (c) double (Livermore).

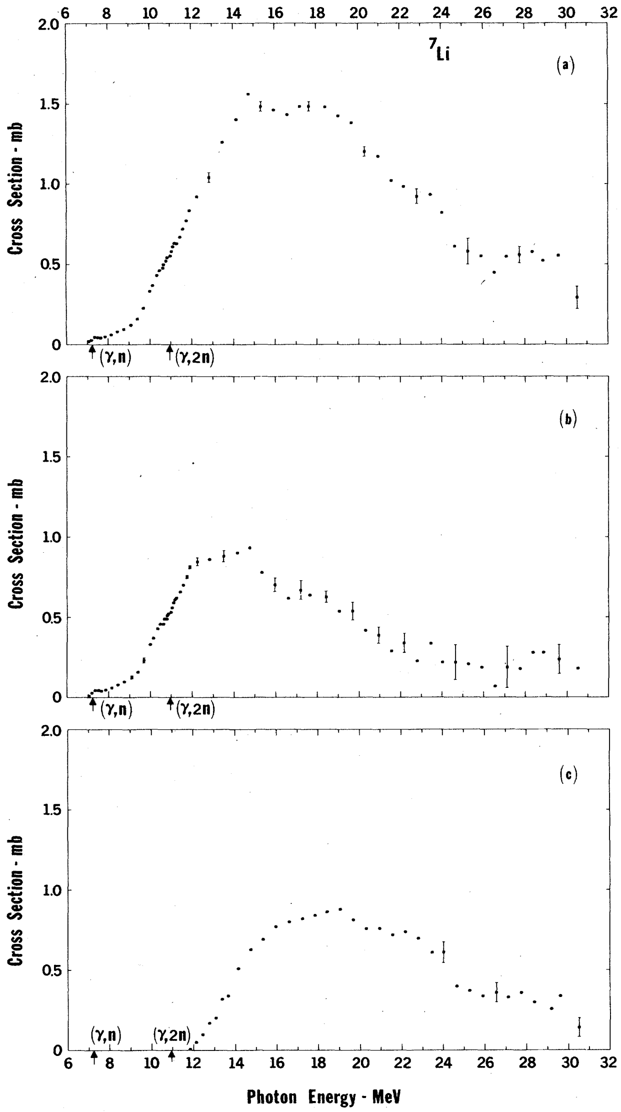

FIG. 12. Photoneutron cross sections for ^{7}Li. (a) Total; (b) single; (c) double (Livermore).

for the total, single, double, and triple photoneutron cross sections, respectively; and the tenth and eleventh columns give the energy-weighted moments of the integrated total photoneutron cross sections

$$\sigma_{-1} = \int[\sigma(E)/E]dE \quad \text{and} \quad \sigma_{-2} = \int[\sigma(E)/E^2]dE,$$

respectively, with the same limits of integration.

Table II gives the photoneutron cross sections obtained for single photon energies (below the giant resonance) by Donahue and collaborators (Welsh and Donahue, 1961; Green and Donahue, 1964; Hurst and Donahue, 1967) using neutron-capture γ rays as the source of radiation. In general, the agreement between the cross-section values for medium and heavy nuclei listed in Table II and the annihilation-photon results is satisfactory. However, since the neutron-capture γ-ray lines are sharp and the nuclear levels in the threshold region do not overlap strongly, any single entry in Table II might be appreciably larger (smaller) than the corresponding annihilation-photon result if the (n,γ) photon energy matches a narrow peak (valley) in the threshold photoneutron cross section.

Comments on individual nuclei follow. For references to recent or relevant bremsstrahlung data for comparison purposes, see Berman (1974b). In general, while the bremsstrahlung results usually are not seriously different in magnitude and overall shape from the monoenergetic-photon results, they frequently differ considerably with regard to structure in the cross sections; this is especially the case for energies above the peak of the giant resonance, where the results of unfolding slowly-rising yield curves become increasingly less accurate.

^{3}*He* [Livermore, Fig. 10(a)]. This experiment was performed with a liquid sample and the neutron detector used by Kelly *et al.* for the polarized holmium experiment (Sec. III.B). The detector geometry was such that the fore–aft photoneutron asymmetry could be measured as well. Sharp structures (1 to 2 MeV wide), unexpected theoretically, possibly are indicated at several energies between 11.5 and 23.5 MeV.

^{4}*He* [Livermore, Fig. 10(b)]. This measurement also was performed with a liquid sample, with the same experimental arrangement as for ^{3}He. The shape of the cross section, together with the fore–aft asymmetry data, show that there are two broad peaks, at 24.7 MeV (photoneutrons forward) and 27.4 MeV (photoneutrons backward). The magnitude of the peak cross section ($\sim$1 mb), however, is controversial, and might be incorrect (see Berman *et al.*, 1972, Irish *et al.*, 1973, Webb *et al.*, 1973, and Dodge and Murphy, 1972).

^{6}*Li* (Livermore, Fig. 11). Since the ^{6}Li sample absorbed the photoneutrons strongly, special precautions were taken (Berman *et al.*, 1965). The ring-ratio data show a monotonic increase of average neutron energy with increasing photon energy (see Shakin and Weiss, 1973). The $(\gamma,2n)$ cross section is very small. It should be noted that the single photoneutron cross section for ^{6}Li includes the (γ,p) channel, since ^{5}He is unstable; this means that the only major reaction channel not measured is $^6\text{Li}(\gamma,t)^3\text{He}$.

^{7}*Li* (Livermore, Fig. 12). The $(\gamma,2n)$ cross section is very

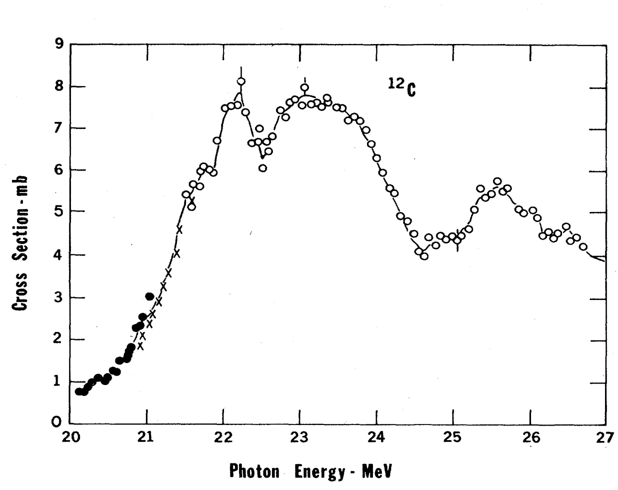

FIG. 13. Photoneutron cross section for ^{12}C (Pennsylvania).

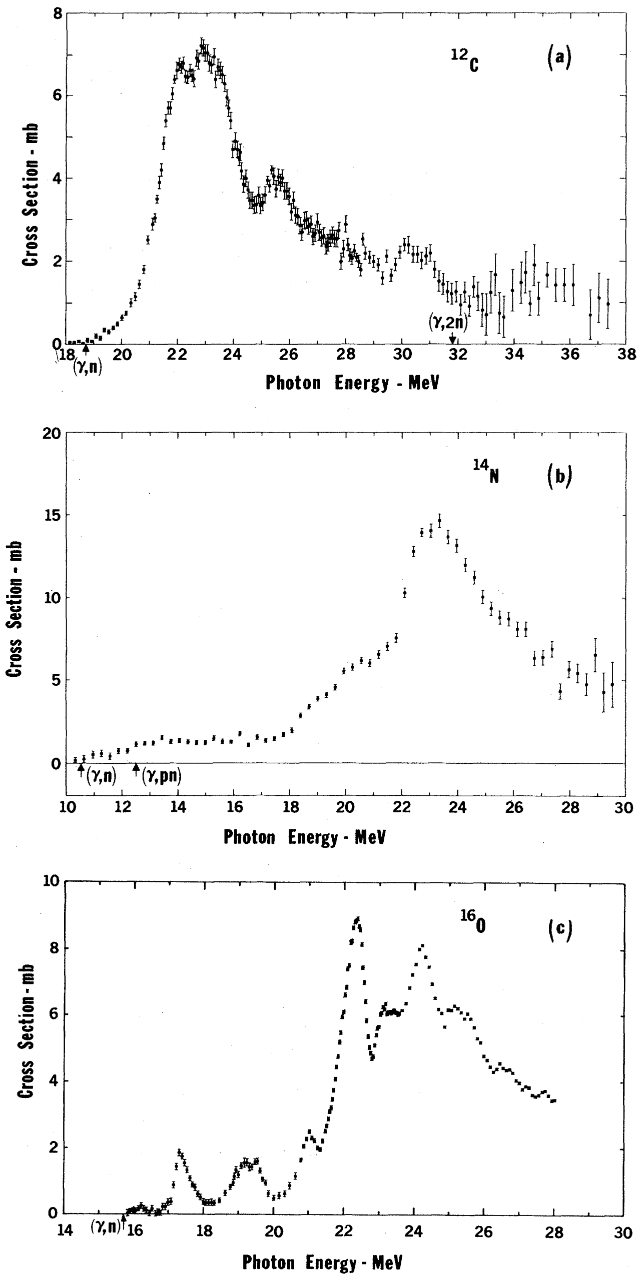

FIG. 14. (a) Photoneutron cross section for ^{12}C (Livermore). (b) Photoneutron cross section for ^{14}N (Livermore). (c) Photoneutron cross section for ^{16}O (Livermore).

large, comprising half of the integrated total cross section up to 31 MeV.

^{12}C (3 laboratories). The early Saclay data of Miller *et al.* (Miller *et al.*, 1966) agree with the Livermore data both in magnitude and in the position of the (gross) structure. The Livermore data [Fig. 14(a)] cover the widest energy range, and include weak evidence for a broad peak at 35.2 MeV. The ring-ratio data show that nearly all (83%) of the photoneutrons from the giant resonance of ^{12}C leave the residual ^{11}C nucleus in its ground state. The superior resolution of the Pennsylvania data (Fig. 13) brings out an additional peak just below 22 MeV and hints at several others at higher energies; these and more were confirmed by a recent Livermore measurement (Berman *et al.*, 1973c) with ~70-keV resolution.

^{14}N [Livermore, Fig. 14(b)]. From this $\sigma[(\gamma,n)+(\gamma,pn)]$ measurement and $\sigma(\gamma,n)$ measurements with bremsstrahlung (King *et al.*, 1960; Gellie *et al.*, 1972), it is clear that about 80% of this cross section is comprised of (γ,pn) reactions. Since the ^{14}N(γ,p) cross section also is small (Baglin *et al.*, 1971), $\sigma[(\gamma,n)+(\gamma,pn)]$ represents about 75% of the total photon absorption cross section.

^{16}O (Livermore and Saclay). The Livermore cross-section data [Fig. 14(c)] above 20.7 MeV have statistics as good as 1%. This was done to bring out all the structure possible with ~250-keV resolution, and to lay the basis for the $(\gamma,n\gamma')$ and $(\gamma,x\gamma')$ experiment of Caldwell *et al.* (Sec. III.B). The old Saclay data agree in magnitude and structure. Recent Saclay data (Bergère *et al.*, 1973) appear to have somewhat better resolution, extend to higher energies (up to 37 MeV), and include a moderate (γ,pn) contribution above 27 MeV. Recent Livermore data (Phillips *et al.*, 1973) show that the 17.3-MeV peak is fragmented into several substructures.

^{23}Na, ^{25}Mg (Livermore); ^{19}F, ^{31}P, ^{39}K [recent Saclay (Bergère *et al.*, 1973)]; ^{27}Al (both). These odd-mass *s*-*d*-shell

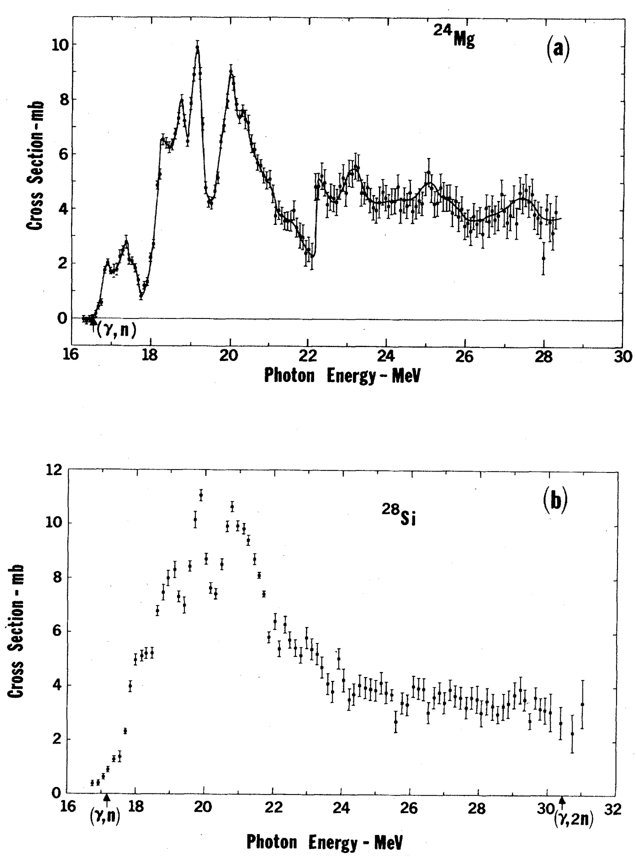

FIG. 15. (a) Photoneutron cross section for ^{24}Mg (Livermore). The curve is drawn to guide the eye. (b) Photoneutron cross section for ^{28}Si (Livermore).

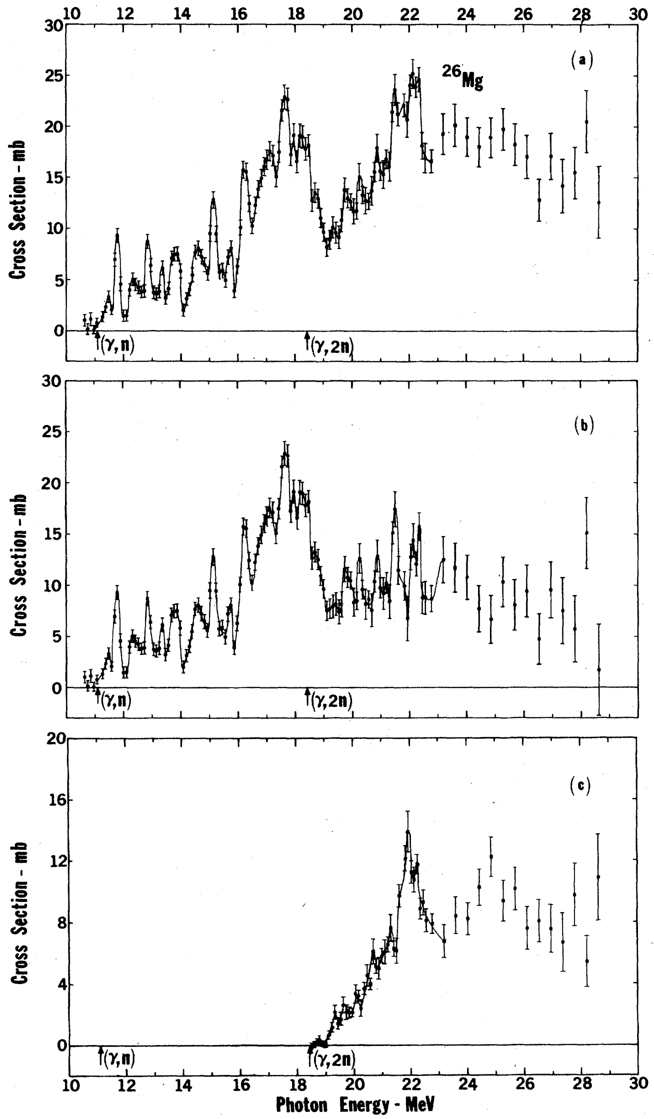

FIG. 16. Photoneutron cross sections for ^{26}Mg. (a) Total; (b) single; (c) double (Livermore). The curves are drawn to guide the eye.

nuclei all show shallow or washed-out structure atop broad giant resonances, probably because the fine structure has not yet been resolved (see Sec. IV.E), and have small or negligible $(\gamma,2n)$ cross sections. Both ^{31}P and ^{39}K have sizeable (γ,pn) cross sections. The ^{27}Al results from the two laboratories agree remarkably well in both magnitude and shape. The ^{27}Al (γ,n) ^{26m}Al cross-section result of Thompson *et al.* (1965) has the same general shape as the Livermore result.

^{24}*Mg* [Livermore, Fig. 15(a)]; ^{32}*S*, ^{40}*Ca* (Saclay); ^{Nat}*Si* (both). These self-conjugate even–even nuclei show considerably more structure than nearby odd-mass nuclei, especially ^{24}Mg and ^{28}Si, whose giant-resonance cross sections look very similar. However, even these measurements were not done with fine enough resolution to see all the fine structure, at least for ^{28}Si, ^{32}S, and ^{40}Ca, as can be seen from the (γ,n_0) photoneutron time-of-flight measurements of Wu *et al.*, at Yale (1970a). The magnitude of the recent Saclay cross section for ^{Nat}Si exceeds the old Livermore one [Fig. 15(b)] by about 20%. The ^{32}S(γ,pn) cross section is appreciable above about 24 MeV.

^{26}*Mg* (Livermore, Fig. 16) and ^{40}*Ar* (recent Saclay). The ^{26}Mg cross sections, including the large $\sigma(\gamma,2n)$, show ex-

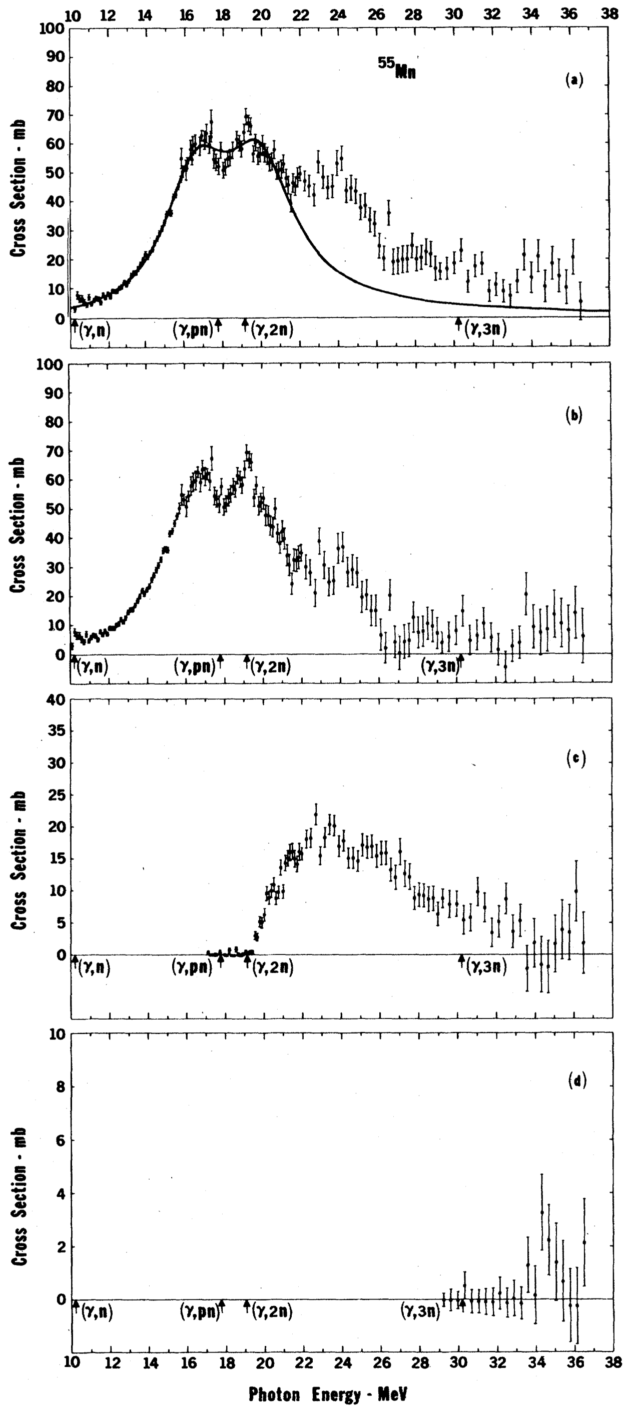

FIG. 17. Photoneutron cross sections for ^{55}Mn. (a) Total; (b) single; (c) double; (d) triple (Livermore). The curve, like the ones in Figs. 19, 21, 27–31, and 35, is a two-line Lorentz curve fitted to the cross-section data (see text).

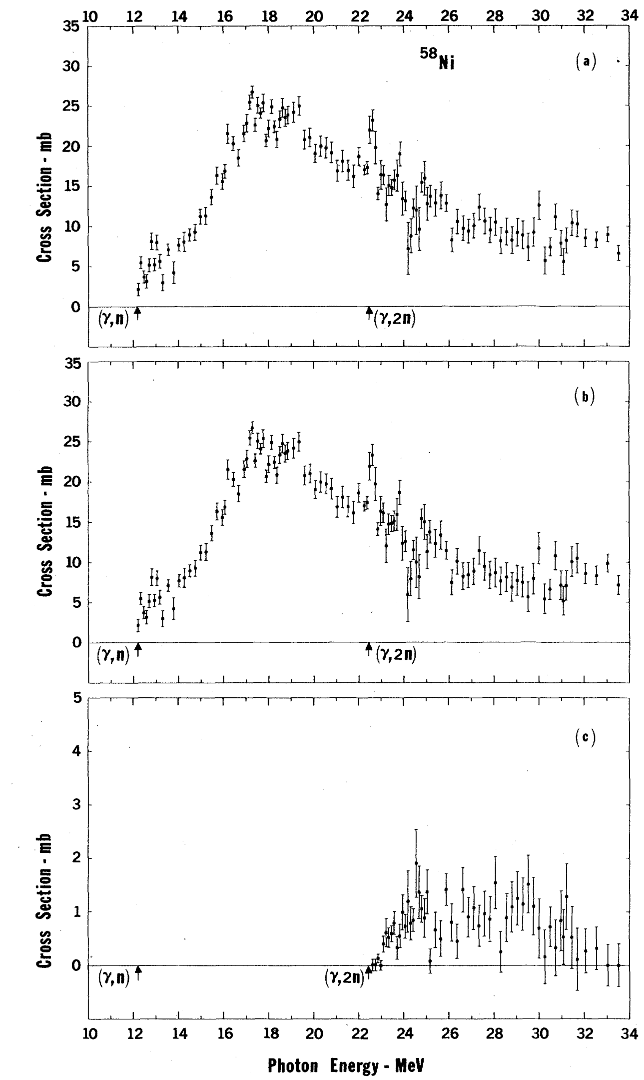

FIG. 18. Photoneutron cross sections for ^{58}Ni. (a) Total; (b) single; (c) double (Livermore).

treme fragmentation of the giant resonance. Moreover, the main strength is divided into two clumps, centered at about 17.5 and 22 MeV (see Sec. IV.F). The Saclay measurement of argon, using a gaseous sample, also shows a large $(\gamma,2n)$ cross section.

^{51}V (Livermore and recent Saclay). The total photoneutron cross section for ^{51}V clearly shows evidence for at least two broad peaks in the giant resonance. The recent Saclay data agree in magnitude with the Livermore total cross section results, but indicate a somewhat larger $\sigma(\gamma,1n)$ and a somewhat smaller $\sigma(\gamma,2n)$ above 23 MeV. This pattern will be seen to be fairly common when comparing the results of the two laboratories, and no doubt has its origin in the complex interplay between detector efficiencies and backgrounds referred to in Sec. II.A, combined with the (larger) overall scale uncertainty arising from the photon flux calibrations.

^{55}Mn, ^{58}Ni, ^{59}Co, ^{60}Ni (new Livermore). The lines shown in Figs. 17(a) and 19(a) are the sums of two noninterfering Lorentz curves. The total cross sections for ^{55}Mn [Fig. 17(a)] and ^{59}Co clearly show a third major hump, on the higher-energy side of the giant resonance. The total photoneutron cross section for ^{58}Ni (Fig. 18) is remarkably small (which is the reason a nickel collimator is used in the Livermore experimental setup), owing to the fact that the ^{58}Ni(γ,p) cross section is very large (see Sec. IV.F); and even compared to the small $(\gamma,1n)$ cross section, the $(\gamma,2n)$ cross section is very small.

^{63}Cu (Livermore and General Atomic). The old Livermore ^{63}Cu data show evidence for a third hump at about 23 MeV, which does not appear in the General Atomic ^{63}Cu$(\gamma,n)^{62}$Cu data, probably implying that this hump is in the (γ,pn) cross section (see Sund *et al.*, 1968). A comparison between the two sets of data is shown in Fig. 20.

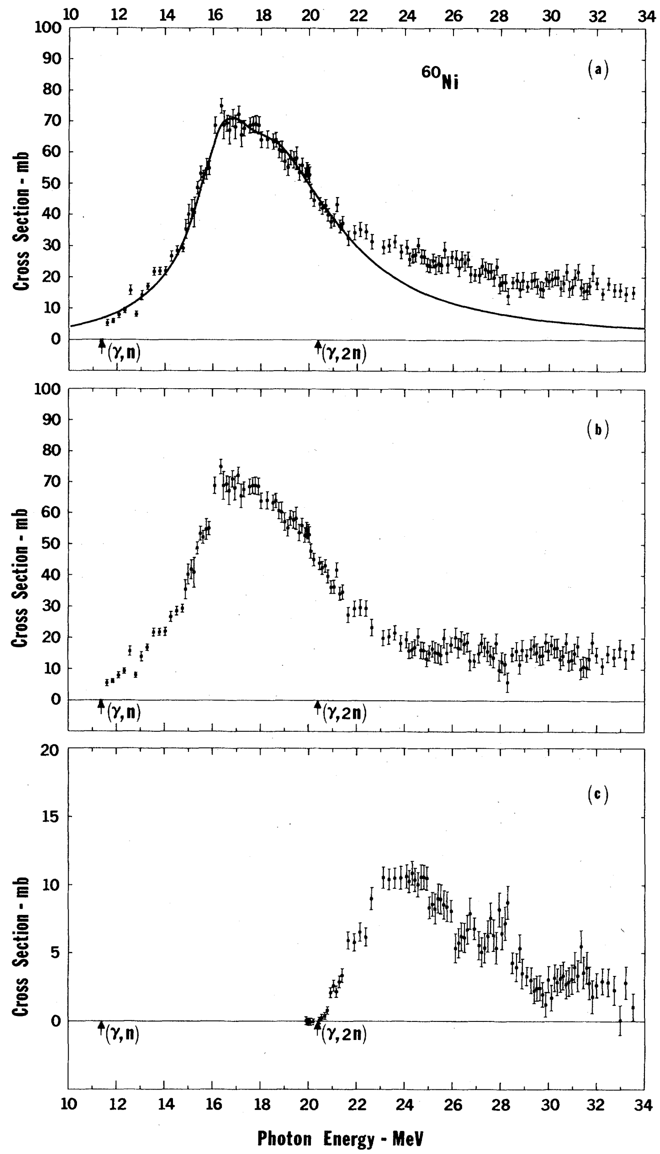

FIG. 19. Photoneutron cross sections for ^{60}Ni. (a) Total; (b) single; (c) double (Livermore).

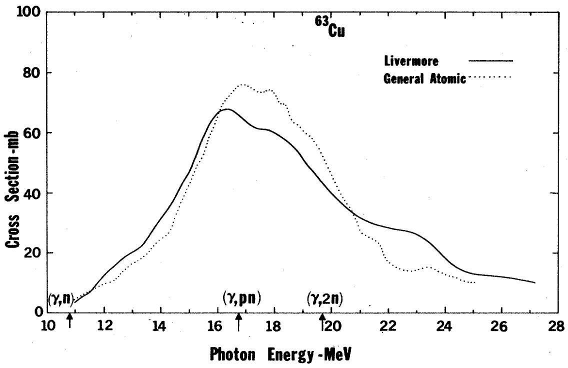

FIG. 20. Comparison of the ^{63}Cu[$(\gamma,n)+(\gamma,pn)$] cross section obtained at Livermore with the ^{63}Cu(γ,n) cross section obtained at General Atomic.

^{75}As (Livermore, Fig. 21). The giant resonance for ^{75}As exhibits a broad, flat top, with no sign of the prominent structure that had been reported previously (Fielder *et al.*, 1965). A recent remeasurement at Livermore with better resolution (Berman *et al.*, 1973c) confirms this absence of prominent structure.

^{Nat}Rb, ^{Nat}Sr, ^{93}Nb (Saclay). These cross sections were measured with good enough statistics (e.g., Fig. 22) to distinguish several very small peaks (as for several other nuclei in this mass region).

^{89}Y (3 laboratories). The higher-resolution Illinois data exhibit more prominent structure on the low-energy side of the giant resonance. The Livermore ring-ratio data for this nucleus show that the average photoneutron energy rises gradually, over an 8-MeV region from the (γ,n) threshold, rather than rising abruptly from threshold like most nuclei, including all the zirconium isotopes (see Berman *et al.*, 1967).

^{90}Zr (Livermore and Saclay). The two measurements agree very well as to shape, the Saclay results being somewhat more detailed than the Livermore results. The comparison plot, Fig. 23, shows the differences.

$^{91,92,94}Zr$ (Livermore). The $(\gamma,2n)$ cross section grows dramatically as one adds neutrons to the closed shell at $N=50$ and the $(\gamma,2n)$ threshold bites into the giant resonance proper. For ^{94}Zr, the integrated $(\gamma,2n)$ cross section actually exceeds the integrated $(\gamma,1n)$ cross section. This also is the lowest-mass nucleus which manifests an appreciable $(\gamma,3n)$ cross section below 30 MeV. Figure 24 shows the broadening of the giant resonance as one adds neutrons to the $N=50$ core.

$^{92,94,96,98,100}Mo$ (recent Saclay). Recent measurements up to 28 MeV on these nuclei show that as the neutron number increases, the giant resonance gets wider, with the high-energy side remaining relatively fixed in photon energy while the low-energy side moves to lower energies (Bergère *et al.*, 1973).

^{115}In, $^{116,117,118,119,120,124}Sn$ (Livermore); $^{116,117,118,120,124}Sn$ (recent Saclay). The tin isotopes (Fig. 25) and indium constitute one of the best-studied series of neighboring nuclei in the periodic table. Moreover, the recent Saclay total cross sections, up to 22 MeV, for five of the tin isotopes (Bergère *et al.*, 1973) are in almost exact agreement with their Livermore counterparts. Figure 25 shows that for these $Z=50$ nuclei, the giant resonance does not change appreciably in width as the number of neutrons in the nucleus varies. The ring-ratio data for ^{115}In, and to a lesser extent for ^{116}Sn, show the same sort of slow rise of $\bar{E}_n$ with photon energy that was obtained for ^{89}Y.

^{127}I (Livermore and Saclay). This nucleus constitutes by far the worst case of disagreement between the two laboratories, the peak total cross section obtained at Saclay being no less than 35% higher than the one obtained at Livermore. [Still, the $(\gamma,2n)$ cross sections are in reasonable agreement.] However, both of these measurements appear to be doubtful, judging by the systematics of the giant resonance for neighboring nuclei (see Secs. IV.B and C). The best compromise probably lies rather closer to the later Saclay

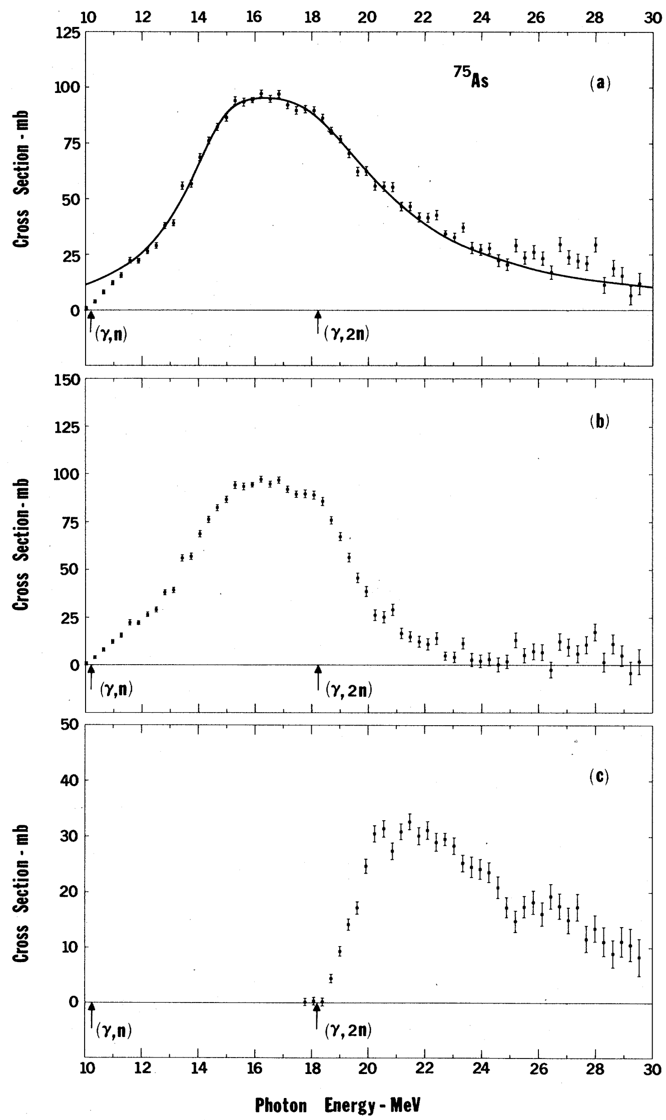

FIG. 21. Photoneutron cross sections for ^{75}As. (a) Total; (b) single; (c) double (Livermore).

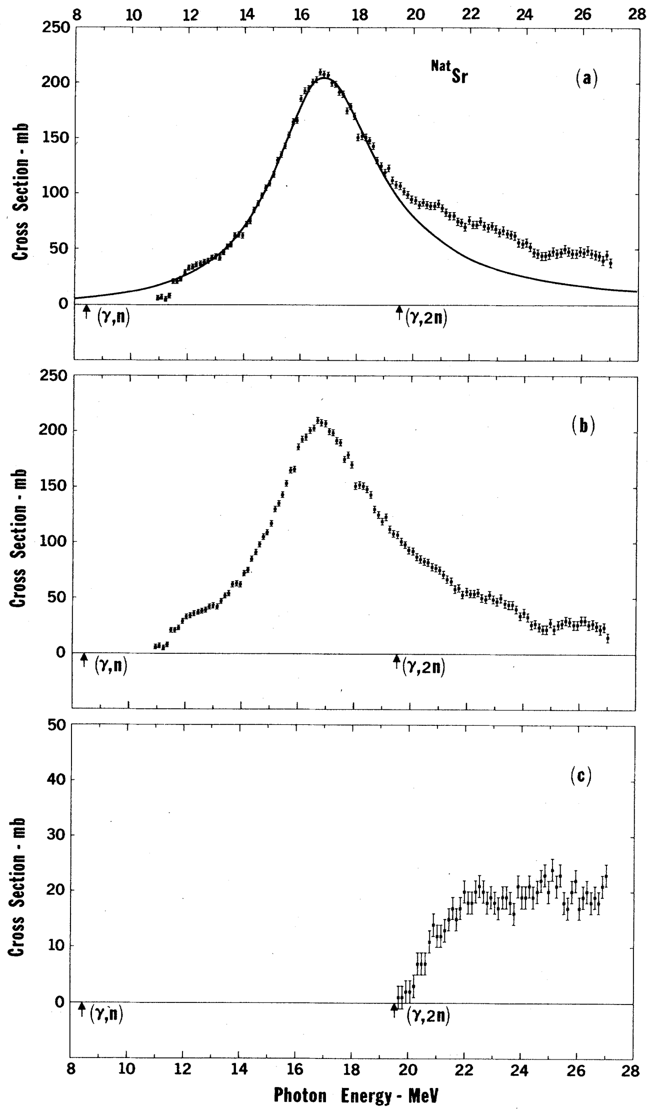

FIG. 22. Photoneutron cross sections for ^{Nat}Sr. (a) Total; (b) single; (c) double (Saclay). The curve, like the ones in Figs. 24, 25, 27, 32, and 33, is a single-line Lorentz curve fitted to the cross-section data (see text).

values than to the earlier Livermore values. This measurement should be repeated.

^{141}Pr (4 laboratories). None of the four measurements yields structure in the giant resonance anywhere near so prominent as that reported from bremsstrahlung measurements (Cook *et al.*, 1966; Cannington *et al.*, 1968); however, the very good statistics of the Saclay data bring out a number of very small peaks which would match up with the large ones of Cannington *et al.* if the Saclay data were shifted upward in energy by about 200 keV (see Bergère *et al.*, 1971). These small peaks also were seen in recent Livermore measurements (Berman *et al.*, 1973c), also about 200 keV higher in energy than the Saclay peaks. However, the most important feature shown in the comparison plot, Fig. 26, is the outstanding agreement in absolute magnitude between the four sets of data: they all are within 7% of each other, with the Saclay data being a bit larger than the rest. Such good agreement between laboratories never before has been obtained for photonuclear measurements; clearly the data for ^{141}Pr set the standard.

$^{Nat,142,143,144,145,146,148,150}Nd$ (Saclay). The data for this series of isotopes are highly variable in quality, owing chiefly to the disparate masses and purities of the samples used. This can be seen most clearly for the case of ^{143}Nd, where the 11.8% ^{144}Nd contaminant makes the $(\gamma,2n)$ cross section look as if it has two thresholds. Still, one can see, in Fig. 27, the general systematic features of the "evolution" of the giant resonance as neutrons are added to the closed-shell ($N = 82$) nucleus ^{142}Nd until the strongly deformed nucleus ^{150}Nd is reached: the giant resonance increases in width until it splits into two distinct peaks, and, like the case for the zirconium isotopes, the relative size of the $(\gamma,2n)$ cross section increases as the $(\gamma,2n)$threshold bites into the main giant-resonance strength.

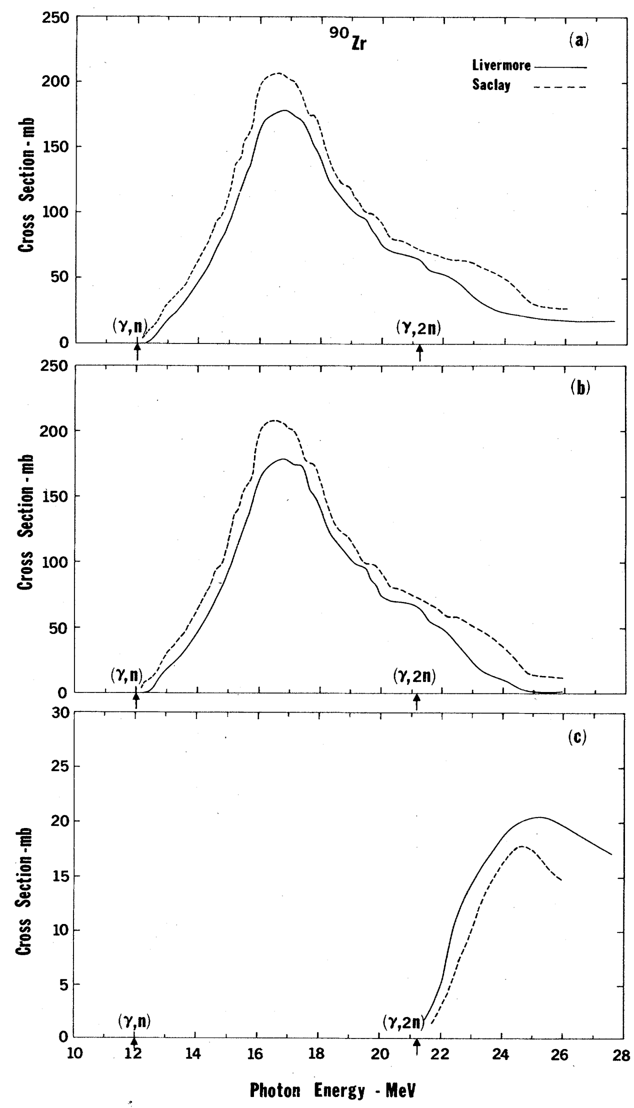

FIG. 23. Comparison of the photoneutron cross sections for ^{90}Zr obtained at Livermore and Saclay.

NatSm, NatEr (Saclay); *144,148,150,152,154Sm* (recent Saclay). A distinct peak appears at 9.5 MeV in the NatEr cross section, which might not have been expected on the grounds that this element is composed of six stable isotopes, four of which have appreciable abundances. It would be interesting to pinpoint the responsible isotope(s) by performing measurements on isotopically enriched samples. Recent Saclay data for the separated samarium isotopes (Bergère *et al.*, 1973) show an evolution of the giant resonance similar to that seen for the neodymium isotopes; ^{144,148,150}Sm are single-peaked (although ^{150}Sm is quite broad), and ^{152,154}Sm are split.

^{153}Eu, ^{160}Gd, ^{186}W (Livermore). These nuclei span the region of statically deformed nuclei; the splitting in ^{186}W is rather small. It is interesting that for the cases of ^{160}Gd (Fig. 28) and ^{186}W (Fig. 31), the higher-energy hump of the giant resonance manifests itself entirely in the $(\gamma,2n)$ cross section, so that activation measurements (Carver and Turchinetz, 1959; Carver *et al.*, 1962), from which only the (γ,n) cross sections are obtained, fail to illustrate the characteristic splitting for these deformed nuclei.

^{175}Lu (Saclay, Fig. 29). This is an excellent example of the "typical" split giant resonance for a statically deformed nucleus.

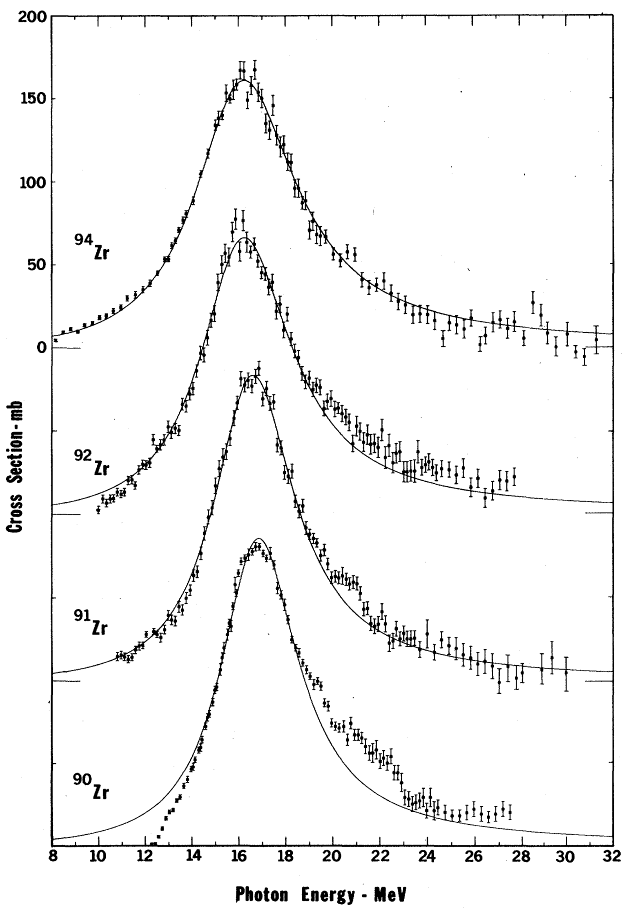

FIG. 24. Total photoneutron cross sections for the zirconium isotopes, showing the broadening of the giant resonance as one adds neutrons to a nucleus having a closed neutron shell (Livermore).

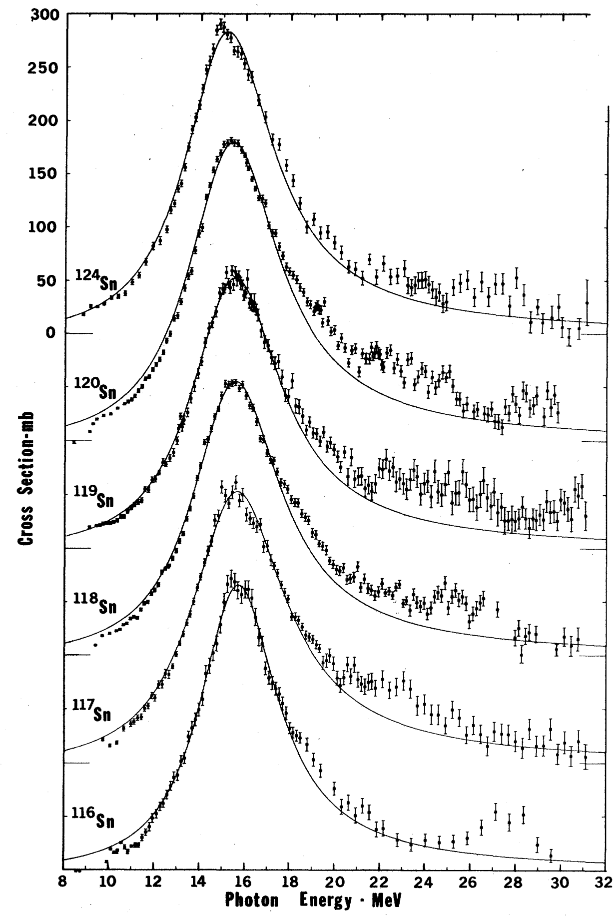

FIG. 25. Total photoneutron cross sections for the tin isotopes, showing the near-constancy of the width of the giant resonance as one adds neutrons to a nucleus having a closed proton shell (Livermore).

^{181}Ta (Livermore and Saclay). The Saclay results (Fig. 30) also include some $(\gamma,4n)$ data, up to 36.4 MeV (not shown).

^{208}Pb (3 laboratories). The Saclay results (Fig. 32) also include some $(\gamma,4n)$ data, up to 37.8 MeV (not shown). The very good statistics of the Saclay data on the lower-energy side of the giant resonance bring out structure which

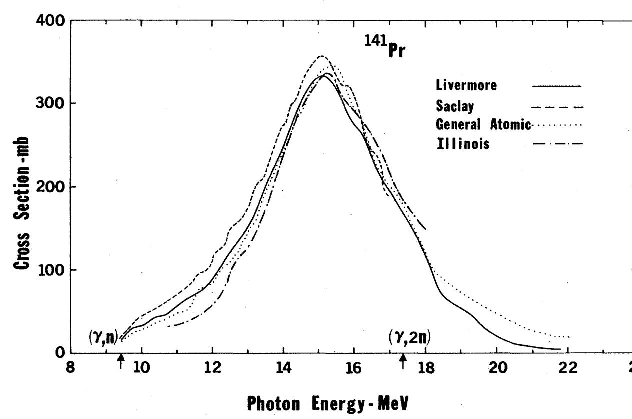

FIG. 26. Comparison of the single photoneutron cross section for ^{141}Pr obtained at Livermore, Saclay, General Atomic, and Illinois.

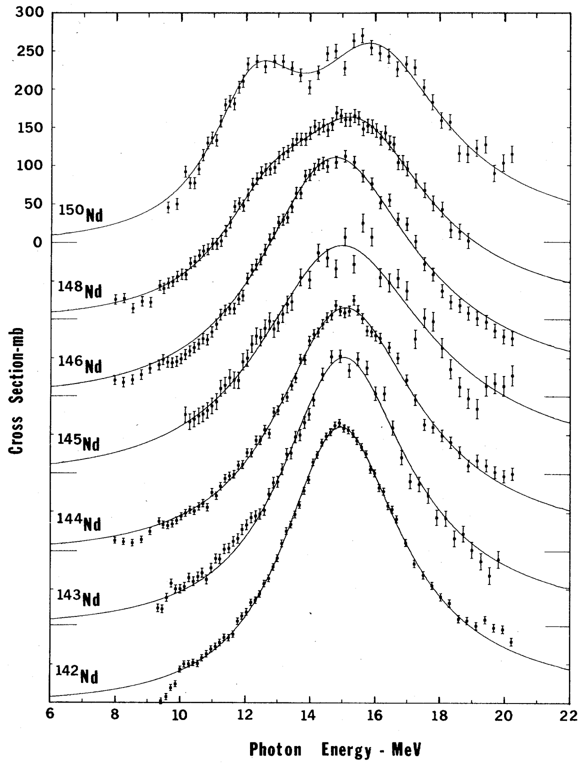

FIG. 27. Total photoneutron cross sections for the neodymium isotopes, showing the "evolution" of the giant resonance as one makes the transition from spherical to statically deformed nuclei (Saclay).

is partly corroborated by the higher-resolution Illinois results (Fig. 33).

^{232}Th, ^{237}Np, ^{238}U (Saclay). All the Saclay (γ,f) results were deduced from neutron multiplicity counting, under assumptions regarding the magnitude and dependence upon incident photon energy of $\bar{\nu}$, the average number of neutrons emitted per fission, for these nuclei (see Veyssière *et al.*, 1973); there was no direct measurement of fission events. Because the thorium and neptunium (oxide) samples were radioactive, the bias on the liquid-scintillator neutron detector had to be raised, thereby reducing the detector efficiency to 0.4 for the thorium measurement, and 0.3 for the neptunium measurement. This in turn resulted in large statistical uncertainties in the ^{237}Np and especially in the ^{232}Th data, in addition to the systematic uncertainty to be associated with any error in the choice of the linear energy dependence for $\bar{\nu}$ and the parameters involved. Nonetheless, within these limitations, the results appear to be reasonable, and constitute an elegant demonstration of the power of the neutron multiplicity-counting technique. The relative sizes of the partial cross sections vary greatly: for ^{232}Th, $\sigma(\gamma,n)$ is large, $\sigma(\gamma,2n)$ is moderate, and $\sigma(\gamma,f)$ [which includes $\sigma(\gamma,nf)$ as well] is small; for ^{237}Np, $\sigma(\gamma,n)$ is moderate, $\sigma(\gamma,2n)$ is small, and $\sigma(\gamma,f)$ is large; and for ^{238}U (Fig. 35), all are about equal (see Table I). From the ratios of partial cross sections, one can extract the ratios of neutron to fission widths Γ_n/Γ_f, which, when plotted against the fissionability parameter Z^2/A, decrease more or less exponentially, in agreement with data from neutron-induced reactions (see Veyssière *et al.*, 1973).

^{235}U (Livermore, Fig. 34). The figure for these data is taken directly from the original paper (Bowman *et al.*, 1964), since the analysis was complex and the values for the individual data points for the (γ,n) and $(\gamma,2n)$ cross sections were not available. The values given in Table I for the integrated cross sections, as well as those for other derived

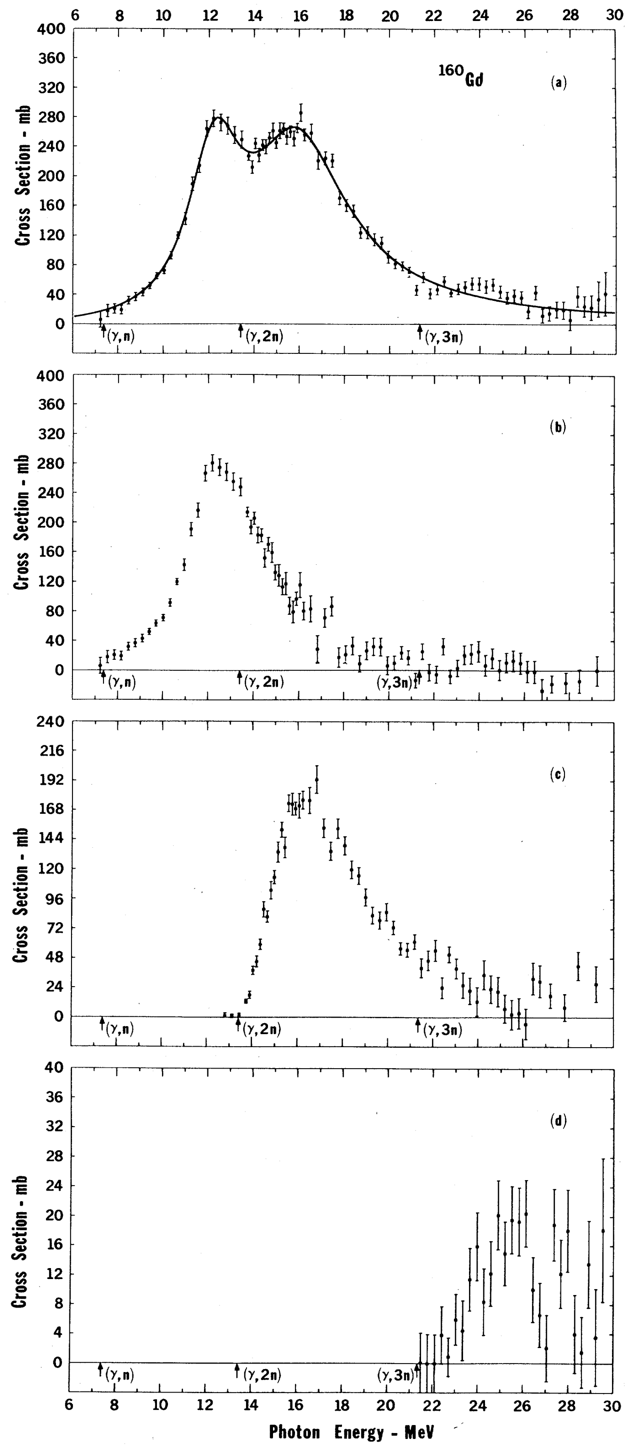

FIG. 28. Photoneutron cross sections for ^{160}Gd. (a) Total; (b) single; (c) double; (d) triple (Livermore).

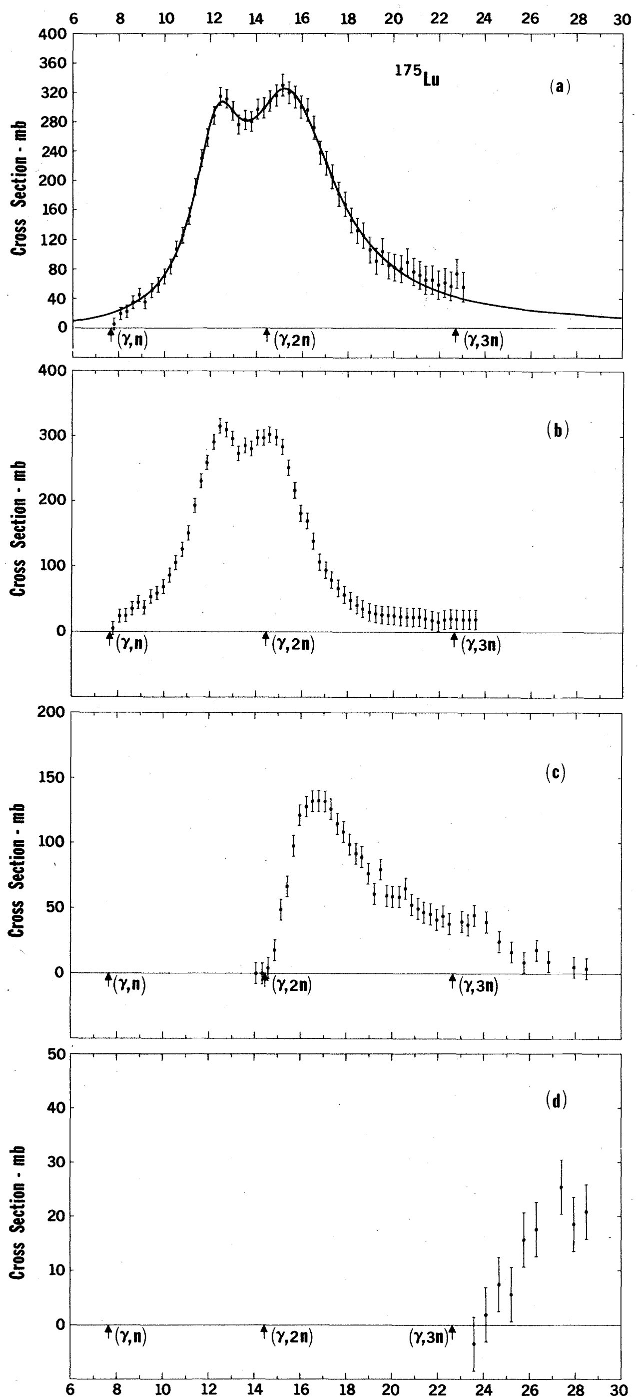

FIG. 29. Photoneutron cross sections for ^{175}Lu. (a) Total; (b) single; (c) double; (d) triple (Saclay).

parameters given in Tables III and V (below), were obtained by digitizing the curves of Fig. 34(a). The photofission measurements [Fig. 34(b)] were made directly, with the use of an ionization chamber to measure the fission fragments. The value of about 6 for Γ_n/Γ_f obtained from the $\sigma(\gamma,n)/\sigma(\gamma,f)$ ratio at 10 MeV does not follow the systematic trend of the Saclay measurements mentioned above. The bremsstrahlung measurements of $\sigma(\gamma,f)$ [the x's in Fig. 34(b)], were made with a wire spark chamber fragment detector.

B. Specialized experiments

In addition to the production of the main body of giant-resonance cross-section data presented in Sec. III.A, monoenergetic photon beams have been used to perform a variety

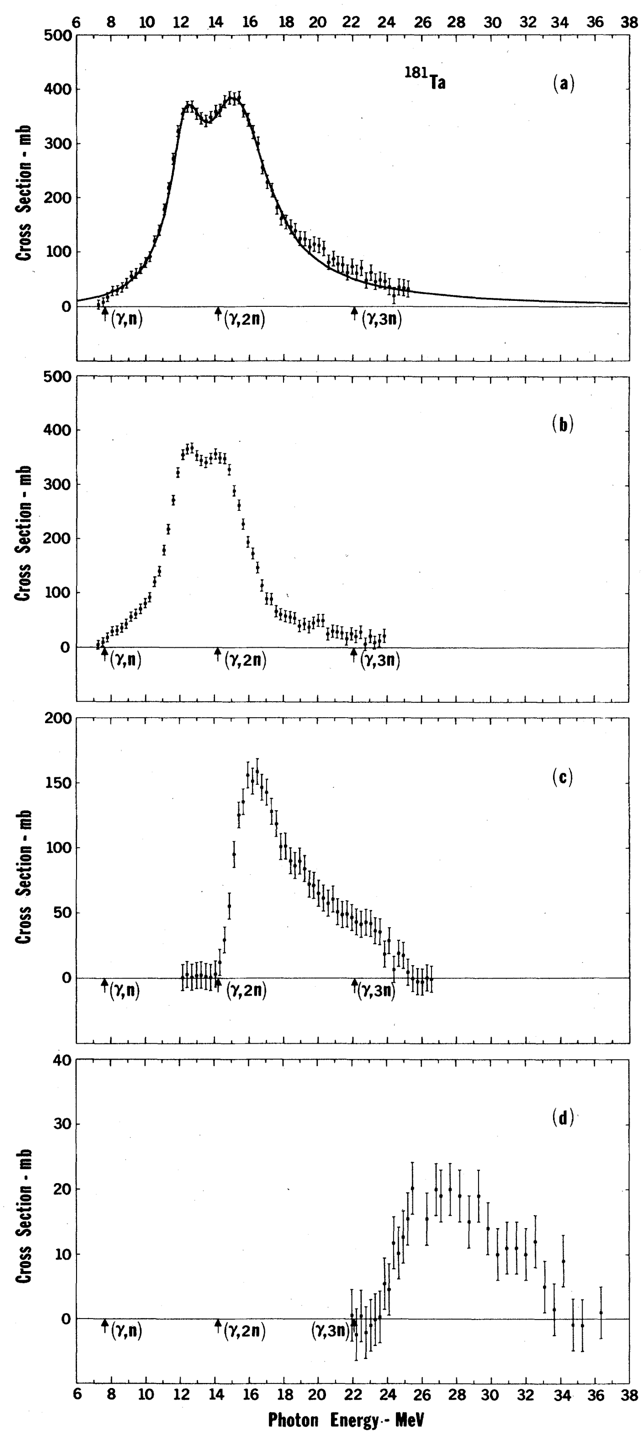

FIG. 30. Photoneutron cross sections for ^{181}Ta. (a) Total; (b) single; (c) double; (d) triple (Saclay).

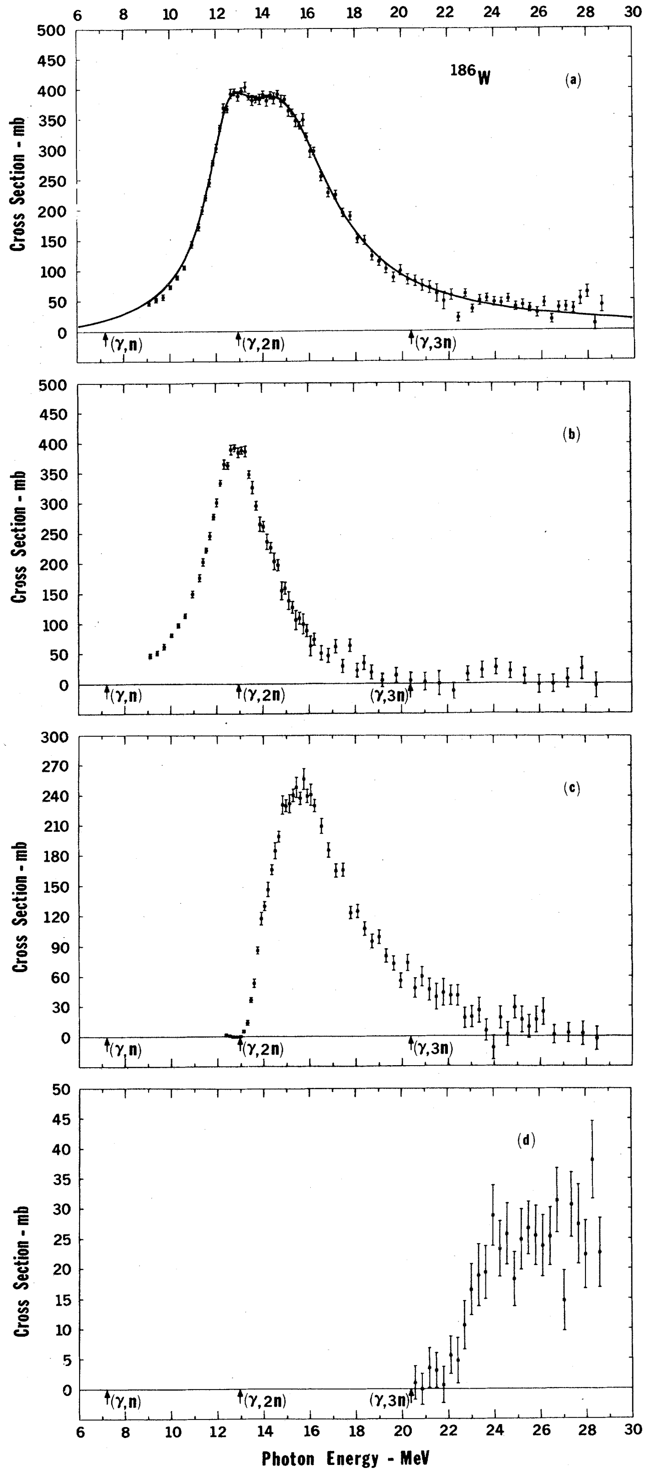

FIG. 31. Photoneutron cross sections for ^{186}W. (a) Total; (b) single; (c) double; (d) triple (Livermore).

of other experiments in the field of photonuclear reactions, some of which bear directly on the theories of the giant resonance. A number of these experiments are discussed in this section.

1. Caldwell's experiment

In order to obtain a complete picture of the giant resonance for light nuclei, it is necessary to perform measurements on all its decay modes and the branching between them, since photoneutron measurements alone, because of the low Coulomb barrier for charged-particle emission, are inadequate. In particular, the case of ^{16}O, for which nu-

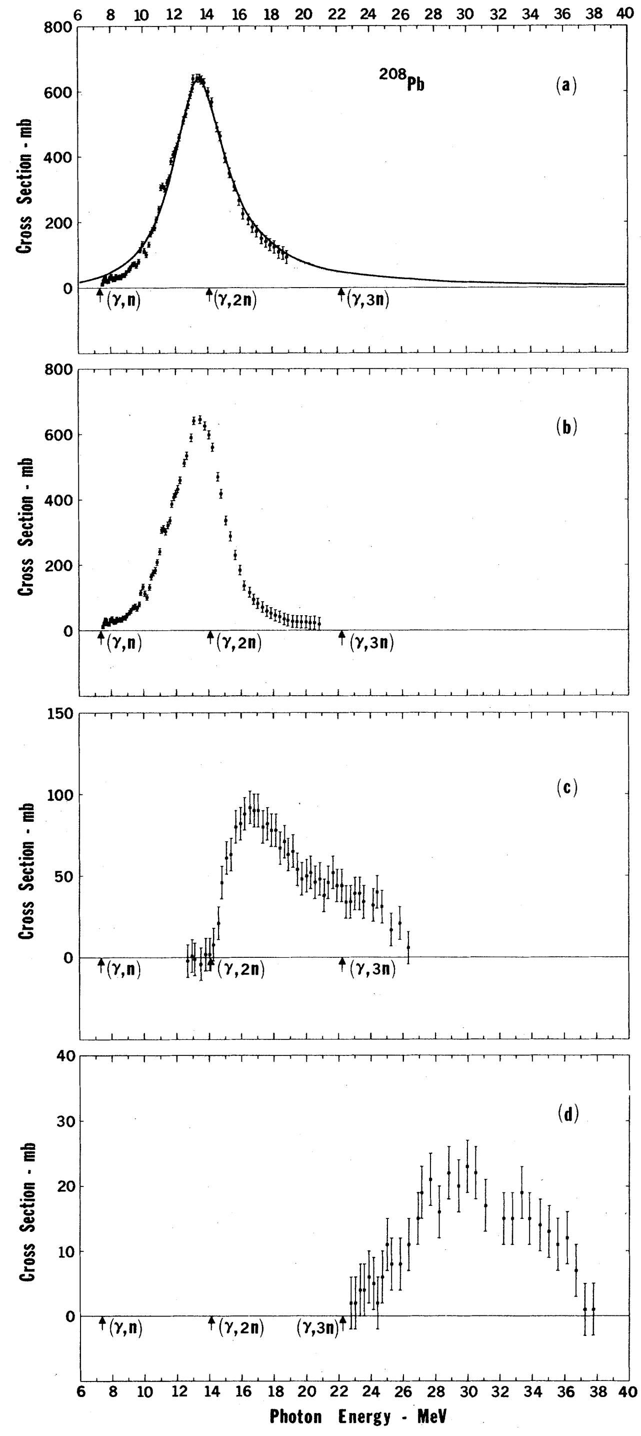

FIG. 32. Photoneutron cross sections for ^{208}Pb. (a) Total; (b) single; (c) double; (d) triple (Saclay).

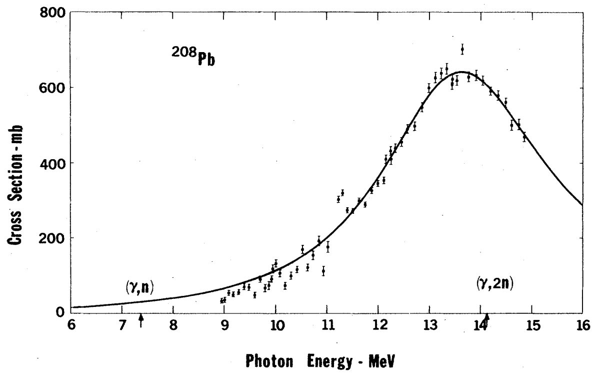

FIG. 33. Photoneutron cross section for ^{208}Pb (Illinois).

merous and extensive theoretical calculations have been performed and for which photoneutron data are available, stands out. In order to measure the branching, Caldwell *et al.* (1967a, 1967b) used a combined neutron and photon detection system.

The results for the decay channels leading to the first four excited states in ^{15}O and ^{15}N are shown in Fig. 36. Since the $^{16}O(\gamma,p_0)^{15}N$ cross section had been measured at several laboratories, both directly and by means of the inverse $^{15}N(p,\gamma_0)$ reaction (Finckh and Hegel, 1961; Dodge and Barber, 1962; Tanner *et al.*, 1964), and is relatively well known, a composite picture could be constructed for the decay of the ^{16}O giant resonance. This synthesis is shown in Fig. 37. Most of the decays can be seen to occur to the negative-parity states of the residual nuclei, as is expected from the elementary particle–hole theory. A significant fraction (16%), however, decay to positive-parity states,

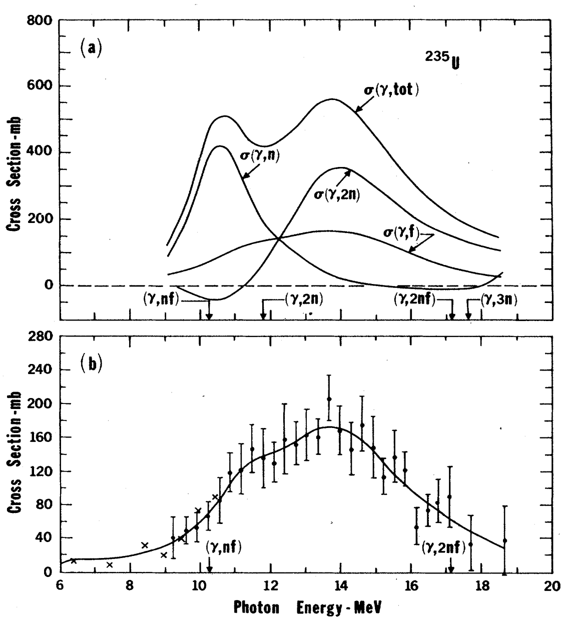

FIG. 34. Photonuclear cross sections for ^{235}U. (a) Curves in lieu of data points for all cross sections (the regions of apparent negative cross sections are an artifact of the analysis); (b) (γ,f); the curve is drawn to guide the eye; the x's are values obtained from a measurement using a bremsstrahlung beam as the source of radiation (Livermore).

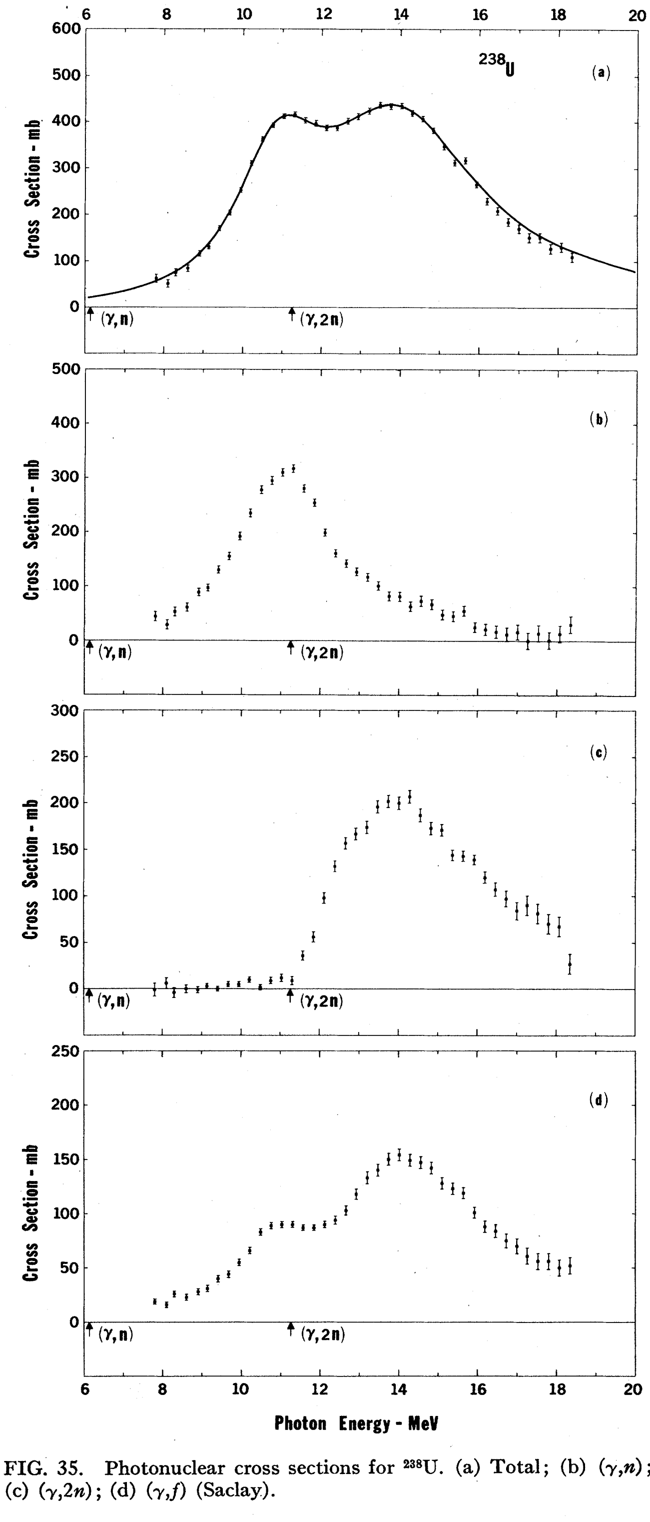

FIG. 35. Photonuclear cross sections for ^{238}U. (a) Total; (b) (γ,n); (c) $(\gamma,2n)$; (d) (γ,f) (Saclay).

thus requiring a more detailed theoretical understanding. The most impressive agreement to date with these data has been achieved by Shakin and Wang (1971, 1972), whose theoretical approach depends critically upon the inclusion of 3 particle–3 hole states in ^{16}O [but also see the eigenchannel calculations of Barrett *et al.* (1973)].

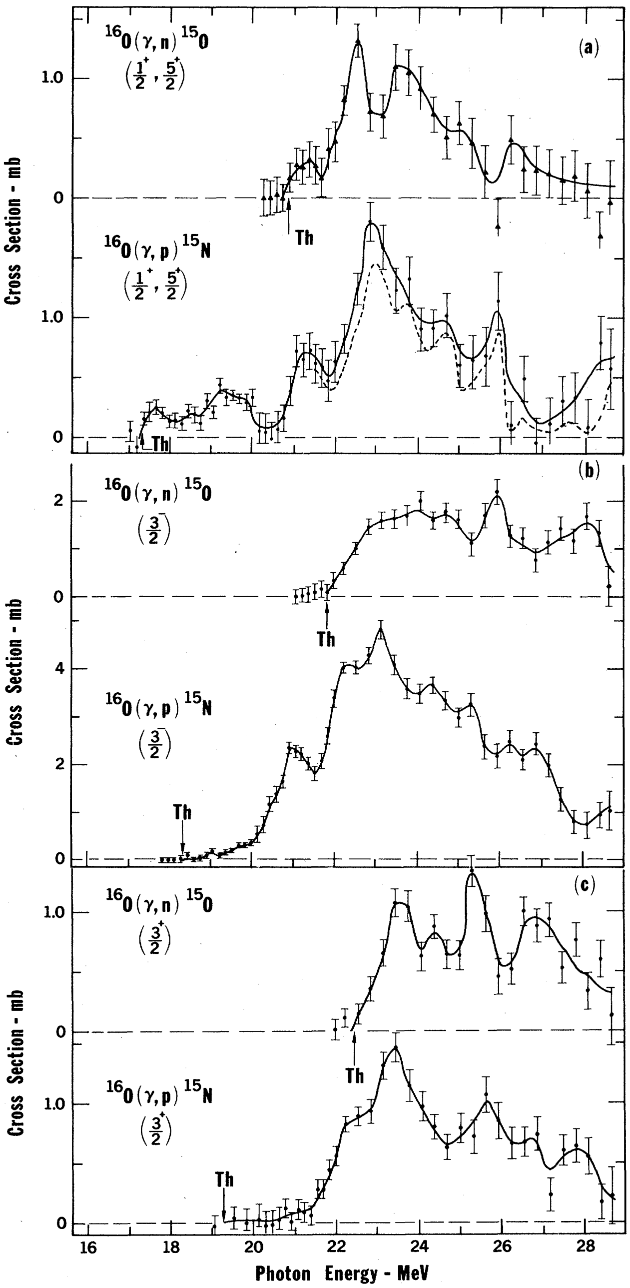

FIG. 36. ^{16}O $(\gamma,n\gamma')$ and $(\gamma,p\gamma')$ mirror-level final-state cross sections. (a) Top: ^{15}O($\frac{1}{2}^+$, $\frac{5}{2}^+$, unresolved) 5.2-MeV final-state cross section; bottom: ^{15}N($\frac{1}{2}^+$, $\frac{5}{2}^+$, unresolved) 5.3-MeV final-state cross section. The dashed line shows the effect of subtracting the 9.22-MeV level cascades. (b) Top: ^{15}O($\frac{3}{2}^-$) 6.18-MeV final-state cross section; bottom: ^{15}N($\frac{3}{2}^-$) 6.33-MeV final-state cross section. (c) Top: ^{15}O($\frac{3}{2}^+$) 6.79-MeV final-state cross section; bottom: ^{15}N($\frac{3}{2}^+$) 7.30-MeV final-state cross section (from Caldwell *et al.*, 1967a).

2. Kelly's experiment

All collective theories of the giant resonance in deformed nuclei predict that it is split into two components (for spheroidal nuclei), corresponding to dipole vibrations parallel and perpendicular to the axis of nuclear symmetry. Furthermore, the degree of splitting, or asymmetry, of the giant resonance is predicted to have a direct relation to the

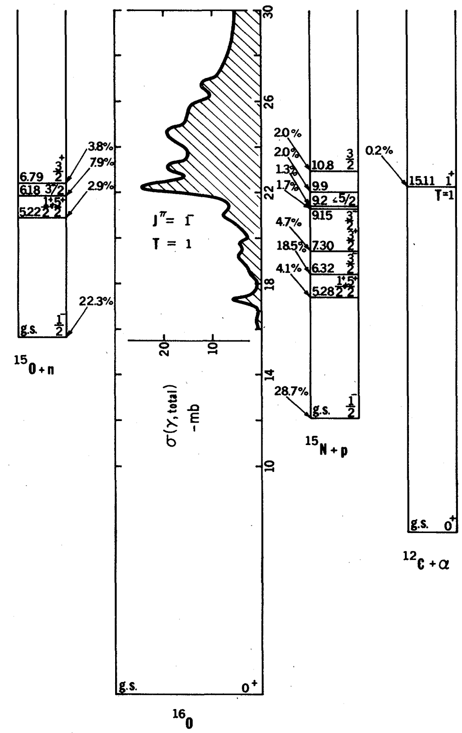

FIG. 37. Decay of the giant resonance of ^{16}O. The branching ratios given are for the total photoabsorption strength integrated up to 28.7 MeV (data taken from Caldwell *et al.*, 1967a).

size of the nuclear deformation. In order to test these predictions, Kelly *et al.* (1968, 1969) used cryogenic techniques to polarize a sample of ^{165}Ho metal composed of nine single crystals whose total mass was 50 g. The sample was mounted on a rotatable and removable assembly inside a 4π BF_3-tube-and-polyethylene neutron detector (the one subsequently used for the ^{3}He and ^{4}He experiments described in Sec. III.A). The sample polarization was measured *in situ* by activating one of the holmium crystals in a reactor and observing the asymmetry of the decay γ rays from ^{166m}Ho with a Ge(Li) detector. The degree of polarization achieved,

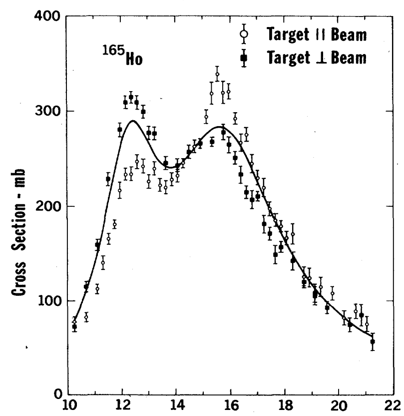

FIG. 38. Total photoneutron cross section for polarized ^{165}Ho, for the ^{165}Ho sample aligned either parallel or perpendicular to the direction of the incident (unpolarized) photon beam. The solid line is the two-component Lorentz curve fitted to the cross-section data for the unpolarized sample (from Kelly *et al.*, 1969).

at 0.13°K in a 15-kOe applied magnetic field, was ~70% of the theoretical maximum (alignment parameter ~0.42). Measurements were made of the photoneutron cross sections from 10 to 21 MeV with the ^{165}Ho sample aligned both along and transverse to the direction of the photon beam, as well as under the same experimental conditions except that the sample was allowed to warm up to 4.2°K and as a consequence was unpolarized.

The results are shown in Fig. 38. The solid line is a two-line Lorentz-curve fit to the warm (unpolarized) data, which matches the more detailed ^{165}Ho cross-section results of Berman *et al.* (1969b). The open data points correspond to the sample alignment parallel to the beam direction (for which dipole vibrations are possible only along the short axes of the prolate nucleus for 100% alignment) and the solid points perpendicular to the beam direction (for which dipole vibrations along the long and short axes are equally probable for 100% alignment). The effect of the polarization is in the direction predicted. The intrinsic cross sections extracted from these data, their asymmetry, and their comparison with theoretical models are discussed in Sec. IV.D. An integral-yield measurement on aligned ^{165}Ho using bremsstrahlung had been performed previously by Ambler *et al.* (1965); they, too, observed the asymmetry effect in the direction expected.

3. Photon scattering

Monoenergetic-photon techniques do not enjoy the same qualitative advantage over bremsstrahlung methods for the study of photon-scattering cross sections as they do for photoneutron cross sections. Since the elastic scattering cross section invariably dominates over the inelastic, a measurement of the scattered photon spectrum is all that is necessary to achieve moderate precision if one knows the approximate shape of the incident bremsstrahlung spectrum (well below its end point). Therefore, photon-difference unfolding procedures are not necessary, and only experimental considerations, such as background levels and the like, dictate the choice of technique. Here, monoenergetic photon beams do have one advantage: since measurements of the scattered radiation normally are made during the beam burst from an electron accelerator, one has to contend with the background from atomic (Compton) scattering, which is several orders of magnitude more intense than the nuclear scattering, and one is obviously better off if the only photons being scattered are at the desired energy. Still, these measurements are difficult, especially with short-duty-cycle accelerators, and particularly in the (continuum) giant-resonance region, so that few experiments have been performed to date; only the great potential importance of the results makes the required effort worthwhile.

Early measurements of (γ,γ) cross sections in the giant-resonance region were made at Saclay (Miller *et al.*, 1961; de Botton *et al.*, 1966) on lead and bismuth, using annihilation photons, and at Illinois (O'Connell *et al.*, 1962; Tipler *et al.*, 1963) on gold and holmium, using tagged bremsstrahlung. Subsequent measurements of the same sort, at photon energies below the (γ,n) thresholds and with better energy resolution, were carried out at Illinois on $^{\mathrm{Nat}}$Zr, $^{\mathrm{Nat}}$Sn, $^{\mathrm{Nat}}$Pb, ^{206}Pb, and ^{209}Bi (Axel *et al.*, 1963). In this work, strong, narrow peaks were found in the (γ,γ) cross section

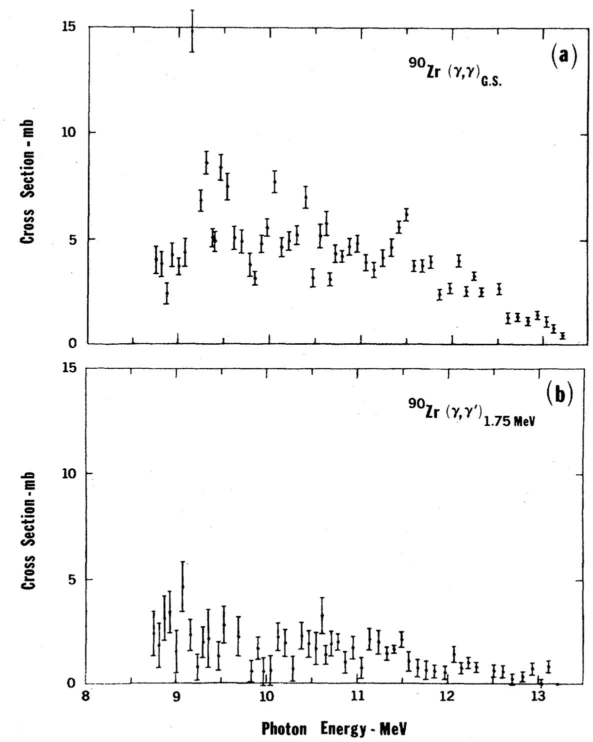

FIG. 39. Low-energy photon-scattering cross sections for ^{90}Zr. (a) Elastic scattering; (b) Inelastic scattering to the 1.75-MeV state of ^{90}Zr (from Ganek, 1972).

for ^{208}Pb at 6.72, 7.03, and 7.29 MeV. More recently, the Illinois group has published measurements on $^{\mathrm{Nat}}$Zr and $^{\mathrm{Nat}}$Sn (Axel *et al.*, 1970). The cross section for $^{\mathrm{Nat}}$Sn has been computed as if only the even-A tin isotopes contribute, since the odd-A tin isotopes have lower (γ,n) thresholds. Also, Kuehne *et al.* (1967) have measured the photon scattering from the 15.11-MeV level in ^{12}C and from four other states near 10 MeV in ^{24}Mg, ^{26}Mg, and ^{28}Si. Finally, new results have been acquired at Illinois for both elastic and inelastic photon scattering on $^{\mathrm{Nat}}$Zr (Ganek, 1972) and $^{\mathrm{Nat}}$Sr (Datta and Allen, 1973). For the zirconium case, only ^{90}Zr (51.4% abundant in $^{\mathrm{Nat}}$Zr; $E_{\mathrm{thr}}(\gamma,n) = 11.98$ MeV) participates in the scattering since the (γ,n) thresholds for all the other zirconium isotopes lie lower in energy; consequently, it was possible, with better energy resolution for detection of the scattered photons, to separate the elastic scattering cross section [Fig. 39(a)] from the inelastic cross section which leaves ^{90}Zr in its first excited state at 1.75 MeV [Fig. 39(b)]. A similar argument applies for the strontium case, where only ^{88}Sr (82.6% abundant in $^{\mathrm{Nat}}$Sr) participates in the scattering. Both elastic and inelastic scattering to the first excited state of ^{88}Sr at 1.84 MeV were measured, and structure similar to that for ^{90}Zr was observed.

These low-energy scattering results are included here because they were obtained with the same tagged-bremsstrahlung facility as the giant-resonance data from Illinois and have not been reviewed previously. Nuclear energy levels in this same region have been studied much more extensively with other monoenergetic-photon techniques, notably with neutron-capture γ rays from reactors, as were used by Donahue and collaborators for (γ,n) measurements (Sec. II.B). Experiments with (n,γ) photons, used either

TABLE III. Quantities derived directly from the data—all nuclei.

Nucleus	$E_{\gamma\max}$ (MeV)	$\sigma_{\rm int}(\gamma,{\rm tot}) / 60NZ/A$	$\sigma_{-1}A^{-4/3}$ (mb)	$\sigma_{-2} / 0.00225A^{5/3}$ (mb-MeV^{-1})	$\sigma_{\rm int}[(\gamma,2n)+(\gamma,3n)] / \sigma_{\rm int}(\gamma,{\rm tot})$	Reference
^{3}He	30.2	0.325	0.178	3.56		Berman *et al.*, 1970a
^{4}He	31.4	0.132	0.047	0.53	0	Berman *et al.*, 1971a
^{6}Li	32.0	0.308	0.172	3.42	0.014	Berman *et al.*, 1965
^{7}Li	30.5	0.195	0.086	1.24	0.50	Bramblett *et al.*, 1973b
^{12}C	37.4	0.260	0.067	0.52	0	Fultz *et al.*, 1966
^{14}N	29.5	0.465	0.129	1.11		Berman *et al.*, 1970c
^{16}O	28.0	0.173	0.044	0.33		Bramblett *et al.*, 1964; Caldwell *et al.*, 1965
^{23}Na	27.1	0.346	0.088	0.69	0.005	Alvarez *et al.*, 1971
^{24}Mg	28.3	0.144	0.034	0.24		Fultz *et al.*, 1971a
^{25}Mg	28.9	0.661	0.157	1.17	0.006	Alvarez *et al.*, 1971
^{26}Mg	28.6	0.608	0.149	1.15	0.31	Fultz *et al.*, 1971a
^{27}Al	36.7	0.408	0.089	0.59	0.046	Fultz *et al.*, 1966
$^{\rm Nat}$Si	31.0	0.288	0.036	0.24	0	Caldwell *et al.*, 1963
^{51}V	27.8	0.728	0.153	0.99	0.184	Fultz *et al.*, 1962a
^{55}Mn	36.5	0.976	0.186	1.13	0.212	Alvarez *et al.*, 1973a
^{58}Ni	33.5	0.329	0.061	0.36	0.027	Fultz *et al.*, 1973a; Fultz *et al.*, 1973c
^{59}Co	36.5	1.007	0.189	1.14	0.162	Alvarez *et al.*, 1973b
^{60}Ni	33.2	0.781	0.151	0.92	0.102	Fultz *et al.*, 1973b; Fultz *et al.*, 1973c
^{63}Cu	27.8	0.643	0.133	0.86	0.125	Fultz *et al.*, 1964
^{65}Cu	27.8	0.643	0.138	0.92	0.319	Fultz *et al.*, 1964
^{75}As	29.5	0.819	0.162	1.02	0.243	Berman *et al.*, 1969a
^{89}Y	28.0	0.805	0.151	0.87	0.093	Berman *et al.*, 1967
	27.0	1.029	0.193	1.12	0.055	Leprêtre *et al.*, 1971
	18.1	0.487[a]	0.101[a]	0.63[a]		Young, 1972
^{90}Zr	27.6	0.795	0.147	0.83	0.092	Berman *et al.*, 1967
	25.9	0.945	0.175	1.00	0.039	Leprêtre *et al.*, 1971
^{91}Zr	30.0	0.820	0.160	0.98	0.181	Berman *et al.*, 1967
^{92}Zr	27.8	0.804	0.154	0.93	0.414	Berman *et al.*, 1967
^{93}Nb	24.3	0.967	0.186	1.12	0.209	Leprêtre *et al.*, 1971
^{94}Zr	31.1	0.813	0.160	1.01	0.547	Berman *et al.*, 1967
^{107}Ag	29.5	0.858	0.155	0.89	0.194	Berman *et al.*, 1969a
^{115}In	31.1	1.111	0.202	1.17	0.278	Fultz *et al.*, 1969
^{116}Sn	29.6	0.978	0.175	0.99	0.248	Fultz *et al.*, 1969
^{117}Sn	31.1	1.102	0.199	1.16	0.271	Fultz *et al.*, 1969
^{118}Sn	30.8	1.072	0.190	1.07	0.297	Fultz *et al.*, 1969
^{119}Sn	31.1	1.145	0.202	1.17	0.334	Fultz *et al.*, 1969
^{120}Sn	29.9	1.185	0.209	1.19	0.330	Fultz *et al.*, 1969
^{124}Sn	31.1	1.123	0.200	1.16	0.361	Fultz *et al.*, 1969
^{127}I	29.5	0.933	0.164	0.93	0.256	Bramblett *et al.*, 1966b
	24.9	1.074	0.201	1.18	0.196	Bergère *et al.*, 1969
^{133}Cs	29.5	1.026	0.182	1.04	0.257	Berman *et al.*, 1969a
^{138}Ba	27.1	1.022	0.183	1.05	0.242	Berman *et al.*, 1970c
^{139}La	24.3	0.980	0.177	1.02	0.147	Beil *et al.*, 71
^{141}Pr	29.8	1.001	0.175	0.97	0.167	Bramblett *et al.*, 1966b
	16.9	0.691	0.138	0.85		Beil *et al.*, 1971
	18.1	0.678[a]	0.128[a]	0.75[a]		Young, 1972
^{142}Nd	20.2	0.901	0.170	1.00	0.024	Carlos *et al.*, 1971
^{143}Nd	19.8	0.910	0.176	1.08	0.094	Carlos *et al.*, 1971
^{144}Nd	20.2	0.896	0.170	1.01	0.299	Carlos *et al.*, 1971
^{145}Nd	20.2	0.965	0.193	1.26	0.323	Carlos *et al.*, 1971
^{146}Nd	20.2	0.905	0.173	1.05	0.347	Carlos *et al.*, 1971
^{148}Nd	18.8	0.795	0.155	0.97	0.491	Carlos *et al.*, 1971
^{150}Nd	20.2	0.931	0.178	1.09	0.416	Carlos *et al.*, 1971
^{153}Eu	28.9	1.022	0.181	1.03	0.311	Berman *et al.*, 1969b
^{159}Tb	28.0	0.997	0.175	1.00	0.386	Bramblett *et al.*, 1964
	27.4	1.109	0.198	1.15	0.243	Bergère *et al.*, 1968
^{160}Gd	29.5	1.099	0.195	1.14	0.448	Berman *et al.*, 1969b
^{165}Ho	28.9	1.057	0.183	1.04	0.312	Berman *et al.*, 1969b
	26.8	1.202	0.215	1.24	0.272	Bergère *et al.*, 1968
^{175}Lu	23.0	0.990	0.177	1.02	0.253	Bergère *et al.*, 1969
^{181}Ta	24.6	0.835	0.146	0.82	0.404	Bramblett *et al.*, 1963
	25.2	1.142	0.201	1.14	0.269	Bergère *et al.*, 1968
^{186}W	28.6	1.123	0.191	1.06	0.449	Berman *et al.*, 1969b
^{197}Au	24.7	1.045	0.179	0.98	0.262	Fultz *et al.*, 1962b
	21.7	1.080	0.190	1.06	0.156	Veyssière *et al.*, 1970
^{206}Pb	26.4	0.982	0.167	0.93	0.183	Harvey *et al.*, 1964

TABLE III. (*Continued*)

Nucleus	$E_{\gamma max}$ (MeV)	$\sigma_{int}(\gamma,tot)$ / $60NZ/A$	$\sigma_{-1}A^{-4/3}$ (mb)	σ_{-2} / $0.00225\,A^{5/3}$ (mb-MeV^{-1})	$\sigma_{int}[(\gamma,2n)+(\gamma,3n)]$ / $\sigma_{int}(\gamma,tot)$	Reference
^{207}Pb	26.4	0.915	0.156	0.87	0.202	Harvey *et al.*, 1964
^{208}Pb	26.4	0.888	0.154	0.87	0.325	Harvey *et al.*, 1964
	18.9	1.027	0.186	1.07	0.107	Veyssière *et al.*, 1970
	14.9	0.701[a]	0.134[a]	0.81[a]		Young, 1972
^{209}Bi	26.4	1.019	0.172	0.96	0.234	Harvey *et al.*, 1964
	14.8	0.709[a]	0.137[a]	0.84[a]		Young, 1972
^{232}Th	16.3	0.815	0.157	0.99		Veyssière *et al.*, 1973
^{235}U	18.5	1.106	0.202	1.20		Bowman *et al.*, 1964
^{237}Np	16.6	0.813	0.153	0.93		Veyssière *et al.*, 1973
^{238}U	18.35	0.894	0.164	0.98		Veyssière *et al.*, 1973

[a] Not corrected for $(\gamma,2n)$; the figures given are for the photoneutron yield cross section $\sigma[(\gamma,n)+(\gamma,pn)+2(\gamma,2n)]$.

directly or after Compton scattering, have been reviewed by Arad and Ben-David (1973a, 1973b).

Another source of monoenergetic photons results from resonant scattering from the 15.11-MeV level in ^{12}C. A beam of these scattered, plane-polarized photons was employed recently by Hayward *et al.*, at NBS, in an important experiment (1973). The ratio of photons scattered parallel to the direction of polarization of the incident beam to those scattered perpendicular to it was measured for a variety of medium and heavy elements. The results showed comparable intensities of incoherent (parallel) scattering from statically deformed nuclei and from spherical but vibrationally deformed nuclei, thus illustrating the tensor nature of the nuclear polarizability, in approximate agreement with the dynamic-collective-model predictions (also see Sec. IV.D), and no incoherent scattering from the hard spherical nucleus ^{209}Bi, as expected.

Arenhövel (1973) recently has given a review of photon scattering theory and experiment.

IV. PROPERTIES OF THE GIANT RESONANCE

The giant dipole resonance is fragmented into considerable structure for nuclei lighter than ^{60}Ni (except for special cases such as ^{4}He); it is composed of one broad peak (two for statically deformed nuclei) for nuclei heavier than ^{75}As; intermediate cases like the copper isotopes are not so clear cut. This fragmentation for light nuclei makes classification of many average properties difficult, but for the medium and heavy nuclei, the data lend themselves well to systematic analysis. Thus the bulk of the subject matter in the following sections is concerned with the delineation of the properties of the giant resonance for medium and heavy nuclei. Although, as noted above (Sec. II.A), most of the photon absorption strength is found in the photoneutron reaction channels for medium and heavy nuclei, one should remember that the systematics of this section apply to the total photon absorption cross section, for which the total photoneutron cross section is only an approximation (albeit a very good one, except as noted, especially for nuclei having $A > 100$).

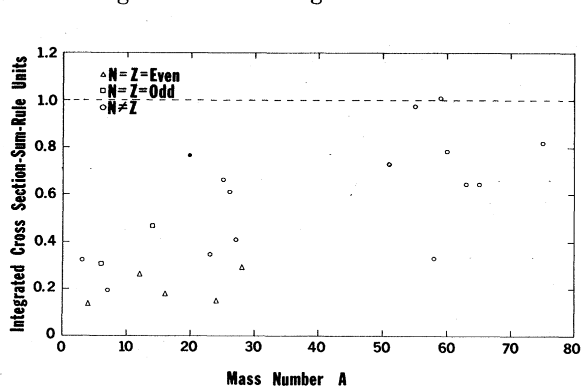

FIG. 40. Measured integrated total photoneutron cross sections $\sigma_{int}(\gamma,\text{total})$ for nuclei having $A < 80$ in units of 60NZ/A MeV-mb, where

$$\sigma_{int} = \int_{E_{thr}(\gamma,n)}^{E_{\gamma max}} \sigma(E)dE.$$

A. Quantities derived directly from the data

In Table III are listed the values for various functions of the integrated cross sections given in Table I. Three of these functions are closely related to the sum rules for photon absorption by nuclei, and the fourth is a sensitive indicator of the shell structure of nuclei.

1. The integrated cross section and the TRK sum rule

The Thomas–Reiche–Kuhn (TRK) sum rule (see Levinger, 1960) is an expression giving the total integrated cross section for electric dipole photon absorption, in the absence of exchange forces, and is given by

$$\int_0^\infty \sigma(E)\,dE = \frac{2\pi^2 e^2 h}{Mc}\frac{NZ}{A} = 60\left(\frac{NZ}{A}\right)\text{MeV-mb},$$

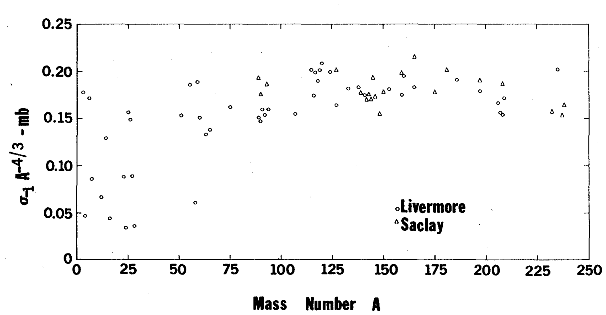

FIG. 41. Measured values for $\sigma_{-1}A^{-4/3}$, where

$$\sigma_{-1} = \int_{E_{thr}(\gamma,n)}^{E_{\gamma max}} [\sigma(E)/E]dE$$

and the $\sigma(E)$ are the total photoneutron cross sections.

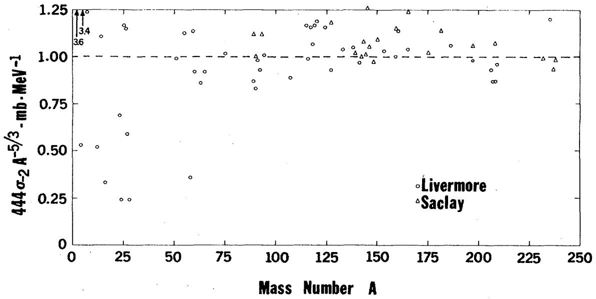

FIG. 42. Measured values for σ_{-2} in units of 0.00225 $A^{5/3}$ mb-MeV^{-1} ($\cong A^{5/3}/444$), where

$$\sigma_{-2}=\int_{E_{\mathrm{thr}}(\gamma,n)}^{E_{\gamma\max}}[\sigma(E)/E^2]dE$$

and the $\sigma(E)$ are the total photoneutron cross sections.

where M is the nucleon mass and the integration is over all energies for which dipole absorption can occur. For up-to-date theoretical discussions of the various photonuclear sum rules, the reader is referred to the papers of Teller and Weiss (1973), Brown (1973), and O'Connell (1973). The third column in Table III gives the integrated total photoneutron cross section in "sum-rule units"; that is, it gives the ratio of the integrated cross section (up to $E_{\gamma\max}$) to the TRK sum-rule value.

The integrated total photoneutron cross sections for nuclei with $A < 80$ are plotted versus mass number in Fig. 40. In general, the TRK sum rule is not nearly exhausted by the data; this results from the fact that the (γ,p) cross sections are not included (except for ^{6}Li), combined with the relatively low (for light nuclei) energy cutoff of the data of about 30 MeV. Both of these effects are especially important for the even–even self-conjugate nuclei (the triangles in Fig. 40), which combine high (γ,n) thresholds with the selection rule forbidding dipole photon absorption into any state having the same isospin as the ground state (namely, zero). One can see, however, that as the mass and charge of the nucleus increase, the integrated photoneutron cross section comes closer to exhausting the TRK sum rule, since (a) the increasing Coulomb barrier progressively inhibits the emission of charged particles, and (b) the giant resonance moves lower in energy and becomes more concentrated in an increasingly narrow energy region. It appears, for instance, that by the time mass 100 is reached the total photoneutron cross section integrated up to about 30 MeV will exhaust the TRK sum rule, and indeed this is the case, as can be seen in Table III. Beyond this point, the question is to what extent is the TRK sum rule exceeded, which then tells us the extent to which it is necessary to invoke exchange-force (or other) contributions in order to account for the total photonuclear absorption strength. This problem will be treated in Sec. IV.C; here we note merely that for the nuclei having mass number between 100 and 200 [since, for the nuclei near $A = 90$, the (γ,p) strength probably still is of the order of 10% of the (γ,n) strength and, for those having $A > 200$, either the measurements have not been carried out to a sufficiently high energy or else the absolute cross-section scale is suspect] for which measurements have been carried out at least up to 23 MeV (21 nuclei, 25 measurements) the average integrated cross section is 1.05 ± 0.07 TRK sum-rule units (for average $E_{\gamma\max} = 28.2$ MeV).

The significant feature of this result is that it differs markedly from earlier measurements in this energy range made with the use of bremsstrahlung radiation sources. In the earlier reports (Fuller and Hayward, 1962a; Hayward, 1965), the experimental integrated cross sections have been given as 1.4 or more times the TRK sum-rule values, with the difference attributed to contributions from exchange forces. The data of Table III do not refute the presence of nuclear exchange forces, but indicate that in the energy region up to 30 MeV such forces make less contribution than has been implied by the early bremsstrahlung data (see Fultz *et al.*, 1967).

2. The first moment of the integrated cross section

The first moment of the integrated cross section, also known as the "bremsstrahlung-weighted" cross section (since the energy dependence of the bremsstrahlung spectrum often is approximated by $1/E$), is given by

$$\sigma_{-1}=\int_0^\infty\left[\frac{\sigma(E)}{E}\right]dE=\frac{4\pi^2}{3}\frac{e^2}{\hbar c}\frac{NZ}{A-1}\langle r^2\rangle$$

for light nuclei (Levinger, 1960), where $\langle r^2\rangle$ is the mean-square radius of the nuclear charge distribution. Indeed, Ahrens *et al.* (1973) have shown that the values for $\langle r^2\rangle$ computed from this expression, using their total photon absorption data integrated up to 140 MeV for nuclei having $A \lesssim 40$, agree very well with those derived from electron-scattering data.

One also can express σ_{-1} as the ratio of the integrated cross section to the harmonic mean energy of the giant resonance $\sigma_{\mathrm{int}}/E_H$; and since this quantity is roughly proportional (Levinger, 1960) to $A^{4/3}$, the proportionality constant is of interest. It is this quantity, $\sigma_{-1}A^{-4/3}$, which is given in the fourth column of Table III, where the values for σ_{-1} used are for the total photoneutron cross section, again integrated up to $E_{\gamma\max}$.

The quantity $\sigma_{-1}A^{-4/3}$ also is plotted versus mass number in Fig. 41. It is seen to be almost independent of mass number for $A \gtrsim 60$, but the average value for the proportionality constant, for the same group of nuclei as above, is 0.186 $\pm$ 0.013 mb, significantly smaller than the value of 0.30

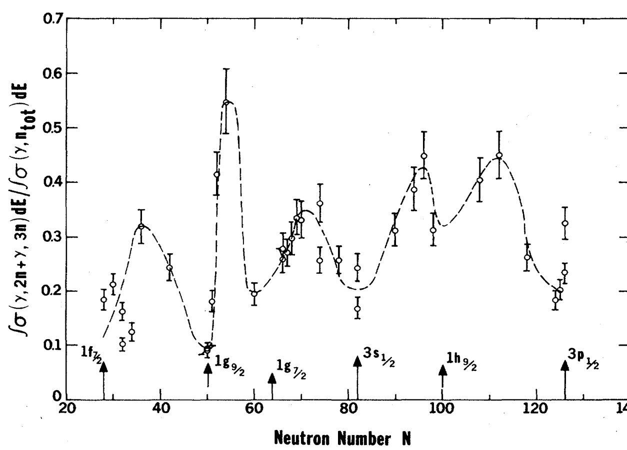

FIG. 43. Measured values for the ratio $\sigma_{\mathrm{int}}[(\gamma,2n)+(\gamma,3n)]/\sigma_{\mathrm{int}}(\gamma,\mathrm{total})$, showing pronounced minima at closed-neutron shells and subshells (adapted from Fultz *et al.*, 1969).

TABLE IV. Quantities derived indirectly from the data—spherical nuclei.

Nucleus	Fitting interval (MeV)	Lorentz parameters E_m (MeV)	σ_m (mb)	Γ (MeV)	K (MeV)	$E_mA^{1/3}$ (MeV)	$E_mA^{1/6}$ (MeV)	$\frac{E_m\sigma_{-1}}{\sigma_{\text{int}}(\gamma,\text{tot})}$	$\frac{(\pi/2)\sigma_m\Gamma}{60NZ/A}$	Reference
^{65}Cu	14–20	16.70	75.2	6.89	18.9	67.1	33.5	0.970	0.844	Fultz *et al.*, 1964
$^{\text{Nat}}$Rb	14–19	16.80	190	4.47						Leprêtre *et al.*, 1971
$^{\text{Nat}}$Sr	14–19	16.84	206	4.50						Leprêtre *et al.*, 1971
^{89}Y	14–19	16.79	185	3.95	23.0	75.0	35.5	0.949	0.872	Berman *et al.*, 1967
	14–19	16.74	226	4.25	22.9	74.8	35.4	0.947	1.147	Leprêtre *et al.*, 1971
	14–19[a]	16.83	205	3.69	23.0	75.2	35.6	1.052	0.903	Young, 1972
^{90}Zr	14–19	16.85	185	4.02	23.2	75.5	35.7	0.939	0.873	Berman *et al.*, 1967
	14–19	16.74	211	4.16	23.0	75.0	35.4	0.940	1.037	Leprêtre *et al.*, 1971
^{91}Zr	14–19	16.58	184	4.20	22.8	74.6	35.2	0.983	0.904	Berman *et al.*, 1967
^{92}Zr	14–19	16.26	166	4.68	22.2	73.4	34.6	0.957	0.898	Berman *et al.*, 1967
^{93}Nb	14–19	16.59	200	5.05	23.3	75.2	35.3	0.979	1.157	Leprêtre *et al.*, 1971
^{94}Zr	14–19	16.22	161	5.29	22.7	73.7	34.6	0.991	0.970	Berman *et al.*, 1967
^{107}Ag	13–19	15.90	150	6.71	24.0	75.5	34.7	0.923	1.003	Berman *et al.*, 1969a
^{115}In	13–18	15.63	266	5.24	24.1	76.0	34.5	0.942	1.297	Fultz *et al.*, 1969
^{116}Sn	13–18	15.68	266	4.19	24.1	76.5	34.6	0.929	1.027	Fultz *et al.*, 1969
^{117}Sn	13–18	15.66	254	5.02	24.4	76.6	34.6	0.942	1.165	Fultz *et al.*, 1969
^{118}Sn	13–18	15.59	256	4.77	24.3	76.5	34.5	0.923	1.108	Fultz *et al.*, 1969
^{119}Sn	13–18	15.53	253	4.81	24.4	76.4	34.4	0.921	1.096	Fultz *et al.*, 1969
^{120}Sn	13–18	15.40	280	4.89	24.2	76.0	34.2	0.920	1.230	Fultz *et al.*, 1969
^{124}Sn	13–18	15.19	283	4.81	24.3	75.7	33.9	0.933	1.194	Fultz *et al.*, 1969
^{133}Cs	12–19	15.25	287	5.01	25.5	77.9	34.5	0.950	1.169	Berman *et al.*, 1969a
^{138}Ba	12–19	15.26	327	4.61	26.2	78.9	34.7	0.976	1.188	Berman *et al.*, 1970c
$^{\text{Nat}}$Ba	12–19	15.29	356	4.89						Beil *et al.*, 1971
^{139}La	12–19	15.24	336	4.47	26.1	78.9	34.7	0.983	1.170	Beil *et al.*, 1971
$^{\text{Nat}}$Ce	12–19	14.95	351	4.64						Beil *et al.*, 1971
^{141}Pr	12–19	15.15	324	4.42	25.9	78.8	34.6	0.942	1.094	Bramblett *et al.*, 1966b
	12–19	15.23	341	4.00	26.1	79.3	34.8		1.042	Sund *et al.*, 1970
	12–19[a]	15.04	347	4.49	25.6	78.3	34.3	1.069	1.186	Beil *et al.*, 1971
	12–19[a]	15.36	332	4.07	26.5	79.9	35.0	1.033	1.030	Young, 1972
$^{\text{Nat}}$Nd	12–19[a]	14.92	315	4.70						Beil *et al.*, 1971
^{142}Nd	12–19	14.94	359	4.44	25.3	78.0	34.1	1.004	1.205	Carlos *et al.*, 1971
^{143}Nd	12–19	15.01	349	4.75	25.7	78.5	34.3	1.041	1.247	Carlos *et al.*, 1971
^{144}Nd	12–19	15.05	317	5.28	26.2	78.9	34.4	1.024	1.251	Carlos *et al.*, 1971
^{145}Nd	12–19	14.95	296	6.31	26.4	78.6	34.3	1.079	1.393	Carlos *et al.*, 1971
^{146}Nd	12–19	14.74	310	5.78	25.7	77.6	33.8	1.023	1.328	Carlos *et al.*, 1971
^{197}Au	11–17	13.82	560	3.84	27.2	80.4	33.3	0.956	1.189	Fultz *et al.*, 1962b
	11–17	13.72	541	4.61	27.1	79.8	33.1	0.972	1.383	Veyssière *et al.*, 1970
^{206}Pb	10–17	13.59	514	3.85	27.2	80.2	33.0	0.950	1.048	Harvey *et al.*, 1964
^{207}Pb	10–17	13.56	481	3.96	27.3	80.2	33.0	0.951	1.008	Harvey *et al.*, 1964
^{208}Pb	10–17	13.46	491	3.90	27.0	79.7	32.8	0.963	1.010	Harvey *et al.*, 1964
	10–17	13.43	639	4.07	26.9	79.6	32.7	1.004	1.369	Veyssière *et al.*, 1970
	10–17[a]	13.63	645	3.94	27.7	80.7	33.2	1.076	1.339	Young, 1972
^{209}Bi	10–17	13.45	521	3.97	27.0	79.8	32.8	0.941	1.084	Harvey *et al.*, 1964
	10–17[a]	13.56	648	3.72	27.4	80.5	33.0	1.083	1.263	Young, 1972

[a] Data do not extend to upper limit of fitting interval (see Table I).

given by Levinger (1960). The value 0.186 mb is a very convenient number to remember, since it has great practical utility for computing activation yields, neutron production yields, and the like, when an incident bremsstrahlung (or electron) beam is the source of radiation. It should be noted that σ_{-1} does not depend nearly so much as σ_{int} does upon the size of the cross section at high energies, because of the inverse-energy weighting in the integrand. Hence the values plotted in Fig. 41 will not increase as much as those for σ_{int} when the measurements are extended to higher energies.

3. The second moment of the integrated cross section and the Migdal sum rule

The second moment of the integrated cross section σ_{-2} is proportional to the nuclear polarizability $p = (e^2R^2A/40K)$, and hence increases with the diffuseness of the nucleus. Here R is the radius of the equivalent spherical nucleus and K is the nuclear symmetry energy. Then the Migdal sum rule (Levinger, 1960; Migdal *et al.*, 1966) states that

$$\sigma_{-2} = \int_0^\infty \left[\frac{\sigma(E)}{E^2}\right] dE = \frac{2\pi^2}{hc}\, p = \frac{\pi^2}{20}\frac{e^2}{hc}\frac{R^2A}{K}$$

which, for $R = 1.20\ A^{1/3}$ F and $K = 23$ MeV, reduces to $\sigma_{-2} = 0.00225\ A^{5/3}$ mb-MeV^{-1}. The fifth column of Table III gives the ratio of the second moment of the integrated total photoneutron cross section to the Migdal sum-rule value, and this ratio is plotted versus mass number in Fig. 42. This sum rule is seen to be exhausted even for some of the light nuclei (indeed, it is greatly exceeded for ^{3}He and ^{6}Li, since these nuclei are so loosely bound and hence diffuse), and again is fairly constant for nuclei having $A \gtrsim 60$. The average value for σ_{-2} for the same group of nuclei as above is $(1.06 \pm 0.09)(0.00225\ A^{5/3})$ mb-MeV^{-1}, or $(2.39 \pm 0.20)\ A^{5/3}$ μb-MeV^{-1}, and of course this quantity is even less dependent upon the size of the high-energy cross section than either σ_{int} or σ_{-1}.

TABLE V. Quantities derived indirectly from the data—deformed nuclei.

Nucleus	Fitting interval (MeV)	Lorentz Parameters E_{m1} (MeV)	σ_{m1} (mb)	Γ_1 (MeV)	E_{m2} (MeV)	σ_{m2} (mb)	Γ_2 (MeV)	K (MeV)	R_A	E_m (MeV)	$E_mA^{1/3}$ (MeV)	$E_mA^{1/6}$ (MeV)	ϵ	R_0 (F)	Q_0 (b)	Q_0[a] (b)	$E_m\sigma_{-1}/\sigma_{int}(\gamma,tot)$	$(\pi/2)(\sigma_{m1}\Gamma_1+\sigma_{m2}\Gamma_2)/60NZ/A$	Reference
^{51}V	14–23	17.86	58.8	4.42	21.22	28.8	5.10	(19.8)	1.77	18.98	70.3	36.5					0.991	0.843	Fultz *et al.*, 1962a
^{55}Mn	14–21	16.62	47.4	4.24	19.91	44.9	4.16	(20.2)	1.08	18.27	69.4	35.6					0.888	0.745	Alvarez *et al.*, 1973a
^{59}Co	14–21	16.37	26.3	2.56	18.90	64.5	7.61	(20.4)	0.14	18.06	70.3	35.6					0.888	0.997	Alvarez *et al.*, 1973b
^{60}Ni	14–21	16.30	34.1	2.44	18.51	55.2	6.37	(19.6)	0.24	17.77	69.6	35.2					0.900	0.761	{Fultz *et al.*, 1973b; Fultz *et al.*, 1973c
^{63}Cu	14–21	16.24	60.8	4.65	19.65	26.8	4.59	(19.0)	2.30	17.38	69.1	34.7					0.961	0.678	Fultz *et al.*, 1964
	14–21	16.72	66.1	4.19	19.10	30.1	3.56	(19.6)	2.58	17.51	69.7	34.9						0.642	Sund *et al.*, 1968
^{75}As	13–21	14.98	41.1	3.64	17.61	76.9	7.26	(20.9)	0.27	16.73	70.6	34.4					0.946	1.003	Berman *et al.*, 1969a
^{127}I	12–20	14.24	118	3.24	16.27	149	5.27	(24.9)	0.49	15.60	78.4	35.0					0.945	0.991	Bramblett *et al.*, 1966b
	12–20	14.57	239	4.08	16.69	118	4.92	(24.4)	1.68	15.28	76.7	34.2					0.984	1.319	Bergère *et al.*, 1969
^{148}Nd	10.8–18.8	12.76	107	3.97	15.48	220	5.30	25.4	0.36	14.58	77.1	33.5	0.454	1.25	4.77		1.042	1.167	Carlos *et al.*, 1971
^{150}Nd	10.8–18.8	12.30	175	3.38	16.04	223	5.17	26.6	0.51	14.79	78.6	34.1	0.643	1.25	6.81	5.15±0.1	1.041	1.266	Carlos *et al.*, 1971
^{153}Eu	10.8–18.8	12.33	155	2.75	15.79	222	5.83	25.9	0.33	14.63	78.3	33.8	0.594	1.25	6.70	7.0±0.1	0.952	1.213	Berman *et al.*, 1969b
^{159}Tb	10.8–18.8	12.22	181	2.64	15.67	220	4.97	26.2	0.44	14.52	78.7	33.8	0.598	1.25	7.13	7.35±0.15	0.953	1.072	Bramblett *et al.*, 1964
	10.8–18.8	12.07	196	2.98	15.88	248	5.10	26.7	0.46	14.61	79.1	34.0	0.667	1.25	7.96	7.35±0.15	0.973	1.259	Bergère *et al.*, 1968
^{160}Gd	10.8–18.8	12.23	215	2.77	15.96	233	5.28	27.3	0.48	14.72	79.9	34.3	0.645	1.25	7.60	7.25±0.1	0.984	1.244	Berman *et al.*, 1969b
^{165}Ho		12.02	236	2.35	15.59	308	4.85	26.4	0.37	14.40	79.0	33.7	0.628	1.25	7.92	7.7±0.15		1.347	Axel *et al.*, 1966
	10.8–18.8	12.28	214	2.57	15.78	246	5.00	27.2	0.45	14.62	80.2	34.2	0.604	1.25	7.60	7.7±0.15	0.960	1.171	Berman *et al.*, 1969b
	10.8–18.8	12.01	239	2.52	15.59	291	5.12	26.4	0.40	14.40	79.0	33.7	0.630	1.25	7.95	7.7±0.15	0.973	1.376	Bergère *et al.*, 1968
^{Nat}Er	10.8–18.8	12.12	242	2.76	15.58	259	4.74												Bergère *et al.*, 1969
^{175}Lu	10.8–18.8	12.32	217	2.57	15.47	287	4.70	27.5	0.41	14.42	80.6	34.1	0.543	1.25	7.54	7.5±0.2	0.997	1.184	Bergère *et al.*, 1969
^{181}Ta	10.8–18.8	12.54	154	1.67	14.95	273	5.23												Bramblett *et al.*, 1963
	10.8–18.8	12.30	259	2.43	15.23	341	4.48	27.4	0.41	14.25	80.6	33.9	0.507	1.25	7.40	7.0±0.25	0.982	1.297	Bergère *et al.*, 1968
^{186}W	10.8–18.8	12.59	211	2.29	14.88	334	5.18	27.4	0.28	14.11	80.6	33.7	0.389	1.25	5.86	6.0±0.2	0.954	1.298	Berman *et al.*, 1969b
^{232}Th	9.0–16.5[b]	11.26	283	4.32	14.18	306	4.48	29.0	0.89	13.21	81.2	32.7	0.550	1.15	9.9	9.75±0.1	1.099	1.232	Veyssière *et al.*, 1973
^{235}U	9.0–16.5	10.58	380	1.77	13.84	531	4.55	(26.5)	0.28	12.75	78.7	31.7	0.651	1.15	12.1	10.7±0.2	1.005	1.445	Bowman *et al.*, 1964
^{237}Np	9.0–16.5	11.00	250	2.88	14.10	394	4.85	28.2	0.38	13.07	80.9	32.5	0.597	1.15	11.2	10.7±0.5	1.063	1.219	Veyssière *et al.*, 1973
^{238}U	9.0–16.5	10.92	291	2.60	13.98	383	4.72	27.9	0.42	12.96	80.3	32.3	0.594	1.15	11.1	11.3±0.1	1.035	1.188	Veyssière *et al.*, 1973

[a] Values from literature (see text).
[b] Data do not extend to upper limit of fitting interval (see Table I).

4. The ratio of integrated cross sections and the shell model

The ratio of the integrated cross section for multiple neutron emission $\sigma_{\rm int}[(\gamma,2n)+(\gamma,3n)]$ to the integrated total photoneutron cross section should be lower for nuclei having closed neutron shells, where the $(\gamma,2n)$ thresholds are high and appreciably above the main part of the giant resonance, than for non-closed-shell nuclei, where these thresholds are lower. This quantity, which, like the other quantities listed in Table III, is obtained directly from the data, is given in the sixth column of Table III for all nuclei for which the higher-multiplicity cross-section data are available.

The ratio $\sigma_{\rm int}[(\gamma,2n)+(\gamma,3n)]/\sigma_{\rm int}(\gamma,{\rm tot})$ is plotted versus *neutron* number N in Fig. 43, for those nuclei having $N\geq 28$ and for which the measurements were carried out at Livermore [except for ^{58}Ni, which is anomalous (see Sec. III.A)]. The reasons the Saclay data are not included are (a) because very few of them were measured at sufficiently high energies [i.e., to a point well up on the high-energy tail of the giant resonance], and (b) for those that were (^{89}Y, ^{159}Tb, ^{165}Ho, and ^{181}Ta) there are sizable discrepancies with the Livermore data (except for ^{165}Ho) in the measured cross-section ratios [since these quantities emphasize the differences in both the $(\gamma,1n)$ and $(\gamma,2n)$ cross sections discussed in Sec. III.A].

If the dominant giant-resonance decay process for medium and heavy nuclei were by neutron emission, then one would expect that the neutron shell structure would influence the decay branching ratios. That this is the case is obvious from a glance at Fig. 43, from which it can be seen that marked minima occur at the neutron numbers which correspond to closed neutron shells and subshells. For the zirconium and tin isotopes, the plotted ratio increases as valence neutrons are added to closed-shell configurations (this is also the case for the neodymium isotopes, which are not plotted in Fig. 43). Moreover, for pairs of nuclei which have the same neutron number but different proton number, notably ^{89}Y–^{90}Zr and ^{115}In–^{116}Sn, similar values for this ratio are obtained. Finally, it should be noted that this effect is pronounced; the scale of the ordinate does not have a depressed zero. Thus, this plot provides another striking affirmation for nuclear shell structure.

B. Lorentz curves fitted to the data and their parameters

In the semiclassical theory of the interaction of photons with nuclei, the shape of a fundamental resonance in the absorption cross section is that of the Lorentz curve (Steinwedel and Jensen, 1950; Danos, 1958):

$$\sigma(E)=\frac{\sigma_m}{1+[(E^2-E_m{}^2)^2/E^2\Gamma^2]},$$

where the Lorentz parameters E_m, σ_m, and Γ are the resonance energy, peak cross section, and full width at half-maximum, respectively. In the hydrodynamic theory of photonuclear reactions, the giant dipole resonance consists of one such Lorentz line for spherical nuclei (Goldhaber and Teller, 1948; Steinwedel and Jensen, 1950), corresponding to the absorption of photons which induce oscillations of the neutron and proton fluids in the nucleus against each other, and the superposition of two such lines for statically deformed spheroidal nuclei (Okamoto, 1956; Danos, 1958), corresponding to oscillations along each of the nondegenerate axes of the spheroid. (The lower-energy line corresponds to oscillations along the longer axis and the higher-energy line along the shorter, since the absorption frequency decreases with increasing nuclear dimensions.)

$$\sigma(E)=\sum_{i=1}^{2}\frac{\sigma_{mi}}{1+[(E^2-E_{mi}{}^2)^2/E^2\Gamma_i{}^2]},$$

where $i=1, 2$ correspond to the lower- and higher-energy lines. Note that the two Lorentz lines are noninterfering, and that the damping parameters Γ_i are assumed not to be energy-dependent.

Accordingly, Lorentz curves have been fitted to the giant-resonance data for nuclei with $A>50$ (with certain exceptions, noted below). The resulting cross-section curves are shown on the figures of the total cross-section data, and the parameters of these fitted curves are given in Tables IV and V. Columns three through five of Table IV list the parameters E_m, σ_m, and Γ, respectively, for spherical nuclei for a single Lorentz line fitted to the data within the fitting interval given in column two. Columns three through eight of Table V list the parameters E_{m1}, σ_{m1}, Γ_1, E_{m2}, σ_{m2}, and Γ_2, respectively, for deformed nuclei for two Lorentz lines whose sum was fitted to the data within the fitting interval given in column two.

The fitting intervals were chosen on the basis of four criteria: (a) that they follow a smooth mass dependence, tracking the mass dependence of the central energy of the giant resonance; (b) that they include as much as possible of the cross section in the giant-resonance region, subject to (c), that they do not encompass the region immediately above the (γ,n) threshold and, insofar as is possible, any prominent structure below or above the main giant resonance (since the presence of such structure clearly is not consistent with a theoretical fit using only one or two Lorentz curves, and its origin is not accounted for by the simple theory); and (d) that they are the same for all members of a group of nuclei whose giant-resonance characteristics are similar (e.g., the tin isotopes, the statically deformed rare-earth nuclei, etc.). Sometimes these fitting intervals are the ones used in the original references, but more often they are not, and the data have been reanalyzed for purposes of this review, in order to make possible a consistent comparison between nuclei and consequently a consistent determination of the systematic properties of the giant resonance.

A least-squares fitting procedure was employed, in which the data points were weighted according to the inverse square of their statistical uncertainties. That is, a minimum value was sought for χ^2:

$$\chi^2=\frac{1}{D}\sum_i\frac{[\sigma(E_i)-\sigma_i(E_i)]^2}{[\Delta\sigma_i(E_i)]^2},$$

where $\sigma(E_i)$ is the value for the Lorentz-curve fit to the cross-section data at energy E_i, $\sigma_i(E_i)$ is the measured value for the total photoneutron cross section at that energy, $\Delta\sigma_i(E_i)$ is the statistical uncertainty in that measured value, and D is the number of degrees of freedom for the data set fitted; D is equal to the number of data points within the fitting interval minus the number of arbitrary parameters used (3 for each Lorentz curve). This minimization of χ^2

is the procedure which has been used by the Livermore group for obtaining Lorentz parameters, and has two advantages. First, the absolute value for χ^2 has a physical meaning: if it is appreciably larger than unity, then the simple theory is inadequate, while if it is much less than unity, then the experimental statistics are inadequate. Second, because the factor D depends (to a certain extent) on the number of Lorentz lines used to fit the data, it gives one a criterion for choice between a one- and a two-line fit for marginal cases. [Of course, the absolute χ^2 determination has meaning only if the data points are statistically independent; that is, if no smoothing of the data has been done.]

This is not, however, the same procedure as the one which has been used by the Saclay group; rather, they replace the weighting factor $[\Delta\sigma_i(E_i)]^{-2}$ by $\sigma_i(E_i)$. In practice, however, the differences between the Lorentz parameters given in the Saclay papers and those in Tables IV and V are small for most cases.

Comments on selected nuclei follow:

^{55}Mn, ^{59}Co (Livermore). For ^{59}Co and especially for ^{55}Mn (Fig. 17), there is considerable strength a few MeV above the two main giant-resonance peaks. It might very well be the case that one should consider this third hump as part of the main giant resonance, as if these nuclei were triaxially deformed (or if there were a clustering of high-lying shell-model states). Fitting these data with three Lorentz curves, however, requires very large values for Γ_3, and does not appear to be a fruitful approach. Indeed, treating vibrational nuclei such as these and all the other nuclei up through ^{127}I in Table V as if they were statically (and not vibrationally) deformed is somewhat artificial to begin with (see Bramblett *et al.*, 1966b; Berman *et al.*, 1969a). [An alternative approach is that of Kerman and Quang (1964), or that of the dynamic collective model of Danos and Greiner (1964a).] The view taken here, therefore, is that this third hump is not part of the main giant resonance, and the data are fitted, accordingly, only up to 21 MeV. There also is present, for these nuclei, as well as for the nickel isotopes, a large amount of fine structure in the cross sections throughout the giant-resonance region. The giant resonance, therefore, must be regarded either as the envelope of a finite number of not-quite-overlapping dipole states (as in *s-d* shell nuclei, particularly ^{26}Mg, for example) or else as the gross underlying macrostructure atop which these narrow fine-structure states lie. Which of these points of view is more nearly correct is currently a topic of speculation, and probably is not given to a universal answer.

$^{58,60}Ni$ (Livermore, Figs. 18, 19). Since the ^{58}Ni(γ,p) cross section is so large [it is about three times the size of the (γ,n) cross section (Ishkhanov *et al.*, 1970; Miyase *et al.*, 1973; Shoda, 1973)], no attempt is made here to fit the (γ,n) cross section alone with Lorentz lines (see Sec. IV.F). The ^{60}Ni total photoneutron cross section exhibits appreciable high-energy strength (above the Lorentz-curve fit), but it is not concentrated into a distinct clump as is the case for ^{55}Mn and ^{59}Co. Even here, however, the (γ,p) cross section comprises about 25% of the total absorption strength (Ishkhanov *et al.*, 1970; Miyase *et al.*, 1973; Shoda, 1973), and thus plays an important role, so that one should not take too seriously the values given in Table V. [Indeed, this probably is the case for ^{51}V, ^{55}Mn, ^{59}Co, and ^{63,65}Cu as well.] A detailed discussion of ^{58,60}Ni can be found in Fultz *et al.* (1973c).

^{63}Cu (Livermore and General Atomic). The excess high-energy cross section seen in the Livermore data, which seems to form a third hump centered at about 23 MeV, probably results largely from the (γ,pn) channel; and the two-line fit to the General Atomic data continues to match the data very well above the 21-MeV upper bound of the fitting interval, which lends support to the view that this third hump is not part of the main giant resonance, but is more likely an isospin or quadrupole effect (see Sec. IV.F).

^{90}Zr (Livermore and Saclay). A substantial amount of excess strength, centered at about 22 MeV, is present in both sets of data (see Sec. IV.F).

$^{117,118,119,120}Sn$ (Livermore, Fig. 25). All these nuclei have appreciable excess strength centered at 23–25 MeV.

^{148}Nd (Saclay, Fig. 27). A far better fit for ^{148}Nd is achieved with a two-line fit than with a one-line fit, as was employed in the original reference (Carlos *et al.*, 1971), which implies that this nucleus is statically deformed.

^{235}U (Livermore, Fig. 36). The values for the Lorentz parameters given in Table V were obtained from fitting the digitized data mentioned in Sec. III.A, with error bars deduced from those of the data points of the photoneutron yield cross section $\sigma[(\gamma,n)+2(\gamma,2n)+\bar{\nu}(\gamma,f)]$ plotted by Bowman *et al.* (1964).

C. Quantities derived from the Lorentz parameters

In addition to the Lorentz parameters and fitting intervals discussed in Sec. IV.B, Tables IV and V list a number of functions of the Lorentz parameters which can be compared with the predictions of nuclear theories. These include, for both spherical (Table IV) and deformed (Table V) nuclei, the nuclear symmetry energy K, which is the coefficient of the $(N-Z)^2/A$ term in the semiempirical mass formulae; the central energy of the giant resonance E_m; the harmonic mean energy $E_H=\sigma_{\rm int}/\sigma_{-1}$; and the total integrated strength derived from the areas under the Lorentz fits. In addition, the following quantities for deformed nuclei are listed in Table V: the area ratio of the two Lorentz lines $R_A=(\sigma_{m1}\Gamma_1)/(\sigma_{m2}\Gamma_2)$; the nuclear eccentricity ϵ; and the intrinsic quadrupole moment Q_0. These quantities are discussed in detail in the following paragraphs.

1. The nuclear symmetry energy

The nuclear symmetry energy K which appears, for example, in the Weizsäcker semiempirical mass formula, is computed from the giant-resonance energies and widths according to the hydrodynamic theory as given by Danos (1958) from the expression

$$E_m=\frac{hk}{A}\left\{\frac{8KNZ}{M}\left[1-\left(\frac{\Gamma}{2E_m}\right)^2\right]\right\}^{1/2},$$

where M is the nucleon mass, $kR=2.082$ for spherical

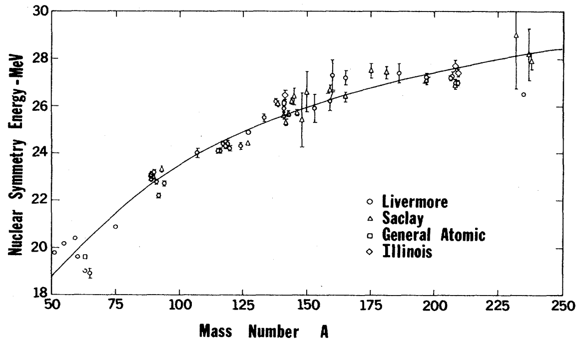

FIG. 44. The nuclear symmetry energy derived from the Lorentz parameters, fitted with the function $K = K_0(1 - cA^{-1/3})$ from which $K_0 = 42.3$ MeV and $cK_0 = 86.6$ MeV (see text). The values without error bars were not used in the fitting procedure.

nuclei, and R is the (sharp) nuclear radius. This reduces to

$$K = 9.935 \times 10^{-4}\left(\frac{A^{8/3}}{NZ}\right)\left[\frac{(E_m)^2}{1-(\Gamma/2E_m)^2}\right]$$

for K in MeV, where $R = R_0A^{1/3}$ and $R_0 = 1.20$ F. For prolate deformed nuclei, this relation, using the parameters of the lower-energy Lorentz line, becomes

$$K = 9.935 \times 10^{-4}\left(\frac{A^{8/3}}{NZ}\right)\left[\frac{(E_m)^2}{1-(\Gamma_1/2E_{m1})^2}\right] \times \left[\frac{\eta^{4/3}}{(1+0.01860\epsilon - 0.03314\epsilon^2)^2}\right],$$

where η and ϵ, the nuclear deformation and eccentricity, respectively, are defined below. The parameters of the higher-energy Lorentz line could have been used as well, with the final term in the formula suitably modified, but in general the data in the lower-energy hump are more reliable because of the smaller positron-bremsstrahlung-yield subtraction. The values for K are given in column 6 of Table IV and column 9 of Table V, and are plotted, along with their statistical uncertainties, versus mass number in Fig. 44. The values for K for vibrationally deformed nuclei (^{51}V through ^{127}I in Table V, whose assumed equilibrium shape is spherical) were computed from one-line Lorentz fits to the data; under these circumstances, these values for K are only approximate, and were neither assigned error bars nor used in the fitting procedure to be described below. (Nevertheless, they agree rather well with the curve fitted to the other values for K, as can be seen in Fig. 44.) The value for ^{235}U was computed normally, but could neither be assigned an error bar nor used for fitting purposes.

It is clear from Fig. 44 that K, as derived in this way, is not a constant for all nuclei, as was assumed to be the case some time ago [e.g., see Green (1954)]; rather, it increases with mass number. Therefore, the values for K (the ones having assigned error bars) were fitted using the same least-squares procedure as was used for the Lorentz-curve fitting, with a function of the form

$$K = K_0(1 - cA^{-1/3})$$

which takes account of the modification of the (volume) symmetry energy by the nuclear surface (see Berman, 1973b). The asymptotic value K_0 then corresponds to the volume symmetry energy and the quantity cK_0 to the surface symmetry energy, as appear, for example, in the mass formula of Myers and Swiatecki (1966, 1969). The value for K_0 obtained from this fit is 42.3 MeV, to be compared with the latest value of 36.5 MeV of Myers and Swiatecki (Swiatecki, 1973). It is not surprising that these values are not quite equal, since one does not expect the elementary hydrodynamic theory to give results even this close. Indeed, it is remarkable that the simple theory does so well, and a better representation of the nuclear surface, such as the inclusion of a diffuse radius [perhaps along the lines of the work of Brennan and Werntz (1970)], might well improve the results.

Recognizing that this derivation of K results from the application of an elementary semiclassical theory, let us nevertheless see where it leads: The value for $cK_0 = 86.6$ MeV obtained here, divided by the latest value (Swiatecki, 1973) for the surface energy, 20.0 MeV, yields a new value for the ratio of the surface symmetry energy to the surface energy of 4.33. This large value for this ratio favors a close-in neutron drip line for heavy elements, and hence argues against the production of superheavy elements by the r process in supernovae.

In a sense, the nuclear symmetry energy can be considered to be the fundamental parameter of the giant resonance. It arises naturally from the hydrodynamic theory, is easily consistent with the mass formulae, and exhibits no large fluctuations resulting from shell or deformation effects. Experimentally it is well determined, with a spread at a given value for A of about $\pm\frac{1}{3}$ MeV from the average. Consequently, using K as determined from systematics (for deformed nuclei, the intrinsic quadrupole moment is needed in order to determine the splitting), the giant-resonance energies for any nucleus having $A > 80$ can be predicted with an accuracy of about 100 keV, which usually is at least as good as is obtained from a single experiment. (The value assumed for Γ is not very important: a 1-MeV change in Γ results in about a 70-keV change in E_m.)

2. The energy of the giant resonance

The peak energy E_m has been predicted by collective models of the giant resonance to be proportional either to $A^{-1/3}$ or $A^{-1/6}$. The $A^{-1/3}$ dependence (Goldhaber and Teller, 1948) arises from the concept that when displacement of the neutron and proton fluids occurs, the restoring force is proportional to the density gradient of those fluids. The $A^{-1/6}$ dependence of E_m (Goldhaber and Teller, 1948; Steinwedel and Jensen, 1950) is based on the concept that the restoring force is proportional to the nuclear surface area. Both of these elementary models employ a sharp cut-off model for the nuclear surface boundary.

The quantities $E_mA^{1/3}$ and $E_mA^{1/6}$ are given in columns 7 and 8, respectively, of Table IV for spherical nuclei, where E_m is the fitted Lorentz parameter. For deformed nuclei, the values for E_m in column 11 of Table V were computed from the Lorentz parameters E_{m1} and E_{m2} as follows:

$$E_m = (E_{m1} + 2E_{m2})/3 \text{ [for prolate nuclei } (R_A < 1)]$$
$$E_m = (2E_{m1} + E_{m2})/3 \text{ [for oblate nuclei } (R_A > 1)]$$

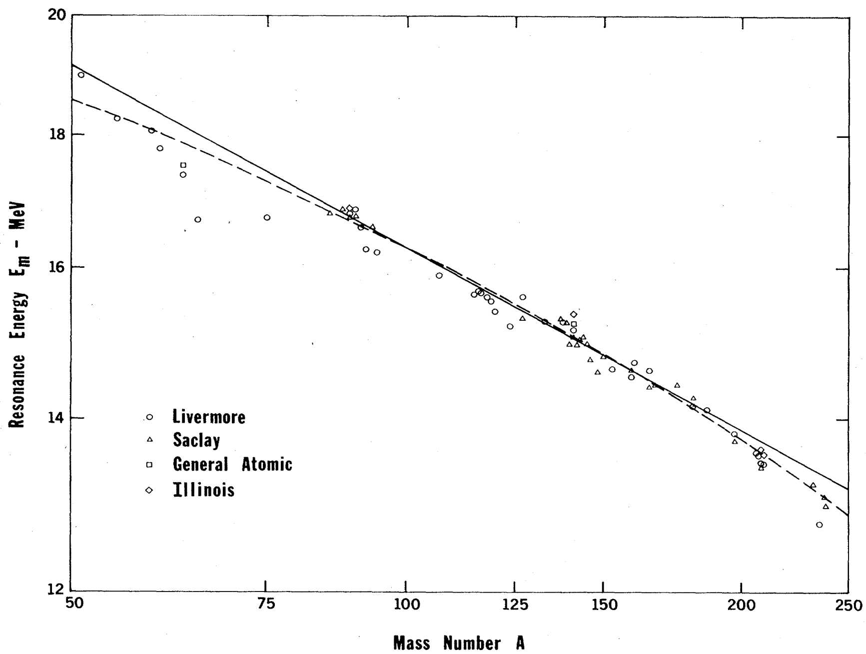

FIG. 45. The giant-resonance energy derived from the Lorentz-curve fits plotted versus mass number on a log–log scale. The solid line is the best two-parameter fit to the data of the form $E_m = c_1A^{-1/c_2}$, from which $c_1 = 47.9$ MeV and $c_2 = 4.27$; the dashed line is the best three-parameter fit of the form $E_m = c_5A^{1/3}(1-e^{-A/A_0}) + c_6A^{-1/6}e^{-A/A_0}$, from which $c_5 = 77.9$ MeV, $c_6 = 34.5$ MeV, and $A_0 = 238$.

except for the anomalous case of ^{55}Mn ($R_A = 1.08$), where $E_m = (E_{m1} + E_{m2})/2$ was used. Although this is somewhat arbitrary, and leads to a strange result for ^{127}I (where the two measurements give opposite deformations), it turns out not to matter very much in the over-all picture since the uncertainties in these values for deformed nuclei are much larger than those for spherical nuclei, where a single Lorentz line gives the best fit to the data. The values for $E_mA^{1/3}$ and $E_mA^{1/6}$ for deformed nuclei are given in columns 12 and 13, respectively, of Table V.

As can be seen from the tables, the product $E_mA^{1/3}$ increases with mass number, i.e., the $A^{1/3}$ power is too strong, while $E_mA^{1/6}$ decreases with mass number—the $A^{1/6}$ power is too weak. The 61 values for E_m resulting from the measurements on monoisotopic or separated-isotope samples (except for ^{235}U) given in Tables IV and V have been fitted (again with the same least-squares method as above) in several ways: (a) with a single power law

$$E_m = c_1A^{-1/c_2}$$

with the result that $c_1 = 47.9$ MeV and $c_2 = 4.27$; (b) with the combined power relation

$$E_m = c_3A^{-1/3} + c_4A^{-1/6}$$

with the result that $c_3 = 31.2$ MeV and $c_4 = 20.6$ MeV; and (c) with a three-parameter relation, analogous to radioactivity expressions, that yields the rate of transition from an $A^{-1/6}$ power law at low mass numbers into an $A^{-1/3}$ power law at high mass numbers, where the transition rate is assumed to follow an exponential function

$$E_m = c_5A^{-1/3}(1 - e^{-A/A_0}) + c_6A^{-1/6}e^{-A/A_0}$$

with the result that $c_5 = 77.9$ MeV, $c_6 = 34.5$ MeV, and $A_0 = 238$. Figure 45 shows the values for E_m plotted versus mass number, together with the fitted expressions in (a) and (c) (the solid and dashed curves, respectively). The expression in (b), over the mass range of the figure, yields a result indistinguishable from that in (a) (which is not surprising, since both contain two arbitrary parameters). Error flags are not shown on the figure, since for most of the spherical nuclei of Table IV, they are not much larger than the data points, and it is these that dominate the fit.

Inspection of the values for c_3 and c_4 in (b) above reveals that the $A^{-1/3}$ term accounts for about 40% (and the $A^{-1/6}$ term $\sim$60%) of the value for E_m throughout the mass region of Fig. 45. This is consistent with the value for A_0 in expression (c) being large ($A_0 = 238$) and is reasonable, in view of the collective theories; it merely states that for nuclei in this mass range neither the effect of the density gradient nor that of the nuclear surface dominates the restoring force. Moreover, as can be seen from the dashed curve in Fig. 45, and better, from the data points themselves, the trend of the experimental results is such that the $A^{-1/3}$ dependence of E_m becomes increasingly dominant for increasing values for A. This too, is eminently reasonable, since for heavier nuclei, a greater fraction of the nucleons are located in the interior (rather than on the surface), so that the effect of the density gradient on the restoring force gradually becomes more important than the effect of the nuclear surface.

The harmonic mean energy $E_H = \sigma_{\rm int}(\gamma,{\rm total})/\sigma_{-1}$ is another measure of the centroid of the giant-resonance strength (Levinger, 1960). Values for the ratio of E_m to E_H are given in the ninth column of Table IV and the 18th column of Table V. Insofar as this ratio is unity, the two methods of estimating the mean energy of the giant resonance agree. One can see from these tables that this is largely the case. The average value for this ratio for all the entries in Tables IV and V is 0.98 ± 0.04, and the distribution of values is such that the (slightly) larger ones tend to be associated with nuclei having the larger mass numbers.

3. The width of the giant resonance

The width of the giant resonance has been in one sense the easiest and in another the hardest feature of the giant reso-

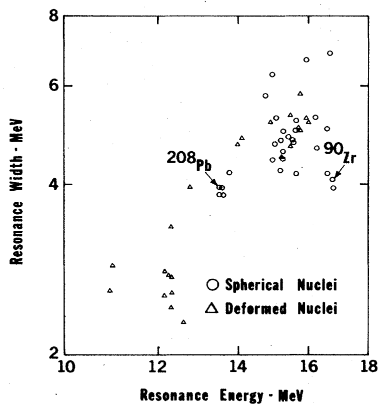

FIG. 46. The width of the giant resonance as determined from the Lorentz curves fitted to the data plotted versus the giant-resonance energy on a log–log scale. A straight-line fit to the data would imply a power-law dependence of Γ upon E_m as assumed by Danos and Greiner (1965b) for ^{165}Ho.

nance to explain. As has been known for many years (Nathans and Halpern, 1953; Okamoto, 1958) and can be seen from Tables IV and V, the giant-resonance width follows the shell structure of the nucleus; it is small (about 4 to 5 MeV) for closed-shell nuclei, larger for nuclei between closed shells or vibrationally deformed (soft) nuclei, and split in two for statically deformed nuclei. But from the viewpoint of the collective theories, there is no fundamental explanation for the width other than as a damping term akin to friction between the two fluids. This situation has led Danos, Greiner, and others (Danos and Greiner, 1965b) to assign to it an energy dependence in the form of a power law

$$\Gamma = \Gamma_0(E/E_0)^\delta.$$

One can ask if a single value for δ can be applied to all nuclei, as has been attempted by Carlos *et al.* (1973). [Danos and Greiner (1965b) were concerned only with a single nucleus (^{165}Ho), and Huber *et al.* (1967) found that the energy dependence which applied to ^{165}Ho was much too strong for spherical nuclei.] But it appears, from Fig. 46, wherein the widths in Tables IV and V are shown on a log–log plot versus photon energy, that the use of a simple power-law dependence of Γ on E is fruitless or is of use only in a limited mass region; and that unless one takes into account shell effects, or the resultant level density in the giant-resonance region (even granted that one could ignore direct reactions), one cannot generalize the behavior of the giant-resonance decay width in this way. Perhaps a more promising approach is the semiclassical treatment of Dover *et al.* (1972), wherein the analogy is drawn between the photoabsorption cross section and the response of a system to a weak external electromagnetic probe, resulting in a damping width for particle–hole excitations owing to collisions between excited particle–hole pairs and the "nuclear background" (also see Ligensa and Greiner, 1969 and Mshelia *et al.*, 1973).

4. The extrapolated integrated cross section

The area beneath a Lorentz-curve fit to the giant resonance for a medium or heavy nucleus gives an estimate of the total electric dipole absorption strength for the nucleus. This procedure amounts to an extrapolation of the total photon absorption cross section in the giant-resonance region down to zero [below the (γ,n) threshold this gives an estimate of the average photon scattering cross section (see Axel, 1962)] and up to the meson thresholds, by which point exchange effects and direct reactions clearly are dominant. The principal failing of this view is that this procedure neglects the contributions of other $E1$ processes, such as $T_>$ strength ($T_> = T_0 + 1$), the quasideuteron effect (Levinger, 1960), and $E1$ "overtones" above the giant resonance proper, and so underestimates the total $E1$ strength. But it is hard to measure the multipolarity of the absorbed radiation, especially at high energies, because of all the competing and complicating continuum effects which can take place there. The Lorentz-curve extrapolation at least has the virtue that it does not include contributions of multipolarities other than $E1$ [such as those resulting from electric quadrupole absorption (see Sec. IV.F)].

The area under a Lorentz curve is given by

$$\int_0^\infty \sigma(E)dE = \frac{\pi}{2}\sigma_m\Gamma,$$

where the form of $\sigma(E)$ is given in Sec. IV.B. The tenth column in Table IV gives the areas under the single-line Lorentz curves (for spherical nuclei) fitted to the total photoneutron cross sections, in TRK sum-rule units. The 19th column in Table V does the same for deformed nuclei, where the summed area under the two-line Lorentz-curve fit is $(\pi/2)(\sigma_{m1}\Gamma_1 + \sigma_{m2}\Gamma_2)$. These values for the extrapolated integrated $E1$ cross section are plotted versus mass number in Fig. 47. One can see that for nuclei having $A < 70$ the TRK sum rule is not exhausted, but this doubtless results from the neglect of the (γ,p) cross sections for these nuclei. For the mass region $70 < A < 100$, the values center about one sum-rule unit, with the Saclay values on the higher side and the Livermore and Illinois values on the the lower side. Here one expects, from $(e,e'p)$ and (p,γ) data, an enhancement of about 10% or so from the (γ,p) reaction channel, even though most of the (γ,p) strength is centered above 20 MeV in this mass region. For the rest of the periodic table ($A > 100$) the plotted values center about 1.2 TRK sum-rule units, with the Saclay values typically about 10% higher than those from Livermore, as discussed in Sec. III.A. For ^{141}Pr, the General Atomic and Illinois results are even lower than the Livermore value, while for ^{208}Pb and ^{209}Bi the Illinois results are close to the

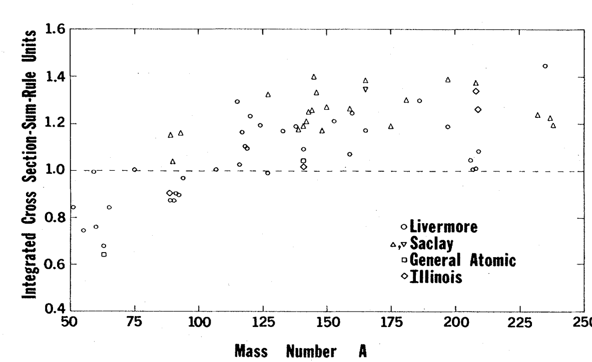

FIG. 47. Extrapolated integrated cross sections derived from the Lorentz parameters in units of 60NZ/A MeV-mb.

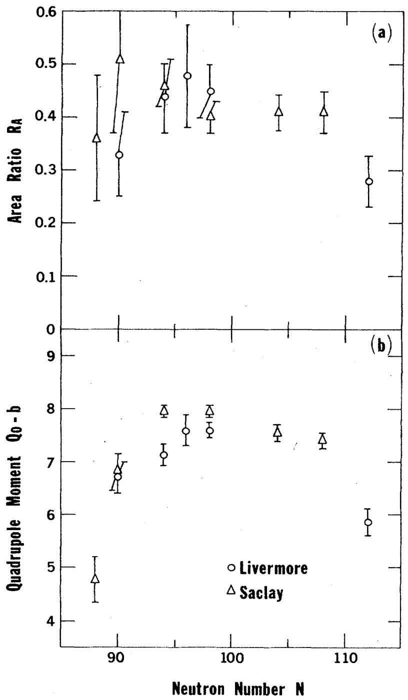

FIG. 48. (a) The area ratio and (b) the intrinsic quadrupole moment derived from the Lorentz parameters for statically deformed rare-earth nuclei plotted versus neutron number, showing that these two quantities vary with deformation in much the same way.

Saclay value and considerably higher than the Livermore points. The old Saclay result (Axel *et al.*, 1966) for ^{165}Ho is closer to the newer Saclay value than to the Livermore result. The average of these integrated cross-section values for $A > 100$, including both measurements for ^{127}I (which tend to balance each other) but not including the Livermore measurements for ^{206,207,208}Pb, ^{209}Bi, and ^{235}U, is 1.21 ± 0.11 sum-rule units, which is still considerably below the old "bremsstrahlung" figure of 1.4 units, even though the present values are for an infinite extrapolation. This says that the giant $E1$ resonance alone requires an exchange-force contribution [or one of a similar nature, e.g., from velocity-dependent (or nonlocal) forces] of about 20% of the TRK sum rule. Of course, other electric-dipole effects which are not a part of the giant resonance proper, such as the three enumerated above, will raise this figure, and thus this figure should be considered to be a minimum value. Clearly, total photon absorption and/or photoneutron cross-section measurements for medium and heavy nuclei for energies between 30 and 150 MeV which will yield a maximum (because of the absorption strength for radiation of other multipolarities) but probably more reasonable value, are needed.

5. The area ratio and quadrupole moment for statically deformed nuclei

The hydrodynamic model of the giant resonance, as applied to deformed nuclei (Okamoto, 1956; Danos, 1958; Okamoto, 1958), makes two major predictions which lend themselves particularly to experimental scrutiny: (a) that the giant resonance is split into two components for spheroidal nuclei, corresponding to dipole vibrations along the major and minor axes of the spheroid of the two interpenetrating fluids made up of the neutrons and protons in the nucleus; and (b) that the strengths of these two components have the simple ratio of 1:2, corresponding to the number of degrees of freedom for these vibrations. The first condition gives a prescription for the nuclear shape parameters (for prolate nuclei) through the relation

$$E_{m2}/E_{m1} = 0.911\eta + 0.089,$$

where the deformation parameter η is the ratio of the major axis b to the minor axis a. The nuclear eccentricity ϵ is given by $\epsilon = (b^2 - a^2)/R^2$, where R is the radius of a sphere of equal volume; for a prolate spheroid, $R^3 = a^2 b$. The intrinsic quadrupole moment Q_0 for the nucleus then can be obtained from the expression

$$Q_0 = \tfrac{2}{5}ZR^2(\eta^2 - 1)\eta^{-2/3} = \tfrac{2}{5}ZR^2\epsilon$$

and $R = R_0 A^{1/3}$. It should be pointed out that while the Coulomb-excitation method for obtaining quadrupole moments depends upon the transition probability $B(E2)$ according to the relation

$$Q_0^2 = (16\pi/5)B(E2)$$

(for even-even nuclei) and hence gives only the magnitude of Q_0, the photonuclear method gives its sign as well. Of course, both of these methods for computing Q_0 are model dependent.

The second condition above predicts that the ratio of the area under the lower-energy component of the giant resonance to that under the higher-energy component be $\frac{1}{2}$ for prolate and 2 for oblate nuclei. Values for this area ratio

$$R_A = \sigma_{m1}\Gamma_1/\sigma_{m2}\Gamma_2$$

derived from the Lorentz parameters are given in column 10 of Table V. The values for R_A for the vibrationally deformed nuclei (the first nine entries in Table V) are not very meaningful, since the static equilibrium shape of these nuclei is spherical (or nearly so), and a different theoretical approach must be employed (see Sec. IV.D). In fact, since these nuclei certainly do not have low-lying rotational spectra, one can presume that the only reason their giant resonances are fitted better with two Lorentz lines than with one is that more arbitrary parameters are available. The values for the fissionable nuclei (with the exception of ^{238}U) suffer from the variety of experimental uncertainties mentioned above. Those for the statically deformed rare-earth nuclei, however, constitute a set of information which provides an important test for the hydrodynamic model, namely, the test of the prediction that R_A for all these prolate nuclei should equal $\frac{1}{2}$. These values for R_A, together with their statistical uncertainties, are plotted versus neutron number in the upper part of Fig. 48. It can be seen that the prediction $R_A = 0.5$ is verified only for the most deformed nuclei ^{159}Tb, ^{160}Gd, and ^{165}Ho, in the middle of the deformed rare-earth region (the data for ^{150}Nd are not sufficiently good to give a definitive value for R_A, as can be seen from its large statistical uncertainty).

The values for the eccentricity ϵ for the statically deformed nuclei are given in column 14 of Table V. These quantities, since they depend only upon the resonance energies, are determined with great precision, usually around 2 to 4%. Therefore, the largest uncertainty by far in the determination of Q_0 is that in the value used for R_0, since

R_0 is known currently for these nuclei, from electron-scattering experiments or otherwise, to no better than 5% and also appears as the square in the expression for Q_0. Therefore, the value used for R_0 for these nuclei, given in column 15 of Table V, was determined from a comparison of the best values for Q_0 from Coulomb-excitation and mu-mesic x-ray experiments in the literature, given in column 17 of Table V, with the photonuclear results. [The "literature" results are taken from the compilation of Löbner *et al.* (1970), but have been reevaluated for the nuclei listed here, since the results of the evaluation given in Löbner *et al.* were deemed to be unsatisfactory.] Since it was observed that the photonuclear results for the fissionable nuclei required appreciably smaller values for R_0 in order to bring them into agreement with the literature values, the statically deformed nuclei were split into two groups as can be seen in the table. Then the best values for R_0 were found to be 1.25 F for the rare-earth nuclei and 1.15 F for the fissionable nuclei. The final values for Q_0, using the values for ϵ from column 14 and these values for R_0, given in column 15, are given in column 16 of Table V and are plotted versus neutron number in the bottom part of Fig. 48. The error bars are those resulting from statistical uncertainties only (that is, uncertainties in ϵ), and do not include possible errors in R_0. One can see from Fig. 48 that the dependence upon N of R_A and of Q_0 are similar; this suggests that the virtues of the hydrodynamic theory for deformed nuclei diminish *proportionately* as the nucleus becomes less deformed.

D. Application of the data to other collective theories of the giant resonance

More sophisticated than the elementary hydrodynamic theory of the giant resonance are the theories that include the coupling of quadrupole (surface) oscillations to the main dipole (volume) vibrations of the nucleus. These include the early theory of Kerman and Quang (1964), the dynamic collective theory of Danos and Greiner (1964a), and its extensions (Danos and Greiner, 1965b; Drechsel *et al.*, 1967; Huber *et al.*, 1967; Arenhövel and Greiner, 1968; Rezwani *et al.*, 1972b), and others (Le Tourneux, 1965; Semenko, 1965). Although the Kerman–Quang theory, which relates the parameters of the giant resonance of a nucleus to its ground-state vibrational character, has been reexamined recently (Berman, 1973a; Faul and Berman, 1974), only the much more extensively pursued dynamic collective model approach will be discussed here.

The dynamic collective treatment of the giant resonance results in the sharing of the dipole strength among several states which arise from terms in the nuclear Hamiltonian which specifically describe the coupling between the dipole vibrations on the one hand and the vibrational and rotational degrees of freedom of the nucleus on the other. These states appear as "satellites" to the main giant-resonance state(s) for stiff spherical and statically deformed nuclei, although they are more distinctive for the softer vibrational nuclei. Like the elementary hydrodynamic theory, however, this model says nothing about the widths (which characterize the damping of the giant-resonance states into the nuclear continuum) of the various peaks. Consequently, the question of intermediate structure in the giant resonance of medium and heavy vibrationally or statically deformed nuclei is ambiguous theoretically, and has been the subject of much controversy (see Huber *et al.*, 1967; Spicer, 1969).

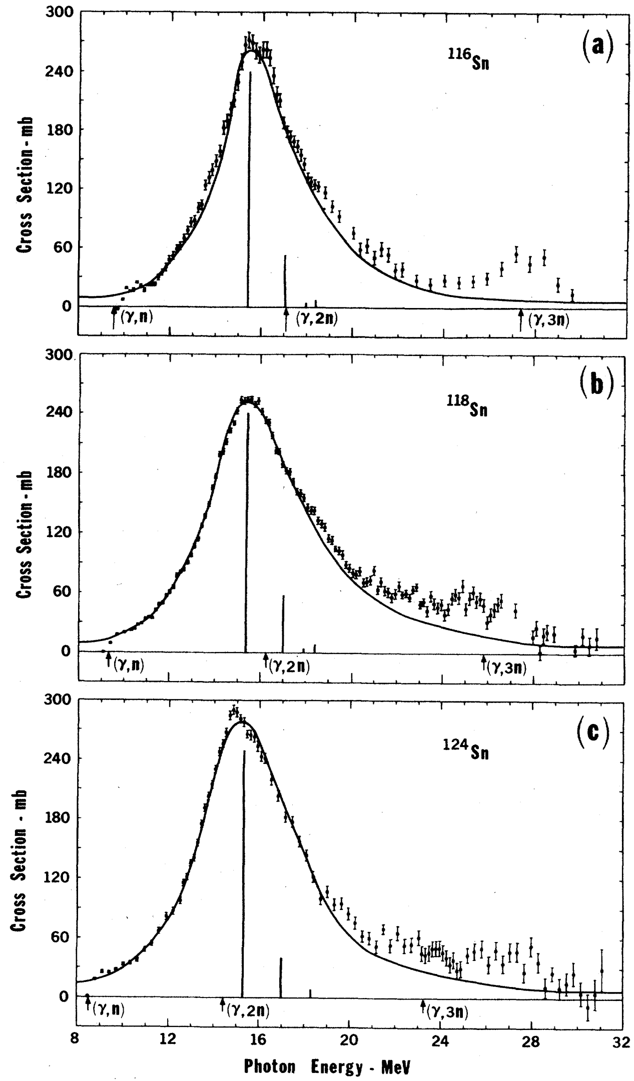

FIG. 49. Total photoneutron cross sections for (a) ^{116}Sn, (b) ^{118}Sn, and (c) ^{124}Sn (from Fig. 25), fitted with dipole strengths and locations calculated using the dynamic collective model (Arenhövel and Greiner, 1969) and shown in the figures as the vertical lines.

For example, earlier reported gross structure for ^{75}As (Fielder *et al.*, 1965) and ^{141}Pr (Cook *et al.*, 1966; Cannington *et al.*, 1968), which indicated an apparent width of about 1.5 MeV for these states, were superseded by the better data presented in Sec. III.A. Also, the best fit to the dynamic-collective-model calculations (Arenhövel and Greiner, 1969) for the three tin isotopes shown in Fig. 49 requires such large values for the widths of the peaks (also see Bergère *et al.*, 1973) that the result is practically indistinguishable from the single-line Lorentz curves of Fig. 25; and the results of the most modern (Rezwani *et al.*, 1972a) such calculations, for the five neodymium isotopes shown in Fig. 50, are no better than the Lorentz fits of Fig. 27. Experiments which can link the giant resonance with surface oscillations more directly are those that detect photons which populate vibrational levels, like the photon-scattering measurements of Arenhövel and Maison [(1970); also see Hayward *et al.* (1973), described in Sec. III.B].

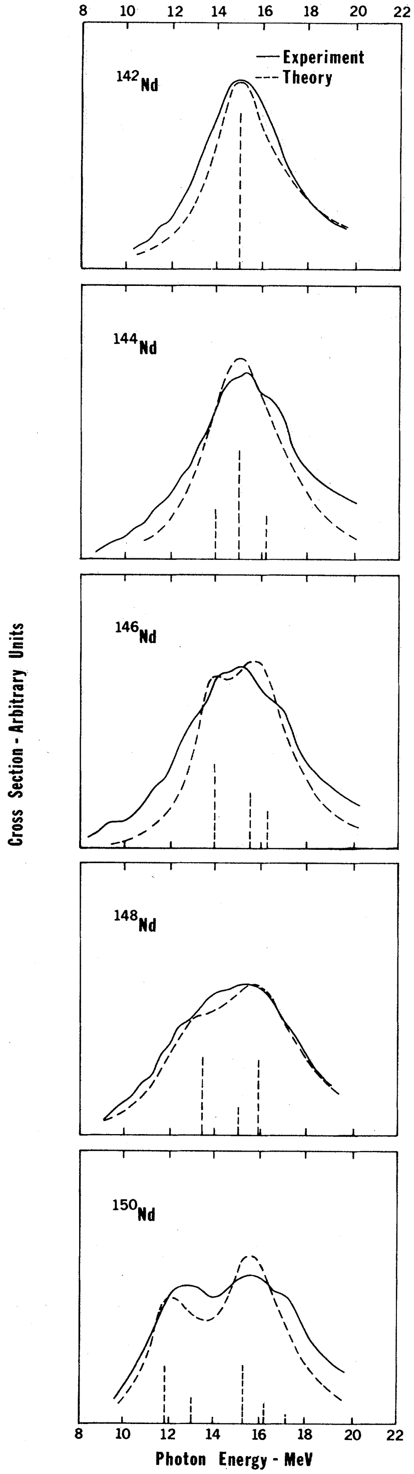

FIG. 50. Total photoneutron cross sections for the even neodymium isotopes (from Fig. 27), together with dipole strengths and locations (shown in the figures as vertical dashed lines) calculated with the modern version of the dynamic collective model which is fitted to the low-energy spectrum of excited states for these nuclei (from Rezwani *et al.*, 1972a).

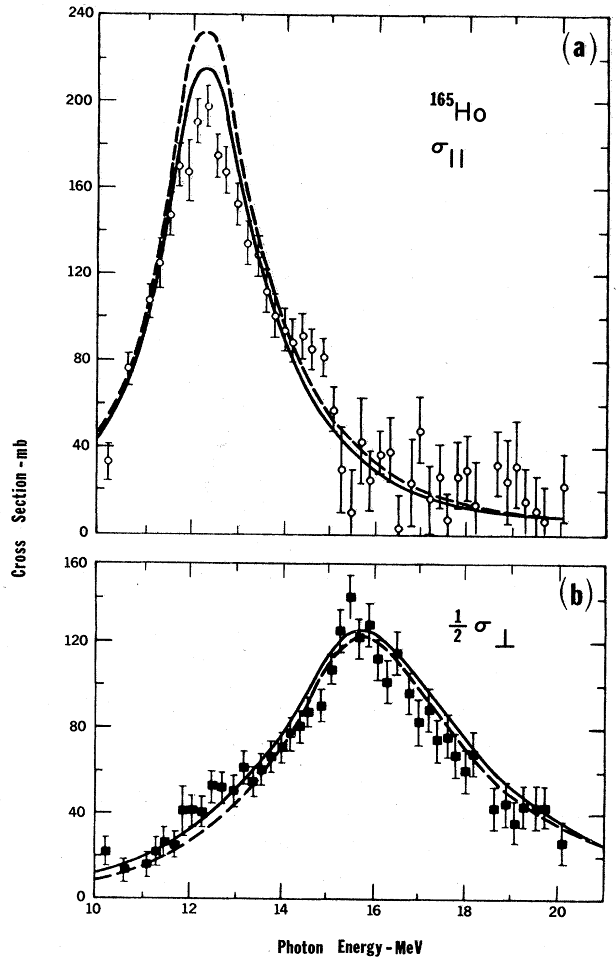

FIG. 51. Intrinsic cross sections for ^{165}Ho: (a) $\sigma_{\parallel}$, associated with dipole vibrations along the nuclear symmetry axis, and (b) $\sigma_{\perp}$, associated with vibrations perpendicular to this axis, derived from the data of Fig. 38. The solid curves are those derived from the elementary hydrodynamic model; the dashed one are calculated using the dynamic collective model (from Kelly *et al.*, 1969).

The great value of the dynamic collective model rests in the fact that it relates the giant-resonance properties of a nucleus to its spectrum of low-lying excited states, rotational and vibrational, and to the detailed shape parameters of its potential-energy surface (Rezwani *et al.*, 1972b; also see Danos, 1973); and it succeeds very well indeed in fitting all these data simultaneously.

An extension of the dynamic collective model which couples each of the basic particle–hole states to the surface vibrations has been applied to ^{12}C, ^{28}Si, and ^{60}Ni (Drechsel *et al.*, 1967). This "collective-correlations" model introduces more structure than the simple particle–hole treatments, in better agreement with the data. The agreement is especially good for ^{12}C, particularly in the high-energy (>24 MeV)region (also see Mshelia and Barrett, 1973).

Another giant-resonance measurement that tests the collective theories, including the dynamic collective model, is that of Kelly *et al.* (1969) on polarized ^{165}Ho (Sec. III.B). From the data presented in Fig. 38 and the measured nuclear alignment, Kelly *et al.* deduced the intrinsic cross sections $\sigma_{\parallel}$ and $\sigma_{\perp}$ for photoexcitation of the ^{165}Ho nucleus by radiation polarized parallel and perpendicular, respectively, to its nuclear symmetry axis. These intrinsic cross

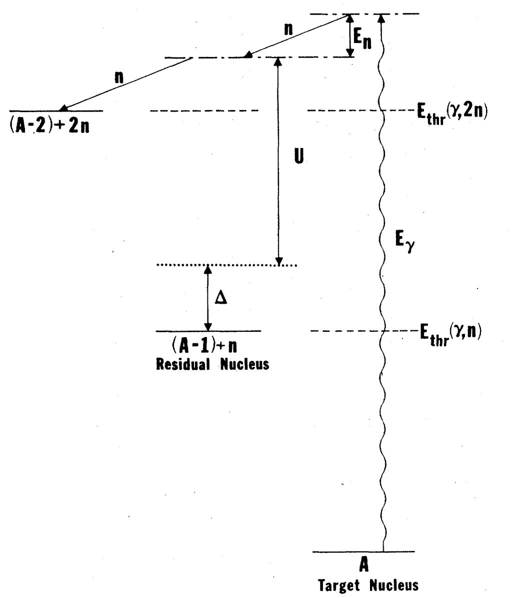

FIG. 52. Schematic diagram of the various energies encountered in the formulae for nuclear level-density calculations.

sections are shown in Fig. 51, together with the predictions of the collective theories. The asymmetry parameter A_t for the giant resonance given by the expression

$$A_t = \int_{\text{giant resonance}} |\sigma_{\parallel}(\gamma,\text{total}) - \sigma_{\perp}(\gamma,\text{total})| \, dE$$

was measured to be only 0.74 ± 0.13 as large as that predicted by either the elementary hydrodynamic theory or the dynamic collective model. The reason that neither collective theory can accommodate this result is that both are based upon the sum rule which requires σ_{int} to be the same for dipole absorption along each of the three intrinsic axes. [That 10% to 20% of the absorption cross section does not depend upon orientation had been found earlier in the photon-scattering measurement of Fuller and Hayward (1962b).] This result, as well as the departure from simple Lorentzian shape of the intrinsic cross sections, suggests some coupling *between* the two major dipole vibrational modes and/or an appreciable amount of underlying direct photoneutron emission. Neither of these possibilities is allowed for in the collective theories, but a measurement of photoneutron spectra from an aligned target could differentiate between them.

E. Statistical parameters

Although the photon absorption process, even for a medium or heavy nucleus, is a one-body effect, that is, the photon excites a single nucleon into a higher shell-model orbit, such a nucleus does not often deexcite by direct nucleon emission or even by precompound decay. Rather, the decay of the giant resonance for medium and heavy nuclei is dominated by statistical processes in the sense of the compound-nucleus picture of Bohr. This allows one to extract statistical parameters of the nucleus from an analysis of the decay products of the giant resonance. In particular, when measurements of the average photoneutron energy exist, the nuclear level density in the range of excitation energy a few MeV above the (γ,n) threshold in the nucleus having one neutron less than the target nucleus can be determined, together with the effect on the level density of shell and pairing forces in the nucleus, from the formula

$$\frac{\sigma(\gamma,2n)}{\sigma(\gamma,\text{total})} = \int_0^{E_\gamma - E_{\text{thr}}(\gamma,2n)} \rho(U) E_n dE_n \Big/ \int_0^{E_\gamma - E_{\text{thr}}(\gamma,n)-\Delta} \rho(U) E_n dE_n,$$

where the excitation energy $U = E_\gamma - E_{\text{thr}}(\gamma,n) - E_n - \Delta$ (see the energy-level diagram of Fig. 52), Δ is the correction resulting from shell and pairing effects, ρ is the density of states, and it is assumed that the inverse neutron-capture cross section is constant.

The functional form of ρ has been given by Ericson (1960) as

$$\rho \propto U^{-2} \exp[2(aU)^{1/2}]$$

and by Blatt and Weisskopf (1952) as

$$\rho \propto \exp[2(aU)^{1/2}],$$

where a is the nuclear level density parameter. A parameter search was carried out for a and Δ, using the same least-squares fitting technique as defined in Sec. IV.B, for the ratio $\sigma(\gamma,2n)/\sigma(\gamma,\text{total})$ in the photon energy range between the $(\gamma,2n)$ threshold and the point where the scatter and uncertainty in the data dictate that the fit to this cross-section ratio could not be improved further. This procedure gives a family of curves corresponding to pairs of values for a and Δ, all of which have approximately the same values for χ^2. In order to choose the correct pair, the average neutron energy $\bar{E}_n$ of the first neutron emitted from the target nucleus was computed for each fit, according to the formula

$$\bar{E}_n = \int_0^{E_\gamma - E_{\text{thr}}(\gamma,n)-\Delta} \rho(U) E_n^2 dE_n \Big/ \int_0^{E_\gamma - E_{\text{thr}}(\gamma,n)-\Delta} \rho(U) E_n dE_n.$$

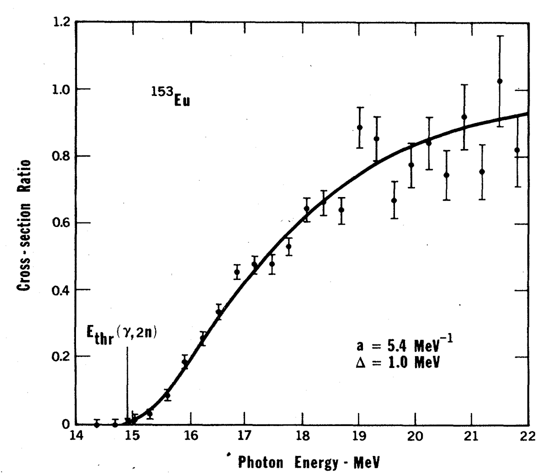

FIG. 53. Measured ratio of the double to the total photoneutron cross section for ^{153}Eu. The solid line is derived using the Ericson formula for the nuclear density of states and is evaluated for a level-density parameter $a = 5.4$ MeV^{-1} and a shell-plus-pairing energy $\Delta = 1.0$ MeV (from Berman *et al.*, 1969b).

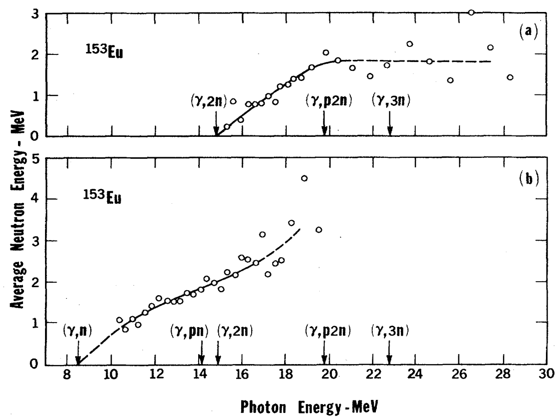

FIG. 54. Average neutron energies for ^{153}Eu obtained from ring-ratio data: (a) for $[(\gamma,2n)+(\gamma,p2n)]$ events, (b) for $[(\gamma,n)+(\gamma,pn)]$ events (from Berman *et al.*, 1969b).

The correct pair of values for a and Δ now was chosen by comparing these calculated $\bar{E}_n$ with the measured $\bar{E}_n$ from the ring-ratio data (see Sec. II.A), at the point where the latter are most reliable, i.e., at the peak of the giant resonance.

An example is shown in Fig. 53, where the ratio $\sigma(\gamma,2n)/\sigma(\gamma,\text{total})$ for ^{153}Eu is plotted versus photon energy. The solid curve is the theoretical fit when the Ericson formula for the density of states is used. The values for a and Δ give the value for $\bar{E}_n = 1.4$ MeV for the photon energy $E_\gamma = E_{m1} = 12.3$ MeV, in agreement with the ring-ratio value for $\bar{E}_n$ at that photon energy, as can be seen from the ring-ratio data for ^{153}Eu shown in Fig. 54.

This analysis was carried out for each nucleus for which ring-ratio data were available, and the results are listed in Table VI. The second and third columns give the pairing and shell properties, respectively, of the residual (target-minus-one-neutron) nucleus, to which the tabulated statistical parameters apply. The fourth and fifth columns of Table VI give the values for a obtained with the Ericson and the Blatt and Weiskopf formulae, respectively, for the density of states, and the sixth and seventh columns give the respective values for Δ.

There seems to be no particular trend in the values for a given in Table VI, although they do lie in the range expected from other kinds of determinations, such as inelastic neutron scattering. (It should be noted that the range of excitation energy to which these values for a applies brackets the region between the energies sampled with slow neutrons and with 14-MeV neutrons.) The values for Δ, however, seem to be independent of the specific functional form for the density of states, so that this can be taken to be a reasonable determination of the shell-and-pairing-effect energy for the nuclei measured.

Of course, justification for the above analysis depends upon the fact that most of the giant-resonance decays are statistical in nature; that is, that most often, when a medium or heavy nucleus is excited into its giant resonance, it lives a long time ($\gg 10^{-22}$ sec), forms a compound nucleus in which the excitation energy is shared by all the nucleons, and then subsequently decays by the evaporation of one or more neutrons. However, not all the giant-resonance decays follow this "resonance-compound" pattern; the $(\gamma,1n)$ cross sections do not always fall to zero within a few MeV of the $(\gamma,2n)$ threshold. More importantly, there is some experimental evidence from photoneutron-spectrum measurements (Bertozzi, 1958; Mutchler, 1966; Kuchnir *et al.*, 1967; Calarco, 1969; Young, 1972) that for medium and heavy nuclei as many as 25%, but more typically 10% to 15% of the giant-resonance decays are nonstatistical. These manifest themselves as an excess of high-energy photoneutrons over the fraction expected from a Maxwellian

TABLE VI. Nuclear level-density parameter a and shell-plus-pairing parameter Δ.

Nucleus	Pair type	Closed shell	a_E (MeV^{-1})	a_W (MeV^{-1})	Δ_E (MeV)	Δ_W (MeV)	Reference
^{74}As	Odd–odd		7.2	3.2	0.9	1.3	Berman *et al.*, 1969a
^{88}Y	Odd–odd		7.4	3.7	1.0	1.2	Berman *et al.*, 1967
^{89}Zr	Odd A		5.1	1.9	1.5	1.6	Berman *et al.*, 1967
^{90}Zr	Even–even	50 neutrons	8.1	4.0	4.8	5.0	Berman *et al.*, 1967
^{91}Zr	Odd A		10.0	4.0	1.9	2.8	Berman *et al.*, 1967
^{93}Zr	Odd A		7.6	1.6	3.1	3.9	Berman *et al.*, 1967
^{106}Ag	Odd–odd		6.9	2.9	2.0	2.2	Berman *et al.*, 1969a
^{114}In	Odd–odd		7.0	2.5	2.9	3.0	Fultz *et al.*, 1969
^{115}Sn	Odd A	50 protons	10.3	4.5	2.7	3.0	Fultz *et al.*, 1969
^{116}Sn	Even–even	50 protons	8.3	2.7	5.0	5.8	Fultz *et al.*, 1969
^{117}Sn	Odd A	50 protons	8.2	2.6	2.7	3.0	Fultz *et al.*, 1969
^{118}Sn	Even–even	50 protons	10.5	6.7	5.0	5.0	Fultz *et al.*, 1969
^{119}Sn	Odd A	50 protons	6.1	1.5	2.6	3.2	Fultz *et al.*, 1969
^{123}Sn	Odd A	50 protons	8.8	3.3	1.9	2.0	Fultz *et al.*, 1969
^{132}Cs	Odd–odd		6.9	2.4	2.3	2.5	Berman *et al.*, 1969a
^{137}Ba	Odd A		5.3	1.4	1.8	2.2	Berman *et al.*, 1970c
^{152}Eu	Odd–odd		5.4	1.8	1.0	1.1	Berman *et al.*, 1969b
^{158}Tb[a]	Odd–odd		(∼13)	(∼8)	∼0	∼0	Berman *et al.*, 1969b
^{159}Gd	Odd A		8.8	3.7	0.7	1.0	Berman *et al.*, 1969b
^{164}Ho	Odd–odd		6.1	2.0	1.6	1.7	Berman *et al.*, 1969b
^{180}Ta[b]	Odd–odd		(∼16)	(∼10)	∼1	∼1	Berman *et al.*, 1969b
^{185}W	Odd A		7.9	2.3	2.5	2.6	Berman *et al.*, 1969b

[a] Original data from Bramblett *et al.*, 1964, reanalyzed in Berman *et al.*, 1969b.
[b] Original data from Bramblett *et al.*, 1963, reanalyzed in Berman *et al.*, 1969b.

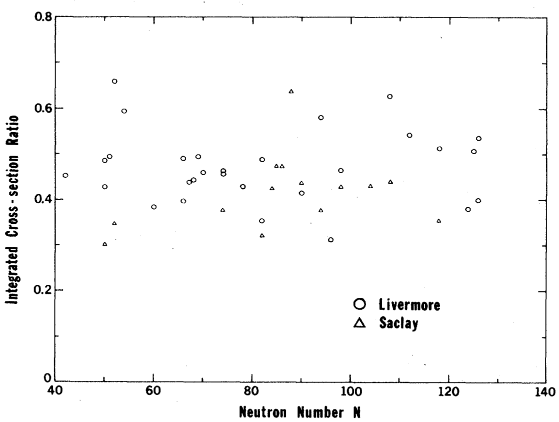

FIG. 55. The measured ratio $\sigma_{int}(\gamma,2n)/\sigma_{int}(\gamma,\text{total})$ plotted versus neutron number, where the integrations are carried out over the energy region from the $(\gamma,2n)$ threshold to the point 6 MeV above it.

distribution. The Livermore results on (γ,n) cross sections above the $(\gamma,2n)$ thresholds for most cases admit of a nonstatistical component of the order of 10%; the Saclay results typically favor a somewhat larger component.

A way of delineating the mass dependence of the nonstatistical component is illustrated in Fig. 55. Here the quantity $\int\sigma(\gamma,2n)dE/\int\sigma(\gamma,\text{total})dE$, where the limits of integration are from the $(\gamma,2n)$ threshold to 6 MeV above it, is plotted versus neutron number N, for all nuclei having $A>70$ for which this information is available. This removes, for practical purposes, the strong shell dependence of this ratio (as shown in Fig. 43) by eliminating the effect of the energy difference between the giant-resonance peak and the $(\gamma,2n)$ threshold. On this plot, a large value for the integrated cross-section ratio indicates a small nonstatistical component, and vice versa. It can be seen that none of the values is less than 0.3, which probably sets an upper limit of about 20% for the nonstatistical fraction, and only three are greater than 0.6, which must correspond to something $\lesssim 10\%$. This illustrates the point that for nuclei having $A>70$, at least, there probably is only slight, if any, mass dependence of the nonstatistical decay component of the giant resonance.

F. Structure above the giant resonance

Although this survey is not concerned primarily with effects which usually manifest themselves outside the main giant-resonance region, some of the data presented do in fact bear upon these subjects, and a brief discussion of two of them, namely, isospin effects and quadrupole effects, will be given here.

Magnetic dipole photon absorption, which occurs at energies well below the main giant resonance, has been seen in other kinds of photonuclear measurements, notably in threshold photoneutron experiments (Bowman *et al.*, 1970; Jackson, 1973) and in inelastic electron scattering (Fagg, 1973). The data surveyed here do not bear strongly upon this subject.

1. Isospin splitting and mixing

For a nucleus having $N-Z=2T_0\neq 0$, the dipole selection rule permits photoexcitation of states having an isospin of either $T_0=T_<$ or $T_0+1=T_>$. The $E1$ strength is apportioned between these two excitation modes roughly according to the ratio $T_0{:}1$ (Fallieros *et al.*, 1965; Fallieros and Goulard, 1970), so that the $T_<$ mode becomes relatively stronger with increasing T_0 and hence with increasing mass number. Thus the $T_<$ mode usually is thought of as the "normal" giant resonance. The simple theories (Fallieros *et al.*, 1965; Morinaga, 1965) also predict a splitting in excitation energy between the two modes roughly proportional to T_0+1, with the higher isospin $T_>$ mode lying higher in energy (Fallieros *et al.*, 1965; Akyüz and Fallieros, 1971; Fallieros, 1973; Paul, 1973). The empirical result given by Paul (1973), for instance, is

$$\Delta E = E_> - E_< \cong (55+15\ \text{MeV})(T_0+1)/A.$$

Thus, for heavy nuclei, the $T_>$ "giant resonance" has very little strength, and what little strength it has is found at energies well above the main part of the giant resonance. For nuclei having $A\lesssim 100$, however, the $T_>$ strength is found just a few MeV above the main $(T_<)$ giant resonance, and is of the order of about 10% to 20% of that of the $T_<$ strength.

Most of our knowledge of the photoexcitation of $T_>$ states comes from (p,γ_0) and $(e,e'p)$ measurements, since, in the absence of mixing into underlying or nearby $T_<$ states, neutron decay of $T_>$ states to low-lying states in the residual nucleus is forbidden by isospin conservation, whereas proton decay is not. [This field has been summarized recently by Paul (1973).] However, for some nuclei, whether resulting from mixing into $T_<$ states and/or from neutron decay to $T_0+\frac{1}{2}$ excited states in the residual nucleus (whose ground state has isospin $T_0-\frac{1}{2}$), $T_>$ effects have been seen in photoneutron reactions. Indeed, the photoneutron cross-section measurements for ^{90}Zr provided the first experimental evidence (Berman *et al.*, 1967) for the existence of this effect in medium or heavy nuclei, in the form of excess strength in the 20- to 23-MeV region, above the Lorentz-curve fit to the $(T_<)$ giant resonance (see Fig. 24). Figure 56 shows the total photoneutron cross section for this nucleus, together with the ^{89}Y(p,γ_0) cross section, which selectively populates $T_>$ states in ^{90}Zr. Similar excess

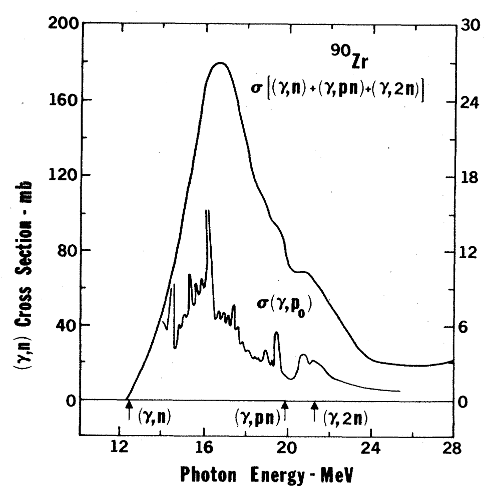

FIG. 56. Comparison of the (γ,n) and (γ,p_0) cross sections for ^{90}Zr, showing that the high-energy structure in the two cross-section curves occurs at the same excitation energies (from Hasinoff *et al.*, 1973).

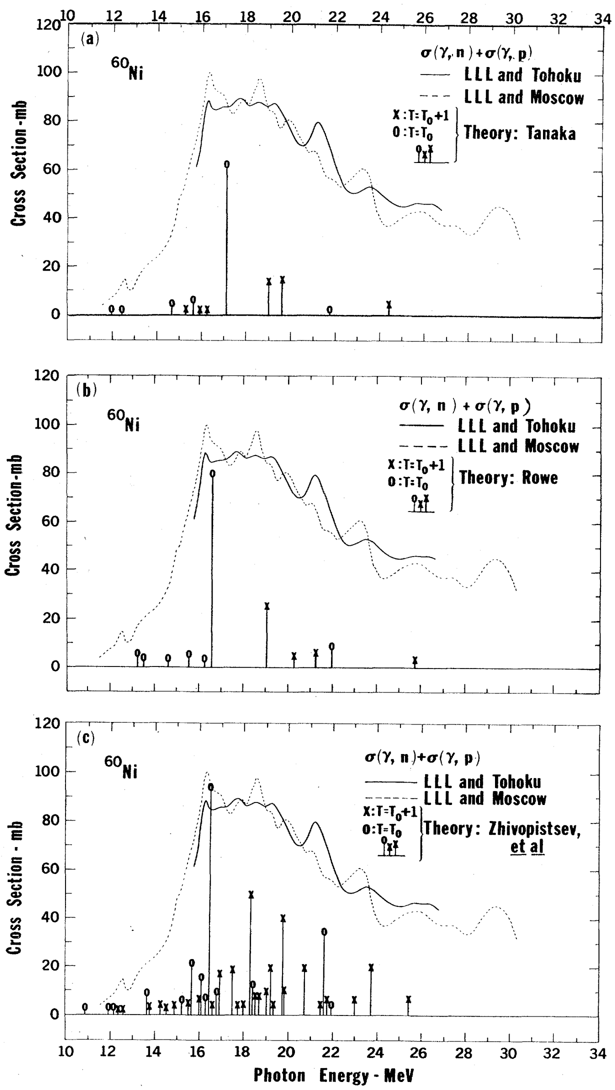

FIG. 57. The total photon absorption cross section for ^{60}Ni, obtained by summing the photoneutron and photoproton cross sections, compared with the theoretical predictions of (a) Tanaka (1971); (b) Rowe; (Ngo-Trong and Rowe, 1971; Rowe, 1973), and (c) Zhivopistsev and Shitikova (Zhivopistsev *et al.*, 1972; Zhivopistsev and Shitikova, 1973). The summed theoretical strengths are not normalized to the data (adapted from Fultz *et al.*, 1973c).

strength, sometimes appearing in clumps, can be seen above the giant resonance for many of the nuclei discussed in Sec. III.A, and this isospin effect is a plausible explanation for much of it. However, there is no conclusive proof that this is the case, and in many cases the quadrupole giant resonance (see below) is predicted to lie in the same energy region, as is the case for the tin isotopes (see Fultz *et al.*, 1969).

For nuclei having $A < 70$ the situation is far more complicated. This is partly because T_0 is smaller than for heavier nuclei, so that the relative $T_>$ strength is larger and the energy splitting is smaller. But more important than this is the fact that in these lighter nuclei the giant resonance is itself fragmented and shell effects play a major role. As a result, isospin mixing effects are so strong that one wonders

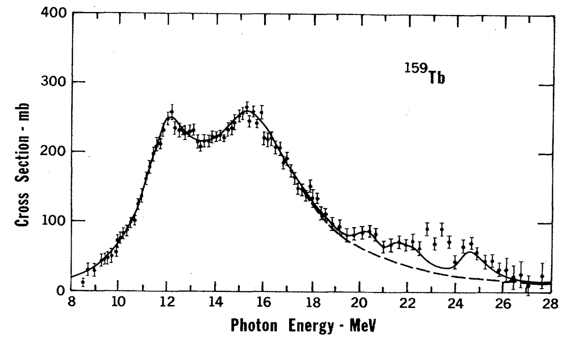

FIG. 58. The total photoneutron cross section for ^{159}Tb (Livermore). The solid curve is calculated with the dynamic collective model, and includes the $E2$ giant resonance; the dashed curve results from $E1$ photon absorption only (from Ligensa and Greiner, 1967).

whether isospin itself is a very fruitful concept here; its conservation law is one that is more honored in the breach than in the observance. A case in point is that for ^{60}Ni, whose total photon absorption cross section {obtained from summing the photoneutron cross section of Fig. 19(a) and the photoproton cross section measured using bremsstrahlung by Ishkhanov *et al.* (1970) or by means of the $(e,e'p)$ reaction by Shoda *et al.* [(1973); Miyase *et al.*, (1973)]} is shown in Fig. 57, together with the predictions of three theoretical calculations. [A similar comparison is given in Fultz *et al.* (1973c) for ^{58}Ni as well, where the (γ,p) reaction channel dominates over the (γ,n).] The theories predict, and the data show, that the situation is so complex that the simple concept of isospin splitting of the giant resonance, which seems to work well for heavier nuclei, cannot be applied in the mass region around $A = 60$, except in some average sense, wherein one refers to the centroids of the $T_<$ and $T_>$ strength distributions.

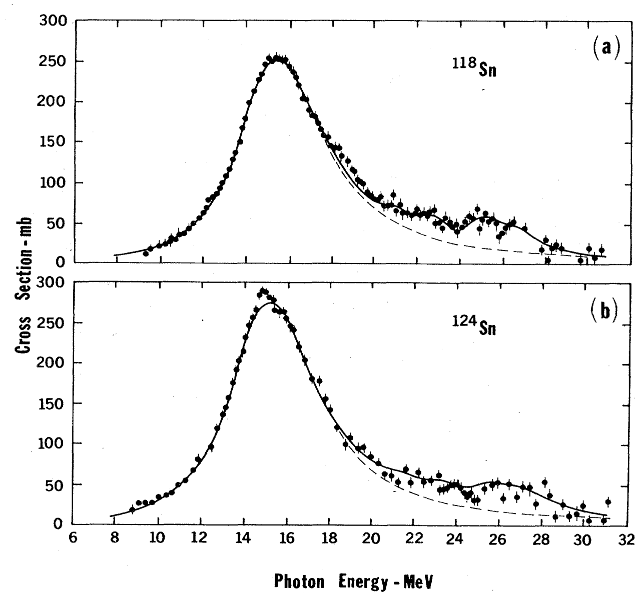

FIG. 59. The total photoneutron cross sections for (a) ^{118}Sn and (b) ^{124}Sn (Fig. 25). The solid curves are calculated with the dynamic collective model, and include the $E2$ giant resonance; the dashed curves result from $E1$ photon absorption only (from Urbas and Greiner, 1970)

For the special case of ^{16}O, where the isospin mixing in the giant resonance is small [see Hanna (1973) for a recent review of isospin mixing in the giant resonance, particularly for light nuclei], the measurements of Caldwell *et al.* (1967a, 1967b) give the value of 0.08 for the average isospin-mixing amplitude ratio.

For the special case of the mass 13 nuclei, Measday *et al.* (1965) have argued that the $^{13}N(\gamma,p_0)$ cross section is composed mainly of $T_<$ strength while the $^{13}C(\gamma,p)$ cross section is mainly $T_>$ [the $^{13}C(\gamma,n)$ cross section contains both isospin components]; that the $T_> = \frac{3}{2}$ component is the stronger (as expected); and that the energy splitting is of the order of 6 to 8 MeV (as expected).

For the special case of ^{26}Mg, the fact that the two clumps of strength below 19 MeV and from 19 to 23 MeV seen in Fig. 16(a) are characterized predominantly by different isospin was shown in a photoneutron time-of-flight measurement using bremsstrahlung by Wu *et al.* (1970b; see also Fultz *et al.*, 1971).

2. Electric quadrupole absorption

It has long been speculated that absorption of $E2$ radiation plays a role both above and below the giant dipole resonance, but since the expected magnitude of this effect was at least an order of magnitude smaller than dipole absorption, it has been hard to observe experimentally. Now it appears that $E2$ absorption has been seen below the giant resonance in medium and heavy nuclei by inelastic scattering of electrons and charged hadrons (Buskirk *et al.*, 1972; Torizuka *et al.*, 1972; Lewis, 1973), and above the giant resonance in some of the data presented here. [In light nuclei, $E2$ strength has been seen in many reaction channels, notably in measurements of (p,γ) angular distributions (see Suffert, 1973) and in $(\gamma,\vec{n})$ and $(\vec{p},\gamma)$ polarization measurements (Firk, 1970; Glavish, 1973)].

Since the effective charge for $E2$ absorption for protons is much larger than for neutrons in medium and heavy nuclei, and since proton emission is inhibited by the Coulomb barrier for modest proton energies, the low-energy $E2$ effects would be very hard to observe in experiments with real photons. But for higher excitation energies, especially energies above the (γ,pn) thresholds, this no longer is true, and one can expect quadrupole effects in the photoneutron cross sections at about 1.6 times the energy of the giant dipole resonance, where the $E2$ absorption is predicted to be centered (Danos and Greiner, 1964b). This situation clearly prevails for the deformed rare-earth nuclei, where $T_>$ effects should be small and prominent high-energy structure is seen in several cross sections, particularly those for ^{159}Tb, ^{160}Gd, and ^{165}Ho. A calculation of this giant quadrupole resonance has been made within the framework of the dynamic collective theory by Ligensa *et al.* (1966; Ligensa and Greiner, 1967) and has been applied by them to the cases of ^{159}Tb and ^{165}Ho. The results for ^{159}Tb are shown in Fig. 58, where the quadrupole effect is included in the calculated solid line. One can see that the energy and strength of the effect agree rather well with the experimental data; and since the widths of the individual peaks are arbitrary in the theory, allowing them to vary for the five quadrupole states (which correspond to the five values for the spherical harmonics Y_{2i}) could produce better agreement still.

For spherical nuclei, the collective theories also predict $E2$ strength centered at 1.6 E_m. Unfortunately, for many nuclei this range of energies overlaps the region of the strong $T_>$ dipole states. A case in point is that of the tin isotopes (Fultz *et al.*, 1969), where the structure above the giant resonance (Fig. 25) could owe its origin to either or both effects. In fact, Urbas and Greiner (1970) achieved excellent fits to the data for $^{118,124}Sn$ of Fultz *et al.* using the dynamic collective model to calculate both the dipole and quadrupole contributions to the cross sections. The results of this calculation are shown in Fig. 59. The goodness of these fits implies that this is a promising approach, and more experimental and theoretical effort along these lines is called for. For the photoneutron channel in particular, however, much firmer evidence than the above is needed, and measurements both of photoneutron angular distributions and of the evolution of the shape of the "$E2$ giant resonance" through a series of transitional nuclei [such as the neodymium isotopes, as has been done for the $E1$ giant resonance by the Saclay group (Carlos *et al.*, 1971)] should be performed (Greiner, 1973).

V. SUMMARY

Various experimental methods for obtaining monoenergetic photon beams were described, and the apparatus and techniques employed at Livermore and Saclay for measuring photoneutron cross sections with monoenergetic photons from the annihilation in flight of fast positrons were analyzed in detail. Sample giant-resonance data obtained over the course of more than a decade with monoenergetic photons were plotted in a uniform format and compared. The data for individual nuclei were discussed. For the most part, the data taken at the various laboratories were found to agree quite well with each other; this situation certainly is far better than that which had prevailed previously for photonuclear cross-section measurements performed with the use of continuous bremsstrahlung radiation sources. In addition to the main body of photoneutron cross-section data, a number of specialized experiments which bear on theories of the giant resonance were described as well.

The properties of the giant resonance which could be determined from this body of data were enumerated, tabulated, plotted, and compared with theoretical predictions. Some quantities, namely, the integrated cross sections, could be derived directly from the data. The TRK sum rule was found to be exhausted by the total photoneutron cross section integrated up to about twice the mean energy of the giant resonance. The first moment of the integrated cross section was found to be roughly proportional to $A^{4/3}$, with a proportionality constant of about 0.19. The second moment of the integrated cross section, which is proportional to the nuclear polarizability, was found to be specified rather well by the Migdal sum rule. The ratio of the integrated cross section for multiple neutron emission to the integrated total photoneutron cross section was found to be a sensitive indicator of nuclear shell effects.

Lorentz curves were fitted to all the giant-resonance data for medium and heavy nuclei in a self-consistent manner, and comments on individual nuclei were offered. Deformed nuclei were fitted with two non-interfering Lorentz curves. The parameters of these Lorentz-curve fits to the data were tabulated, as were several nuclear quantities derived from them. The nuclear symmetry energy was found to increase appreciably with mass number, and was fitted with a functional form which accounts for both volume and surface contributions. The energy of the peak of the giant resonance was found to have a mass dependence midway between the $A^{-1/3}$ and $A^{-1/6}$ predictions of the semiclassical collective theories, showing that neither volume nor surface effects dominate the restoring force in the mass region $51 \leq A \leq 238$. The width of the giant resonance was found to be hard to describe by a simple power of the resonance energy. The area under the Lorentz curves fitted to the data extrapolated to infinite energy was found to exhaust about 1.2 TRK sum-rule units, showing that the contribution from meson exchange forces to the giant-resonance absorption strength was rather smaller than had been believed previously. The hydrodynamic theory of the giant resonance was shown to give an excellent prescription for determining the eccentricity, and hence the intrinsic quadrupole moment, of statically deformed nuclei from the splitting of the giant resonance; however, the ratio of the areas under the two peaks departs from the predicted value of 0.5 for (prolate) nuclei which are not strongly deformed.

A number of other topics were discussed as well, insofar as they are related to the data surveyed here. Collective theories which couple quadrupole surface oscillations of the nucleus to the dipole vibrational modes were applied to the data—particularly the dynamic collective model of Danos, Greiner, and collaborators for spherical, deformed, vibrational, and transitional nuclei. The location and strength of electric quadrupole absorption also can be calculated from the dynamic collective theory, and was shown to fit very well the high-energy structure observed in the cross sections for certain nuclei. Nuclear level-density parameters and shell-and-pairing energies were extracted from the ratio of partial photoneutron cross sections above the $(\gamma,2n)$ thresholds and the fraction of nonstatistical decay products of the giant resonance was estimated. Finally, isospin splitting and mixing effects in the giant-resonance data were noted, and it was seen that for the nickel isotopes at least, both theory and experiment exhibited a very complex structure.

VI. PERSPECTIVE

Owing largely to the development and exploitation of monoenergetic photon beams, it now can be said that, by and large, the systematic properties of the giant $E1$ resonance have been determined well, although there remain a number of outstanding problems that call for further study, particularly among the light nuclei (where it is often the case that each nucleus presents its own unique features of interest). This being the case, it now is appropriate to focus attention on the other collective modes of the nucleus, which manifest themselves through the absorption of electromagnetic radiation of other multipolarities. These other modes usually are excited more readily by electron and hadron scattering, where larger linear and angular momenta can be transferred to the nucleus and for which as a consequence the usual electromagnetic selection rules are modified (for example, $E0$ transitions can be induced). Nevertheless, measurements with real photons, because of their very specificity, have played and will continue to play an important role. A few such measurements have been presented here, particularly of the isovector $E2$ resonance above the giant $E1$ resonance, and others, notably of the giant $M1$ resonance below the giant $E1$ resonance, are in the literature.

In addition to the study of the collective modes of the nucleus which has constituted the core of photonuclear physics, a number of other topics can be studied effectively with monoenergetic photon beams at or near giant-resonance energies, among them nuclear spectroscopy (as well as reaction mechanisms), especially in the continuum region for light nuclei. In particular, a considerably expanded effort is called for in photon scattering and in the measurement of the angular distribution and polarization of photoejected particles. More effort is needed in the too-neglected field of photofission as well. Finally, a number of applications have grown out of the photonuclear field, including those to astrophysics, nuclear reactor technology, and biology and medicine; and these applied fields certainly will continue to need more of the kind of fundamental information which monoenergetic-photon studies can provide.

ACKNOWLEDGMENTS

The authors of this review are deeply indebted to the many persons around the world, and especially to their past and present colleagues in the experimental and theoretical photonuclear groups at Livermore, who, over the years, have contributed in many ways to the production of this survey. Particular thanks are due to Dr. R. Bergère, who made available the Saclay photoneutron data in digital form; to Dr. R. E. Sund, who did the same for the General Atomic data; to Professor P. Axel, who allowed the use of data from Illinois in advance of publication and whose comments are always valued highly; to D. D. Faul and S. S. Dietrich, who helped greatly with the analysis of the data; to C. Hunt, who did most of the computer programming; to W. J. Goodman, who prepared the figures; to B. Brown, who prepared the manuscript, and to Dr. M. S. Weiss and Dr. T. F. Godlove for critically reading the manuscript.

REFERENCES TO THE DATA

Alvarez, R. A., B. L. Berman, D. R. Lasher, T. W. Phillips, and S. C. Fultz, 1971, Phys. Rev. C **4**, 1673.
Alvarez, R. A., B. L. Berman, F. H. Lewis, and P. Meyer, 1973a, in *Proceedings of the International Conference on Photonuclear Reactions and Applications*, Pacific Grove, California, edited by B. L. Berman (Lawrence Livermore Laboratory, Livermore), p. 545.
Alvarez, R. A., B. L. Berman, F. H. Lewis, and P. Meyer, 1973b, in *Proceedings of the International Conference on Photonuclear Reactions and Applications*, Pacific Grove, California, edited by B. L. Berman (Lawrence Livermore Laboratory, Livermore), p. 547.
Axel, P., K. Min, N. Stein, and D. C. Sutton, 1963, Phys. Rev. Lett. **10**, 299.
Axel, P., J. Miller, C. Schuhl, G. Tamas, and C. Tzara, 1966, J. Phys. (Paris) **27**, 262.
Axel, P., K. K. Min, and D. C. Sutton, 1970, Phys. Rev. C **2**, 689.
Beil, H., R. Bergère, P. Carlos, A. Leprêtre, A. Veyssière, and A. Parlag, 1971, Nucl. Phys. A **172**, 426.
Bergère, R., H. Beil, and A. Veyssière, 1968, Nucl. Phys. A **121**, 463.
Bergère, R., H. Beil, P. Carlos, and A. Veyssière, 1969, Nucl. Phys. A **133**, 417.
Bergère, R., H. Beil, P. Carlos, A. Leprêtre, and A. Veyssière, 1973, in *Proceedings of the International Conference on Photonuclear Reactions and Applications*, Pacific Grove, California, edited by B. L. Berman (Lawrence Livermore Laboratory, Livermore), p. 525.

Berman, B. L., R. L. Bramblett, J. T. Caldwell, R. R. Harvey, and S. C. Fultz, 1965, Phys. Rev. Lett. **15**, 727.
Berman, B. L., J. T. Caldwell, R. R. Harvey, M. A. Kelly, R. L. Bramblett, and S. C. Fultz, 1967, Phys. Rev. **162**, 1098.
Berman, B. L., R. L. Bramblett, J. T. Caldwell, H. S. Davis, M. A. Kelly, and S. C. Fultz, 1969a, Phys. Rev. **177**, 1745.
Berman, B. L., M. A. Kelly, R. L. Bramblett, J. T. Caldwell, H. S. Davis, and S. C. Fultz, 1969b, Phys. Rev. **185**, 1576.
Berman, B. L., S. C. Fultz, and P. F. Yergin, 1970a, Phys. Rev. Lett. **24**, 1594.
Berman, B. L., S. C. Fultz, and M. A. Kelly, 1970b, Phys. Rev. Lett. **25**, 938.
Berman, B. L., S. C. Fultz, J. T. Caldwell, M. A. Kelly, and S. S. Dietrich, 1970c, Phys. Rev. C **2**, 2318.
Berman, B. L., S. C. Fultz, and M. A. Kelly, 1971, Phys. Rev. C **4**, 723.
Berman, B. L., R. A. Alvarez, D. D. Faul, F. H. Lewis, Jr., P. Meyer, and T. W. Phillips, 1973c, in *Proceedings of the International Conference on Photonuclear Reactions and Applications*, Pacific Grove, California, edited by B. L. Berman (Lawrence Livermore Laboratory, Livermore), p. 1073.
Bowman, C. D., G. F. Auchampaugh, and S. C. Fultz, 1964, Phys. Rev. **133**, B676.
Bramblett, R. L., J. T. Caldwell, G. F. Auchampaugh, and S. C. Fultz, 1963, Phys. Rev. **129**, 2723.
Bramblett, R. L., J. T. Caldwell, R. R. Harvey, and S. C. Fultz, 1964, Phys. Rev. **133**, B869.
Bramblett, R. L., B. L. Berman, M. A. Kelly, J. T. Caldwell, and S. C. Fultz, 1966a, Bull. Am. Phys. Soc. **11**, 367.
Bramblett, R. L., J. T. Caldwell, B. L. Berman, R. R. Harvey, and S. C. Fultz, 1966b, Phys. Rev. **148**, 1198.
Bramblett, R. L., B. L. Berman, M. A. Kelly, J. T. Caldwell, and S. C. Fultz, 1973b, in *Proceedings of the International Conference on Photonuclear Reactions and Applications*, Pacific Grove, California, edited by B. L. Berman (Lawrence Livermore Laboratory, Livermore), p. 175.
Calarco, J. R., 1969, Ph.D. thesis, University of Illinois (unpublished).
Caldwell, J. T., 1967b, Ph.D. thesis, University of California, Lawrence Radiation Laboratory Report No. UCRL-50287 (unpublished).
Caldwell, J. T., R. R. Harvey, R. L. Bramblett, and S. C. Fultz, 1963, Phys. Lett. **6**, 213.
Caldwell, J. T., R. L. Bramblett, B. L. Berman, R. R. Harvey, and S. C. Fultz, 1965, Phys. Rev. Lett. **15**, 976.
Caldwell, J. T., S. C. Fultz, and R. L. Bramblett, 1967a, Phys. Rev. Lett. **19**, 447.
Carlos, P., H. Beil, R. Bergère, A. Leprêtre, and A. Veyssière, 1971, Nucl. Phys. A **172**, 437.
Carlos, P., R. Bergère, A. Veyssière, H. Beil, A. Leprêtre, and A. Miniac, 1973, in *Proceedings of the International Conference on Photonuclear Reactions and Applications*, Pacific Grove, California, edited by B. L. Berman (Lawrence Livermore Laboratory, Livermore), p. 1053.
Datta, S., and J. S. Allen, 1973, Phys. Rev. C **8**, 1421.
de Botton, N., J. Miller, C. Schuhl, G. Tamas, and C. Tzara, 1966, Nucl. Phys. **75**, 396.
Fultz, S. C., R. L. Bramblett, J. T. Caldwell, N. E. Hansen, and C. P. Jupiter, 1962a, Phys. Rev. **128**, 2345.
Fultz, S. C., R. L. Bramblett, J. T. Caldwell, and N. A. Kerr, 1962b, Phys. Rev. **127**, 1273.
Fultz, S. C., R. L. Bramblett, J. T. Caldwell, and R. R. Harvey, 1964, Phys. Rev. **133**, B1149.
Fultz, S. C., J. T. Caldwell, B. L. Berman, R. L. Bramblett, and R. R. Harvey, 1966, Phys. Rev. **143**, 790.
Fultz, S. C., B. L. Berman, J. T. Caldwell, R. L. Bramblett, and M. A. Kelly, 1969, Phys. Rev. **186**, 1255.
Fultz, S. C., R. A. Alverez, B. L. Berman, M. A. Kelly, D. R. Lasher, T. W. Phillips, and J. McElhinney, 1971a, Phys. Rev. C **4**, 149.
Fultz, S. C., R. A. Alvarez, B. L. Berman, and P. Meyer, 1973a, in *Proceedings of the International Conference on Photonuclear Reactions and Applications*, Pacific Grove, California, edited by B. L. Berman (Lawrence Livermore Laboratory, Livermore), p. 549.
Fultz, S. C., R. A. Alvarez, B. L. Berman, and P. Meyer, 1973b, in *Proceedings of the International Conference on Photonuclear Reactions and Applications*, Pacific Grove, California, edited by B. L. Berman (Lawrence Livermore Laboratory, Livermore), p. 551.
Fultz, S. C., R. A. Alvarez, B. L. Berman, and P. Meyer, 1973c, Lawrence Livermore Laboratory Report No. UCRL-75302, submitted to Phys. Rev. C.
Ganek, D., 1972, Ph.D. thesis, University of Illinois (unpublished).
Harvey, R. R., J. T. Caldwell, R. L. Bramblett, and S. C. Fultz, 1964, Phys. Rev. **136**, B126.
Hayward, E., W. C. Barber, and J. Sazama, 1973, Phys. Rev. C **8**, 1065.
Hurst, R. R., and D. J. Donahue, 1967, Nucl. Phys. A **91**, 365.
Kelly, M. A., 1968, Ph.D. thesis, University of California, Lawrence Radiation Laboratory Report No. UCRL-50421 (unpublished).
Kelly, M. A., B. L. Berman, R. L. Bramblett, and S. C. Fultz, 1969, Phys. Rev. **179**, 1194.
Kuchnir, F. T., P. Axel, L. Criegee, D. M. Drake, A. O. Hanson, and D. C. Sutton, 1967, Phys. Rev. **161**, 1236.
Kuehne, H. W., P. Axel, and D. C. Sutton, 1967, Phys. Rev. **163**, 1278.
Leprêtre, A., H. Beil, R. Bergère, P. Carlos, A. Veyssière, and M. Sugawara, 1971, Nucl. Phys. A **175**, 609.
Lochstet, W. A., and W. E. Stephens, 1966, Phys. Rev. **141**, 1002.
Matsumoto, S., H. Yamashita, T. Kamae, and Y. Nogami, 1964, Phys. Lett. **12**, 49.
Matsumoto, S., H. Yamashita, T. Kamae, and Y. Nogami, 1965, J. Phys. Soc. Jpn. **20**, 1321.
Miller, J., C. Schuhl, and C. Tzara, 1961, J. Phys. Radium **22**, 35.
Miller, J., C. Schuhl, and C. Tzara, 1962a, Nucl. Phys. **32**, 236.
Miller, J., C. Schuhl, G. Tamas, and C. Tzara, 1962b, Phys. Lett. **2**, 76.
Miller, J., C. Schuhl, G. Tamas, and C. Tzara, 1966, J. Phys. (Paris) **27**, 8.
Nagel, M. Z., 1970, Ph.D. thesis, University of Illinois (unpublished).
O'Connell, J. S., P. A. Tipler, and P. Axel, 1962, Phys. Rev. **126**, 228.
Sund, R. E., M. P. Baker, L. A. Kull, and R. B. Walton, 1968, Phys. Rev. **176**, 1366.
Sund, R. E., V. V. Verbinski, H. Weber, and L. A. Kull, 1970, Phys. Rev. C **2**, 1129.
Tipler, P. A., P. Axel, N. Stein, and D. C. Sutton, 1963, Phys. Rev. **129**, 2096.
Veyssière, A., H. Beil, R. Bergère, P. Carlos, and A. Leprêtre, 1970, Nucl. Phys. A **159**, 561.
Veyssière, A., H. Beil, R. Bergère, P. Carlos, A. Leprêtre, and K. Kernbath, 1973, Nucl. Phys. A **199**, 45.
Young, L. M., 1972, Ph.D. thesis, University of Illinois (unpublished).

REFERENCES TO THE TEXT

[Some of the Data References (above) are referred to in the text as well.]

Ahrens, J., H. B. Eppler, H. Gimm, H. Gundrum, M. Kröning, P. Riehn, G. Sita Ram, A. Zieger, and B. Ziegler, 1973, in *Proceedings of the International Conference on Photonuclear Reactions and Applications*, Pacific Grove, California, edited by B. L. Berman (Lawrence Livermore Laboratory, Livermore), p. 23.
Akyüz, R. Ö., and S. Fallieros, 1971, Phys. Rev. Lett. **27**, 1016.
Ambler, E., E. G. Fuller, and H. Marshak, 1965, Phys. Rev. **138**, B117.
Arad, B., and G. Ben-David, 1973a, Rev. Mod. Phys. **45**, 230.
Arad, B., and G. Ben-David, 1973b, in *Proceedings of the International Conference on Photonuclear Reactions and Applications*, Pacific Grove, California, edited by B. L. Berman (Lawrence Livermore Laboratory, Livermore), p. 277.
Arenhövel, H., 1973, in *Proceedings of the International Conference on Photonuclear Reactions and Applications*, Pacific Grove, California, edited by B. L. Berman (Lawrence Livermore Laboratory, Livermore), p. 449.
Arenhövel, H., and W. Greiner, 1968, Prog. Nucl. Phys. **10**, 167.
Arenhövel, H., and W. Greiner, 1969, Private communication quoted in Fultz *et al.* (1969) and Bergère *et al.* (1973).
Arenhövel, H., and J. M. Maison, 1970, Nucl. Phys. A **147**, 305.
Audit, G., N. de Botton, G. Tamas, H. Beil, R. Bergère, and A. Veyssière, 1970, Nucl. Instrum. Methods **79**, 203.
Axel, P., 1962, Phys. Rev. **126**, 671.
Baglin, J. E. E., E. J. Bentz, and R. W. Carr, 1971 (private communication).
Barrett, R. F., L. C. Biedenharn, M. Danos, P. P. Delsanto, W. Greiner, and H. G. Wahsweiler, 1973, Rev. Mod. Phys. **45**, 44.
Bayart, J. A., 1969, Saclay Report No. CEA-N-1161 (unpublished).
Beil, H., R. Bergère, and A. Veyssière, 1969, Nucl. Instrum. Methods **67**, 293.
Berman, B. L., 1973a, in *Proceedings of the International Conference on Photonuclear Reactions and Applications*, Pacific Grove, California

edited by B. L. Berman (Lawrence Livermore Laboratory, Livermore), p. 567.
Berman, B. L., 1973b, in *Proceedings of the International Conference on Photonuclear Reactions and Applications*, Pacific Grove, California, edited by B. L. Berman (Lawrence Livermore Laboratory, Livermore), p. 569.
Berman, B. L., Editor, 1973d, *Proceedings of the International Conference on Photonuclear Reactions and Applications*, Pacific Grove, California (Lawrence Livermore Laboratory, Livermore).
Berman, B. L., 1974a, in *Nuclear Spectroscopy*, edited by J. Cerny (Academic, New York), Chap. VIII.A.
Berman, B. L., 1974b, University of California Lawrence Livermore Laboratory Report No. UCRL-75694, to be published in Atomic Data and Nuclear Data Tables.
Berman, B. L., F. W. K. Firk, and C.-P. Wu, 1972, Nucl. Phys. A **179**, 791.
Berman, B. L., and Fultz, S. C., 1974c, University of California Lawrence Livermore Laboratory Report No. UCRL-75383.
Bertozzi, W., 1958, Ph.D. thesis, M.I.T. (unpublished).
Blatt, J. M., and V. F. Weisskopf, 1952, *Theoretical Nuclear Physics* (Wiley, New York), p. 379.
Bowman, C. D., R. J. Baglan, B. L. Berman, and T. W. Phillips, 1970, Phys. Rev. Lett. **25**, 1302.
Bramblett, R. L., 1962, Livermore Internal Report (unpublished).
Bramblett, R. L., S. C. Fultz, and B. L. Berman, 1973a, in *Proceedings of the International Conference on Photonuclear Reactions and Applications*, Pacific Grove, California, edited by B. L. Berman (Lawrence Livermore Laboratory, Livermore), p. 13.
Bramblett, R. L., S. C. Fultz, B. L. Berman, M. A. Kelly, J. T. Caldwell, and D. C. Sutton, 1973c, in *Proceedings of the International Conference on Photonuclear Reactions and Applications*, Pacific Grove, California, edited by B. L. Berman (Lawrence Livermore Laboratory, Livermore), p. 271.
Brennan, J. G., and C. Werntz, 1970, Phys. Rev. C **1**, 1679.
Brown, G. E., 1973, in *Proceedings of the International Conference on Photonuclear Reactions and Applications*, Pacific Grove, California, edited by B. L. Berman (Lawrence Livermore Laboratory, Livermore), p. 57; also see the discussion following this paper (p. 63).
Brown, G. E., and M. Bolsterli, 1959, Phys. Rev. Lett. **3**, 472.
Buskirk, F. R., H.-D. Gräf, R. Pitthan, H. Theissen, O. Titze, and Th. Walcher, 1972, Phys. Lett. B **42**, 194.
Cannington, P. H., R. J. J. Stewart, and B. M. Spicer, 1968, Nucl. Phys. A **109**, 385.
Carver, J. H., and W. Turchinetz, 1959, Proc. Phys. Soc. Lond. **73**, 69.
Carver, J. H., D. C. Peaslee, and R. B. Taylor, 1962, Phys. Rev. **127**, 2198.
Cook, B. C., D. R. Hutchinson, R. C. Waring, J. N. Bradford, R. G. Johnson, and J. E. Griffin, 1966, Phys. Rev. **143**, 730.
Danos, M., 1958, Nucl. Phys. **5**, 23.
Danos, M., 1973, in *Proceedings of the International Conference on Photonuclear Reactions and Applications*, Pacific Grove, California, edited by B. L. Berman (Lawrence Livermore Laboratory, Livermore), p. 43.
Danos, M., and W. Greiner, 1964a, Phys. Rev. **134**, B284.
Danos, M., W. Greiner, and C. B. Kohr, 1964b, Phys. Lett. **12**, 344.
Danos, M., and E. G. Fuller, 1965a, Annu. Rev. Nucl. Sci. **15**, 29.
Danos, M., and W. Greiner, 1965b, Phys. Rev. **138**, B876.
Del Bianco, W., S. Kundu, and P. Boucher, 1973a, Nucl. Phys. A **209**, 181.
Del Bianco, W., S. Kundu, and P. Boucher, 1973b, in *Proceedings of the International Conference on Photonuclear Reactions and Applications*, Pacific Grove, California, edited by B. L. Berman (Lawrence Livermore Laboratory, Livermore), p. 557.
Dodge, W. R., and W. C. Barber, 1962, Phys. Rev. **127**, 1745.
Dodge, W. R., and J. J. Murphy II, 1972, Phys. Rev. Lett. **28**, 839.
Dover, C. B., R. H. Lemmer, and F. J. W. Hahne, 1972, Ann. Phys. **70**, 458.
Drechsel, D., J. B. Seaborn, and W. Greiner, 1967, Phys. Rev. **162**, 983.
Eisenberg, J. M., and W. Greiner, 1970a, *Nuclear Models* (North-Holland, Amsterdam).
Eisenberg, J. M., and W. Greiner, 1970b, *Excitation Mechanisms of the Nucleus* (North-Holland, Amsterdam).
Eisenberg, J. M., and W. Greiner, 1972, *Microscopic Theory of the Nucleus* (North-Holland, Amsterdam).
Elliott, J. P., and B. H. Flowers, 1957, Proc. R. Soc. Lond. A **242**, 57.
Elliott, R. V., K. Lokan, D. Lobb, and L. Katz, 1964, Saskatchewan Accelerator Laboratory Report No. SAL-3 (unpublished).
Ericson, T., 1960, Adv. Phys. **9**, 425.
Fagg, L., 1973, in *Proceedings of the International Conference on Photonuclear Reactions and Applications*, Pacific Grove, California, edited by B. L. Berman (Lawrence Livermore Laboratory, Livermore), p. 663.
Fallieros, S., 1973, in *Proceedings of the International Conference on Photonuclear Reactions and Applications*, Pacific Grove, California, edited by B. L. Berman (Lawrence Livermore Laboratory, Livermore), p. 401.
Fallieros, S., B. Goulard, and R. H. Venter, 1965, Phys. Lett. **19**, 398.
Fallieros, S., and B. Goulard, 1970, Nucl. Phys. A **147**, 593.
Faul, D. D., and B. L. Berman, 1974, Bull. Am. Phys. Soc. **19**, 110.
Fielder, D. S., J. Le Tourneux, K. Min, and W. D. Whitehead, 1965, Phys. Rev. Lett. **15**, 33.
Finckh, E., and U. Hegel, 1961, Z. Phys. **162**, 154.
Firk, F. W. K., 1970, Annu. Rev. Nucl. Sci. **20**, 39.
Fuller, E. G., and E. Hayward, 1962a, in *Nuclear Reactions*, edited by P. M. Endt and P. B. Smith (North-Holland, Amsterdam), p. 113.
Fuller, E. G., and E. Hayward, 1962b, Nucl. Phys. **30**, 613.
Fuller, E. G., H. M. Gerstenberg, H. Vander Molen, and T. C. Dunn, 1973, NBS Spec. Publ. 380.
Fultz, S. C., R. L. Bramblett, B. L. Berman, J. T. Caldwell, and M. A. Kelly, 1967, in *Proceedings of the International Nuclear Physics Conference*, Gatlinburg, Tennessee, edited by R. L. Becker, C. D. Goodman, P. H. Stelson, and A. Zucker (Academic, New York), p. 397.
Fultz, S. C., B. L. Berman, R. A. Alvarez, and P. Meyer, 1973d, in *Proceedings of the International Conference on Photonuclear Reactions and Applications*, Pacific Grove, California, edited by B. L. Berman (Lawrence Livermore Laboratory, Livermore), p. 273.
Gellie, R. W., K. H. Lokan, N. K. Sherman, R. G. Johnson, and J. I. Lodge, 1972, Can. J. Phys. **50**, 1689.
Glavish, H. F., 1973, in *Proceedings of the International Conference on Photonuclear Reactions and Applications*, Pacific Grove, California, edited by B. L. Berman (Lawrence Livermore Laboratory, Livermore), p. 755.
Goldhaber, M., and E. Teller, 1948, Phys. Rev. **74**, 1046.
Green, A. E. S., 1954, Phys. Rev. **95**, 1006.
Greiner, W., 1973, in *Proceedings of the International Conference on Photonuclear Reactions and Applications*, Pacific Grove, California, edited by B. L. Berman (Lawrence Livermore Laboratory, Livermore), p. 1364.
Haissinski, J., 1967, Nucl. Instrum. Methods **51**, 181.
Hanna, S. S., 1973, in *Proceedings of the International Conference on Photonuclear Reactions and Applications*, Pacific Grove, California, edited by B. L. Berman (Lawrence Livermore Laboratory, Livermore), p. 417.
Hasinoff, M., G. A. Fisher, and S. S. Hanna, 1973, Nucl. Phys. A **216**, 221.
Hatcher, C. R., R. L. Bramblett, N. E. Hansen, and S. C. Fultz, 1961, Nucl. Instrum. Methods **14**, 337.
Hayward, E., 1965, in *Nuclear Structure and Electromagnetic Interactions*, edited by N. MacDonald (Plenum, New York), p. 141.
Hayward, E., 1970, NBS Monograph 118 (unpublished).
Huber, M. G., M. Danos, H. J. Weber, and W. Greiner, 1967, Phys. Rev. **155**, 1073.
Irish, J. D., R. G. Johnson, B. L. Berman, B. J. Thomas, K. G. McNeill, and J. W. Jury, 1973, Phys. Rev. C **8**, 1211.
Ishkhanov, B. S., I. M. Kapitonov, I. M. Piskarev, V. G. Shevchenko, and O. P. Shevchenko, 1970, Sov. J. Nucl. Phys. **11**, 272.
Jackson, H. E., 1973, in *Proceedings of the International Conference on Photonuclear Reactions and Applications*, Pacific Grove, California, edited by B. L. Berman (Lawrence Livermore Laboratory, Livermore), p. 817.
Jupiter, C. P., N. E. Hansen, R. E. Shafer, and S. C. Fultz, 1961, Phys. Rev. **121**, 866.
Kerman, A. K., and H. K. Quang, 1964, Phys. Rev. **135**, B883.
King, J. D., R. N. Haslam, and R. W. Parsons, 1960, Can. J. Phys. **38**, 231.
Le Tourneux, J., 1965, K. Dan. Vidensk. Selsk. Mat.-Fys. Medd. **34**, No. 11.
Levinger, J. S., 1960, *Nuclear Photo-Disintegration* (Oxford University, London).
Lewis, M. B., 1973, in *Proceedings of the International Conference on Photonuclear Reactions and Applications*, Pacific Grove, California, edited by B. L. Berman (Lawrence Livermore Laboratory, Livermore), p. 685.
Ligensa, R., W. Greiner, and M. Danos, 1966, Phys. Rev. Lett. **16**, 364.

Ligensa, R., and W. Greiner, 1967, Nucl. Phys. A **92**, 673.
Ligensa, R., and W. Greiner, 1969, Ann. Phys. (N.Y.) **51**, 28.
Lobb, D. E., 1967, Nucl. Instrum. Methods **46**, 181.
Löbner, K. E. G., M. Vetter, and V. Hönig, 1970, Nucl. Data Tables **7**, 5.
Measday, D. F., A. B. Clegg, and P. S. Fisher, 1965, Nucl. Phys. **61**, 269.
Meyer, P., 1973 (private communication).
Migdal, A. B., A. A. Lushnikov, and D. F. Zaretsky, 1965, Nucl. Phys. **66**, 193.
Miller, J., C. Schuhl, G. Tamas, and C. Tzara, 1960a, J. Phys. Radium **21**, 296.
Miller, J., C. Schuhl, G. Tamas, and C. Tzara, 1960b, J. Phys. Radium **21**, 755.
Miyase, H., S. Oikawa, A. Suzuki, J. Uegaki, T. Saito, M. Sugawara, and K. Shoda, 1973, in *Proceedings of the International Conference on Photonuclear Reactions and Applications*, Pacific Grove, California, edited by B. L. Berman (Lawrence Livermore Laboratory, Livermore), p. 553.
Moreh, R., and T. Bar-Noy, 1972, Nucl. Instrum. Methods **105**, 557.
Morinaga, H., 1965, Z. Phys. **188**, 182.
Mshelia, E. D., K. Roos, and W. Greiner, 1973a, Nucl. Phys. A **212**, 157.
Mshelia, E. D., and R. F. Barrett, 1973b, Nucl. Phys. A **205**, 581.
Mutchler, G. S., 1966, Ph.D. thesis, M.I.T. (unpublished).
Myers, W. D., and W. J. Swiatecki, 1966, Nucl. Phys. **81**, 1.
Myers, W. D., and W. J. Swiatecki, 1969, Ann. Phys. (N.Y.) **55**, 395.
Nathans, R., and J. Halpern, 1953, Phys. Rev. **92**, 207.
Ngo-Trong, C., and D. J. Rowe, 1971, Phys. Lett. B **36**, 553.
Nunan, C. S., 1965, IEEE Nucl. Sci. Trans. **NS-12**, 465.
O'Connell, J. S., 1973, in *Proceedings of the International Conference on Photonuclear Reactions and Applications*, Pacific Grove, California, edited by B. L. Berman (Lawrence Livermore Laboratory, Livermore), p. 71.
Okamoto, K., 1956, Prog. Theor. Phys. **15**, 75L.
Okamoto, K., 1958, Phys. Rev. **110**, 143.
Owens, R. O., and L. S. Cardman, 1969, Nucl. Instrum. Methods **67**, 283.
Paul, P., 1973, in *Proceedings of the International Conference on Photonuclear Reactions and Applications*, Pacific Grove, California, edited by B. L. Berman (Lawrence Livermore Laboratory, Livermore), p. 407.
Phillips, T. W., R. A. Alvarez, and B. L. Berman, 1973 (private communication).
Rezwani, V., M. Brand, R. Sedlmayr, L. v. Bernus, U. Schneider, and W. Greiner, 1972a, in *Proceedings of the International Conference on Nuclear Structure Studies Using Electron Scattering and Photoreaction*, edited by K. Shoda and H. Ui (Sendai, Tohoku), p. 235.
Rezwani, V., G. Gneuss, and H. Arenhövel, 1972b, Nucl. Phys. A **180**, 254.
Rowe, D. J., 1973, in *Proceedings of the International Conference on Photonuclear Reactions and Applications*, Pacific Grove, California, edited by B. L. Berman (Lawrence Livermore Laboratory, Livermore), p. 717.
Schuhl, C., and C. Tzara, 1961, Nucl. Instrum. Methods **10**, 217.
Schuhl, C. G., 1973, in *Proceedings of the International Conference on Photonuclear Reactions and Applications*, Pacific Grove, California, edited by B. L. Berman (Lawrence Livermore Laboratory, Livermore), p. 1249.
Semenko, S. F., 1965, Sov. J. Nucl. Phys. **1**, 295.
Seward, F. D., C. R. Hatcher, and S. C. Fultz, 1961, Phys. Rev. **121**, 605.
Shakin, C. M., and W. L. Wang, 1971, Phys. Rev. Lett. **26**, 902.
Shakin, C. M., and M. S. Weiss, 1973, Phys. Rev. C **7**, 1820.
Shoda, K., 1973 (private communication).
Shoda, K., and H. Ui, Editors, 1972, *Proceedings of the International Conference on Nuclear Structure Studies Using Electron Scattering and Photoreaction* (Sendai, Tohoku).
Spicer, B. M., 1964, Suppl. Nuovo Cimento **2**, 243.
Spicer, B. M., 1969, Adv. Nucl. Phys. **1**, 1.
Steinwedel, H., and J. H. D. Jensen, 1950, Z. Naturforsch. A **5**, 413.
Suffert, M., 1973, in *Proceedings of the International Conference on Photonuclear Reactions and Applications*, Pacific Grove, California, edited by B. L. Berman (Lawrence Livermore Laboratory, Livermore), p. 741.
Sund, R. E., R. B. Walton, M. J. Norris, and M. H. MacGregor, 1964, Nucl. Instrum. Methods **27**, 109.
Swiatecki, W. J., 1973 (private communication).
Tanaka, Y., 1971, Prog. Theor. Phys. **46**, 787.
Tanner, N. W., G. C. Thomas, and E. D. Earle, 1964, Nucl. Phys. **52**, 45.
Teller, E., and M. S. Weiss, 1973, in *Proceedings of the International Conference on Photonuclear Reactions and Applications*, Pacific Grove, California, edited by B. L. Berman (Lawrence Livermore Laboratory, Livermore), p. 7.
Thompson, M. N., J. M. Taylor, B. M. Spicer, and J. E. E. Baglin, 1965, Nucl. Phys. **64**, 486.
Toms, M. E., 1967, Naval Research Laboratory Bibliography No. 31.
Toms, M. E., and T. F. Godlove, 1965, IEEE Nucl. Sci. Trans. **NS-12**, 462.
Torizuka, Y., Y. Kojima, T. Saito, K. Itoh, A. Nakada, S. Mitsunobu, M. Nagao, K. Hosoyama, and S. Fukuda, 1972, in *Proceedings of the International Conference on Nuclear Structure Studies Using Electron Scattering and Photoreaction*, edited by K. Shoda and H. Ui (Sendai, Tohoku), p. 171.
Torizuka, Y., Y. Kojima, T. Saito, K. Itoh, A. Nakada, S. Mitsunobu, M. Nagao, K. Hosoyama, S. Fukuda, and H. Miura, 1973, in *Proceedings of the International Conference on Photonuclear Reactions and Applications*, Pacific Grove, California, edited by B. L. Berman (Lawrence Livermore Laboratory, Livermore), p. 675.
Tzara, C., 1957, C. R. Acad. Sci. (Paris) **56**, 245.
Urbas, T. D., and W. Greiner, 1970, Phys. Rev. Lett. **24**, 1026.
Wang, W. L., and C. M. Shakin, 1972, Phys. Rev. C **5**, 1898.
Wapstra, A. H., and N. B. Gove, 1971, Nucl. Data Tables **9**, 303.
Webb, D. V., C. K. Malcolm, Y. M. Shin, and D. M. Skopik, 1973, in *Proceedings of the International Conference on Photonuclear Reactions and Applications*, Pacific Grove, California, edited by B. L. Berman (Lawrence Livermore Laboratory, Livermore), p. 149.
Wilkinson, D. H., 1956, Physica **22**, 1039.
Wu, C.-P., F. W. K. Firk, and T. W. Phillips, 1970a, Nucl. Phys. A **147**, 19.
Wu, C.-P., F. W. K. Firk, and B. L. Berman, 1970b, Phys. Lett. B **32**, 675.
Yount, D., and J. Pine, 1962, Nucl. Instrum. Methods **15**, 45.
Zhivopistsev, F. A., V. A. Lukashov, K. V. Shitikova, and N. P. Yudin, 1972, Czech. J. Phys. B **22**, 883.
Zhivopistsev, F. A., and K. F. Shitikova, 1973, Sov. J. Nucl. Phys. **16**, 42.